DNA-TR-81-129

TEMPORAL STATISTICS OF SCINTILLATION FOR SATELLITE COMMUNICATION AND RADAR SYSTEMS

Roger A. Dana
Mission Research Corporation
P.O. Drawer 719
Santa Barbara, California 93102

1 April 1982

Technical Report

CONTRACT No. DNA 001-81-C-0081

APPROVED FOR PUBLIC RELEASE;
DISTRIBUTION UNLIMITED.

THIS WORK WAS SPONSORED BY THE DEFENSE NUCLEAR AGENCY
UNDER RDT&E RMSS CODE B322082466 S99QAXHB00005 H2590D

Prepared for
Director
DEFENSE NUCLEAR AGENCY
Washington, DC 20305

Destroy this report when it is no longer needed. Do not return to sender.

PLEASE NOTIFY THE DEFENSE NUCLEAR AGENCY, ATTN: STTI, WASHINGTON, D.C. 20305, IF YOUR ADDRESS IS INCORRECT, IF YOU WISH TO BE DELETED FROM THE DISTRIBUTION LIST, OR IF THE ADDRESSEE IS NO LONGER EMPLOYED BY YOUR ORGANIZATION.

UNCLASSIFIED

SECURITY CLASSIFICATION OF THIS PAGE (When Data Entered)

REPORT DOCUMENTATION PAGE	READ INSTRUCTIONS BEFORE COMPLETING FORM
1 REPORT NUMBER: DNA-TR-81-129	2 GOVT ACCESSION NO: AD-A135 735
	3 RECIPIENT'S CATALOG NUMBER:
4 TITLE (and Subtitle): TEMPORAL STATISTICS OF SCINTILLATION FOR SATELLITE COMMUNICATION AND RADAR SYSTEMS	5 TYPE OF REPORT & PERIOD COVERED: Technical Report
	6 PERFORMING ORG. REPORT NUMBER: MRC-R-692
7 AUTHOR(s): Roger A. Dana	8 CONTRACT OR GRANT NUMBER(s): DNA 001-81-C-0081
9 PERFORMING ORGANIZATION NAME AND ADDRESS: Mission Research Corporation, P. O. Drawer 719, Santa Barbara, California 93102	10 PROGRAM ELEMENT, PROJECT, TASK AREA & WORK UNIT NUMBERS: Task S99QAXHB-00005
11 CONTROLLING OFFICE NAME AND ADDRESS: Director, Defense Nuclear Agency, Washington, DC 20305	12 REPORT DATE: 1 April 1982
	13 NUMBER OF PAGES: 128
14 MONITORING AGENCY NAME & ADDRESS (if different from Controlling Office)	15 SECURITY CLASS (of this report): UNCLASSIFIED
	15a DECLASSIFICATION DOWNGRADING SCHEDULE: N/A since UNCLASSIFIED

16 DISTRIBUTION STATEMENT (of this Report)

Approved for public release; distribution unlimited.

17 DISTRIBUTION STATEMENT (of the abstract entered in Block 20, if different from Report)

18 SUPPLEMENTARY NOTES

This work was sponsored by the Defense Nuclear Agency under RDT&E RMSS Code B322082466 S99QAXHB00005 H2590D.

19 KEY WORDS (Continue on reverse side if necessary and identify by block number)

Satellite Communication
Space Based Radar
Signal Scintillation
Temporal Statistics
Rayleigh Fading

20 ABSTRACT (Continue on reverse side if necessary and identify by block number)

Analytic and simulation results are presented which describe the statistics of the duration and separation of scintillation which results when radio frequency signals propagate through randomly ionized media. This work is applicable to the problems of satellite communication and space based radar observation through disturbed ionospheric channels that result from high altitude chemical release or nuclear detonation. In these environments, a radio frequency signal that traverses the disturbed

DD FORM 1 JAN 73 1473 EDITION OF 1 NOV 65 IS OBSOLETE

UNCLASSIFIED

SECURITY CLASSIFICATION OF THIS PAGE (When Data Entered)

20. ABSTRACT (Continued)

ionosphere a single time has Rayleigh amplitude statistics and power spectral densities that range from f^{-3} in the slow fading limit to Gaussian in the fast fading limit.

The amplitude statistics of the received signal are extended to monostatic and bistatic propagation through the disturbed ionosphere. The bistatic geometry is applicable to either a bistatic radar or to a two-way communication link that utilizes a linear transponder. The statistics of the amplitude used for demodulation in dual channel communication links are presented for systems that use spatial, frequency, or other diversity techniques. The distributions of the received amplitude are used to calculate bit error rates for two-way or dual channel communication links and for various PSK and FSK demodulation techniques. These results are compared with bit error rates in single channel or one-way communication links and with bit error rates in communication links through the ambient ionosphere.

Analytic expressions are obtained for the mean number of level crossings and the mean duration and separation of scintillation above or below arbitrary power levels in the one-way, monostatic, and bistatic propagation geometries. These mean quantities are plotted for a Gaussian power spectral density or, equivalently, for a fast fading environment. The mean duration, separation, and number of level crossings for arbitrary $f^{-\mu}$ power spectral dersities can be obtained from the Gaussian values by scaling factors which are calculated for μ in the range 3 to 10.

The distributions of the number of level crossings and the duration and separation of fast fading scintillation are obtained using Monte Carlo techniques for the one-way, monostatic, and bistatic propagation geometries and for dual channel communication links. The simulation results are presented in tabular form and are compared with analytic results where possible. Histograms of the duration and separation of scintillation for the one-way propagation geometry are also presented. Qualitative comparisons are made of the effects of Rayleigh fading conditions on one-way versus two-way and single channel versus dual channel communication links or monostatic versus bistatic radar systems.

TABLE OF CONTENTS

TABLES OF CONTENTS (continued)

LIST OF ILLUSTRATIONS

LIST OF ILLUSTRATIONS (Continued)

LIST OF ILLUSTRATIONS (Continued)

LIST OF ILLUSTRATIONS (Continued)

LIST OF ILLUSTRATIONS (Continued)

LIST OF TABLES

SECTION 1
INTRODUCTION

The performance of a space based communication or radar system operating in a nuclear environment is degraded by the resulting random amplitude and phase fluctuations of the received radio frequency signal. In general, the random amplitude fluctuations produce an instantaneous signal power that is less than the average power, while occasionally, the instantaneous signal power will be larger than the average power. The first situation is referred to in this report as a fade and the latter as a flare. Because the propagation disturbances are correlated in time, these fades or flares have a finite mean duration and mean separation. More generally, fades below an arbitrary level or flares above that level have varying probability of occurence, mean duration, and mean separation as the level is changed relative to the mean received power. It is the purpose of this report to describe the statistics of the duration and separation of fades and flares for several cases of importance to space based communication and radar systems. This work was performed in response to requests from contractor and SPO personnel involved in the DSP and IONDS programs.

Three propagation geometries are considered and are denoted one-way, monostatic, and bistatic throughout this discussion. The one-way case corresponds to a one-way communication link and the monostatic case corresponds to a monostatic space based radar. The bistatic case corresponds to either a bistatic space based radar or to a two-way communication link. The bistatic case reduces to the one-way case in the event

that only one of the propagation paths is through a Rayleigh fading channel while the other path is through an undisturbed channel. However, it is expected that this situation has a low probability of occurance and it is mentioned here for completeness only. Dual channel communication systems which combine the received signal from two independent one-way communication channels before demodulation are also discussed in this report. In practice the independent channels can be achieved by the use of spatial diversity (e.g., separated receiver antennas or transmitter locations) or other diversity techniques such as multiple transmitter frequencies. Two different algorithms for combining the signals into the amplitude used for demodulation have been considered. The summation algorithm adds the signal amplitudes from the two channels while the maximum algorithm selects the larger of the two amplitudes.

The first and second order statistics of the received signal for the monostatic and bistatic propagation cases are described in the second section assuming Rayleigh amplitude statistics and Gaussian temporal autocorrelation functions or equivalently Gaussian power spectral densities (PSD) for the received one-way voltage. The distribution of the amplitude used for demodulation is also calculated in this section for the two dual channel communication link algorithms and is compared with a single channel or one-way communication link. As an application of the first order statistics results, binary error probabilities are calculated in the third section for two-way and dual channel communication links under slow Rayleigh fading conditions and for various frequency-shift keying and phase-shift keying demodulation techniques.

The mean number of level crossings per unit time for Rayleigh fading with an arbitrary PSD is calculated next in closed form for the three propagation cases. The mean duration and separation of fades and flares is obtained from the mean number of level crossings. These analytic results provide a qualitative comparison of the effects of Rayleigh

fading conditions on one-way versus two-way communication links or monostatic versus bistatic radar systems. The mean number of level crossings and the mean duration and separation of fades and flares are plotted for a Gaussian PSD. These numerical results can be scaled to obtain the mean quantities for an arbitrary $f^{-\mu}$ PSD using scaling factors which are calculated in Appendix A.

The problem of calculating the probability density functions of the duration and separation of fades or flares cannot be solved in closed form for even the simplest propagation geometry. Thus Section 5 briefly outlines the method of generating random sequences of voltages with the desired first and second order statistics. The distributions of the duration and separation of fades and flares for a Gaussian PSD are then obtained in numerical form from the random data. These simulation results are tabulated in Section 6 and are compared with the analytic mean quantities. The one-way results are compared in Appendix C with mean fade duration and separation data from several multiple phase screen (MPS) realizations. Histograms and cumulative distributions of fade and flare separation and duration are presented in Appendix D for the one-way propagation case.

The major conclusions of this study are summarized in the final section. They are:

1) To achieve a demodulator bit error rate of 10^{-3} under slow Rayleigh fading conditions, a two-way communication link* requires about 9 dB more bit energy-to-noise density than does a one-way link while a dual channel communication link requires about 10 dB less bit energy-to-noise density than does a single channel link.

---

* Assuming no satellite processing and a perfect (linear) transponder.

2) The mean duration of fades below the mean power is longest for the monostatic geometry and shortest for the one-way geometry with the bistatic geometry mean fade duration falling between the other two. For fades more than 11 dB below the mean power, the monostatic case also has the shortest mean separation between fades.

3) When compared to fades in single channel communication links which are more than 10 dB below the mean power, the 10 dB fades of dual channel links are, on the average, two thirds as long and spaced three times farther apart.

SECTION 2
FIRST AND SECOND ORDER STATISTICS OF THE RECEIVED SIGNAL

In this section well known empirical descriptions are presented of the first and second order statistics of the one-way received voltage in the strong scattering limit. From these results, the first and second order statistics of the received voltage for the monostatic and bistatic cases are constructed. The distribution of the received power for the three propagation cases are then calculated as are the distributions of the combined power for the two dual channel algorithms.

2.1 STATISTICS OF THE ONE-WAY VOLTAGE

After propagating one-way through an ionized layer, the received voltage can be expressed as two independent quadrature components

$$p(t) = x(t) + iy(t) \tag{2-1}$$

where $p(t)$ is the received complex voltage with in-phase component $x(t)$ and quadrature-phase component $y(t)$. Both MPS calculations[1,2] and theoretical calculations in the strong scattering regime[3] show that transmission of an initially constant amplitude and phase signal one-way through a strongly turbulent layer results in a received signal whose quadrature components $x(t)$ and $y(t)$ are independent Gaussian random variables with joint probability density function

$$f(x,y) = \exp[-(x^2+y^2)/2\sigma^2]/2\pi\sigma^2. \qquad (-\infty < x < \infty, -\infty < y < \infty) \tag{2-2}$$

At two different times, the in-phase components of $p(t_1)$ and $p(t_2)$, denoted x_1 and x_2 respectively, have the joint Gaussian probability density function

$$f(x_1,x_2) = \exp[-(x_1^2-2\rho x_1 x_2+x_2^2)/2\sigma^2(1-\rho^2)]/2\pi\sigma^2\sqrt{1-\rho^2} \quad . \qquad (2\text{-}3)$$

The joint probability density function of the quadrature-phase components y_1 and y_2 is identical to Equation 2-3. The autocorrelation of the complex voltage is then

$$\langle p(t)p^*(t+\tau)\rangle = \langle x(t)x(t+\tau)\rangle + \langle y(t)y(t+\tau)\rangle = 2\sigma^2\rho(\tau). \qquad (2\text{-}4)$$

In the strong scattering limit

$$\rho(\tau) = \exp[-(\tau/\tau_1)^2)] \qquad (2\text{-}5)$$

where τ_1 is the one-way signal decorrelation time. General $f^{-\mu}$ power spectral densities with corresponding Bessel function forms for $\rho(\tau)$ are considered in Appendix A. In subsequent developments, the strong scattering limit Gaussian form of $\rho(\tau)$ will be used as an example with appropriate scaling factors included to render the results valid for any properly behaved PSD. It will be seen later in this section that only in the case of one-way propagation through the ionized medium does the decorrelation time of the received signal, τ_0, equal the one-way decorrelation time τ_1.

The amplitude r of p(t),

$$r = \sqrt{x^2+y^2} \qquad (2\text{-}6)$$

has a Rayleigh probability density function

$$f_R(r) = r\exp(-r^2/2\sigma^2)/\sigma^2, \quad r \geq 0 \qquad (2\text{-}7)$$

and the average power of the signal is

$$\langle p(t)p^*(t)\rangle = \langle r^2\rangle = 2\sigma^2 \quad . \tag{2-8}$$

2.2 GENERAL FIRST ORDER STATISTICS

The received voltage q(t) of a radio frequency signal which traverses an ionized layer either once or twice can be represented as

$$q(t) = \begin{cases} p(t) & \text{one-way} \\ p^2(t) & \text{monostatic} \\ p_1(t)p_2(t) & \text{bistatic} \end{cases} \tag{2-9}$$

when it is assumed that in the radar cases the target cross section is non-fluctuating and that in the two-way communication link case there is no on board satellite processing and the transponder used is perfectly linear. The effect of target cross section fluctuations on the received signal has been discussed in detail elsewhere.[4] In the bistatic case, $p_1(t)$ represents the signal transmitted along path 1 and incident on the transponder or the radar target and $p_2(t)$ represents the signal retransmitted or reflected by the target and received along path 2. The received power S is then given by

$$S = q(t)q^*(t) = \begin{cases} r^2 & \text{one-way} \\ r^4 & \text{monostatic} \\ r_1^2 r_2^2 & \text{bistatic} \end{cases} \tag{2-10}$$

The probability density function of S is easily calculated from the Rayleigh probability density function of r as

$$f(S) = \begin{cases} \exp[-S/\langle S\rangle]/\langle S\rangle & \text{one-way} \\ \exp[-\sqrt{2S/\langle S\rangle}]/\sqrt{2S\langle S\rangle} & \text{monostatic} \\ 2K_0[2\sqrt{S/\langle S\rangle}]/\langle S\rangle & \text{bistatic} \end{cases} \tag{2-11}$$

where K_0 is a modified Bessel function. The mean power is

$$\langle S \rangle = \begin{cases} 2\sigma^2 & \text{one-way} \\ 8\sigma^4 & \text{monostatic} \\ 4\sigma^4 & \text{bistatic} \end{cases} \tag{2-12}$$

where σ^2 is the variance of the underlying Gaussian probability density function of Equation 2-2.

The cumulative distribution function of the received power, defined as

$$F(S) = \text{Prob}\{\text{received power} \leq S\} = \int_0^S f(S')dS' , \tag{2-13}$$

gives an indication of the probability of occurrence of deep fades which are detrimental to the performance of communication or radar systems. This function is readily calculated for the three cases considered with the results

$$F(S) = \begin{cases} 1 - \exp[-S/\langle S \rangle] & \text{one-way} \\ 1 - \exp[-\sqrt{2S/\langle S \rangle}] & \text{monostatic} \\ 1 - 2\sqrt{S/\langle S \rangle}\, K_1[2\sqrt{S/\langle S \rangle}] & \text{bistatic} \end{cases} \tag{2-14}$$

where K_1 is a modified Bessel function.

The median power M, defined by

$$F(M) = 1/2, \tag{2-15}$$

is equal to

$$M/\langle S \rangle = \begin{cases} \ell n(2) = -1.6\text{dB} & \text{one-way} \\ [\ell n(2)]^2/2 = -6.2\text{dB} & \text{monostatic} \\ u_0/4 = -4.0\text{dB} & \text{bistatic} \end{cases} \tag{2-16}$$

where u_0 for the bistatic case is given by solving the equation

$$u_0 K_1(u_0) = 1/2 \tag{2-17}$$

which gives

$$u_0 = 1.25715 \ . \tag{2-18}$$

Thus for the one-way propagation geometry, one half of the time the received power is 1.6 dB or more below the mean power while for a monostatic radar the received power is 6.2 dB or more below the mean power one-half of the time.

The cumulative distributions are plotted on probability paper in Figure 1 for the three cases. It is apparent that the monostatic case has

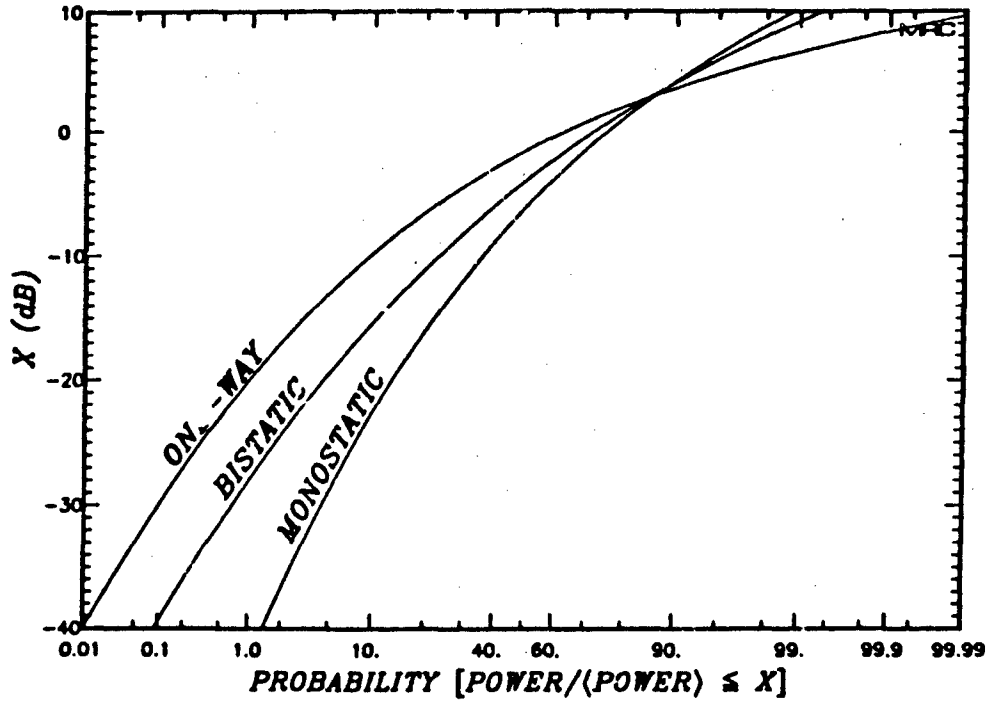

Figure 1. Cumulative distribution of the received power.

the highest probability of deep fades, the one-way case has the lowest probability, and the bistatic case falls between the other two. For example, the one-way case has a probability of 10^{-4} of fades of 40 dB or greater while this probability is about 8×10^{-4} for the bistatic case and is about 1.5×10^{-2} for the monostatic case.

2.3 GENERAL SECOND ORDER STATISTICS

The frequency of occurrence, the duration and the separation of fades or flares is determined by both the first order or amplitude statistics described above and by the second order or correlation properties of the received voltage defined in Equation 2-4. The correlation function for the monostatic case is

$$\begin{aligned} \langle q(t)q^*(t+\tau)\rangle &= \langle p^2(t)p^{2*}(t+\tau)\rangle \\ &= \langle x_1^2 x_2^2 + y_1^2 y_2^2 + 4x_1 x_2 y_1 y_2 - x_1^2 y_2^2 - x_2^2 y_1^2\rangle \qquad (2\text{-}19) \\ &+ 2i\langle x_1 x_2^2 y_1 - x_1 y_1 y_2^2 - x_1^2 x_2 y_2 + x_2 y_1^2 y_2\rangle \ . \end{aligned}$$

Noting that x and y are independent, zero mean random variables, the imaginary part of $\langle q(t)q^*(t+\tau)\rangle$ is identically zero. In addition, it is easy to demonstrate the following using Equation 2-3:

$$\begin{aligned} \langle x_1^2 x_2^2\rangle &= \langle y_1^2 y_2^2\rangle = \sigma^4(1+2\rho^2) \\ \langle x_1 x_2 y_1 y_2\rangle &= \langle x_1 x_2\rangle\langle y_1 y_2\rangle = (\sigma^2\rho)^2 \qquad (2\text{-}20) \\ \langle x_1^2 y_2^2\rangle &= \langle x_2^2 y_1^2\rangle = \langle x^2\rangle\langle y^2\rangle = \sigma^4 \ . \end{aligned}$$

so that for the monostatic case,

$$\langle q(t)q^*(t+\tau)\rangle = \langle S\rangle\rho^2(\tau) \ . \qquad (2\text{-}21)$$

The correlation function for the bistatic case is

$$\langle q(t)q^*(t+\tau)\rangle = \langle p_1(t)p_2(t)p_1^*(t+\tau)p_2^*(t+\tau)\rangle$$

$$= \langle p_1(t)p_1^*(t+\tau)\rangle\langle p_2(t)p_2^*(t+\tau)\rangle \qquad (2\text{-}22)$$

when it is assumed that $p_1(t)$ and $p_2(t)$ are independent. In this case,

$$\langle q(t)q^*(t+\tau)\rangle = \langle S\rangle \rho_1(\tau)\rho_2(\tau) \qquad (2\text{-}23)$$

In general for a Gaussian PSD,

$$\langle q(t)q^*(t+\tau)\rangle = \langle S\rangle \exp[-(\tau/\tau_0)^2] \qquad (2\text{-}24)$$

where τ_0 is the decorrelation time of the received voltage and

$$\tau_0 = \begin{cases} \tau_1 & \text{one-way} \\ \tau_1/\sqrt{2} & \text{monostatic} \\ \sqrt{\dfrac{\tau_{1,1}^2\,\tau_{1,2}^2}{\tau_{1,1}^2+\tau_{1,1}^2}} & \text{bistatic } (\tau_{1,1}\neq\tau_{1,2}) \\ \tau_{1,1}/\sqrt{2} & \text{bistatic } (\tau_{1,1}=\tau_{1,2}) \end{cases} \qquad (2\text{-}25)$$

For bistatic propagation, $\tau_{1,i}$, $i = 1$ or 2, is the one-way decorrelation time of the i^{th} path. It can be seen for the bistatic case, that if one of the paths has a small decorrelation time relative to the other one-way path, the resulting decorrelation time of the received signal corresponds to the smaller decorrelation time. If both one way paths have the same decorrelation time, the resulting τ_0 corresponds to the monostatic case with a decorrelation time of $\tau_1/\sqrt{2}$. In both two-way cases, it is apparent that the decorrelation time of the received signal is smaller

than the decorrelation time of the one-way propagation path. For arbitrary power spectral densities and propagation geometries, the decorrelation time of the received voltage is related to the one-way decorrelation time as

$$\tau_o = \begin{cases} \tau_1 & \text{one way} \\ \delta\tau_1/\sqrt{2} & \text{monostatic} \\ \delta\tau_{1,1}\tau_{1,2}/\sqrt{\tau_{1,1}^2 + \tau_{1,2}^2} & \text{bistatic} \end{cases} \tag{2-26}$$

The scale factor δ differs from unity in general if the PSD is not Gaussian.

2.4 FIRST ORDER STATISTICS FOR DUAL CHANNEL COMMUNICATION SYSTEMS

Dual channel communication systems may combine the amplitudes of two independent channels in order to mitigate the effects of propagation fading. Two possible algorithms for combining the amplitudes of the two channels into the amplitude z used for demodulation are

$$z = \begin{cases} r_1 + r_2 & \text{summation algorithm} \\ \max(r_1, r_2) & \text{maximum algorithm} \end{cases} \tag{2-27}$$

where r_i, i=1 or 2, is the amplitude of the received voltage on the i th channel and the function max(x,y) is equal to the large of x and y. If it is assumed that the two channels utilize propagation paths of sufficient spatial separation that the propagation effects on the received voltages are independent. Then in the strong scattering limit, r_1 and r_2 are independent, Rayleigh distributed random variables. It will also be assumed that the transmitted power is equal in the two channels so that $\langle r_1^2 \rangle = \langle r_2^2 \rangle$.

For the summation algorithm, the cumulative distribution of z has been given by Marcum[5] from which the cumulative distribution of the combined power ($S = z^2$) is obtained as

$$F(S) = 1-\exp[-S/2\sigma^2] - \sqrt{\pi S/4\sigma^2}\; e^{-S/4\sigma^2}\; \mathrm{erf}(\sqrt{S/4\sigma^2}) \qquad (2\text{-}28)$$

where $2\sigma^2$ is the mean power in each of the channels and erf is the error function. The mean power of the combined amplitude is

$$\langle S\rangle = \langle z^2\rangle = \langle r_1^2\rangle + 2\langle r_1\rangle\langle r_2\rangle + \langle r_2^2\rangle = (4+\pi)\sigma^2 \; . \qquad (2\text{-}29)$$

The cumulative distribution of z for the maximum algorithm is

$$F(z) = [1 - \exp(-z^2/2\sigma^2)]^2 \qquad (2\text{-}30)$$

where the term inside the brackets is the probability that one of the Rayleigh distributed amplitudes is less than or equal to z and the square gives the probability that both r_1 and r_2 are less than or equal to z. The mean received power is then easily calculated as

$$\langle S\rangle = \langle z^2\rangle = \int_0^\infty z^2\, dF(z) = 3\sigma^2 \qquad (2\text{-}31)$$

and the cumulative distribution of the combined power is

$$F(S) = \{1 - \exp[-3S/2\langle S\rangle]\}^2 \; . \qquad (2\text{-}32)$$

The probability density function of the combined power is obtained by differentiating Equation 2-32 giving

$$f(S) = (3/\langle S\rangle) \exp(-3S/2\langle S\rangle) \left[1 - \exp(-3S/2\langle S\rangle\right] \qquad (2\text{-}33)$$

The median combined power for the dual channel communication systems is

$$M/\langle S\rangle = \begin{cases} 4u_o/(4+\pi) & = -0.81\text{dB} \quad \text{summation algorithm} \\ 2\ \ell n[\sqrt{2}/(\sqrt{2}-1)] & = -0.87\text{dB} \quad \text{maximum algorithm} \end{cases} \qquad (2\text{-}34)$$

where u_o is the solution of the equation

$$e^{-2u_o} + \sqrt{\pi u_o}\, e^{-u_o}\, \text{erf}(\sqrt{u_o}) = 1/2 \qquad (2\text{-}35)$$

which yields

$$u_o = 1.482227\ . \qquad (2\text{-}36)$$

When compared with the single channel median power of 1.6 dB below the mean power, these results indicate that the dual channel system does in fact mitigate the effects of scintillation.

The cumulative distributions for the combined power are plotted on probability paper in Figure 2 for the two dual channel algorithms along with the cumulative distribution of the received power of the one-way communication link or single channel case. The near coincidence of the dual channel curves is a consequence of the fact that because the amplitudes from the two channels are independent and Rayleigh distributed, it is probable that one amplitude is much smaller than the other and hence that the larger amplitude is nearly equal to the sum of the two amplitudes. It is apparent from the figure that the dual channel system has a lower probability of deep fades than does the single channel system. For

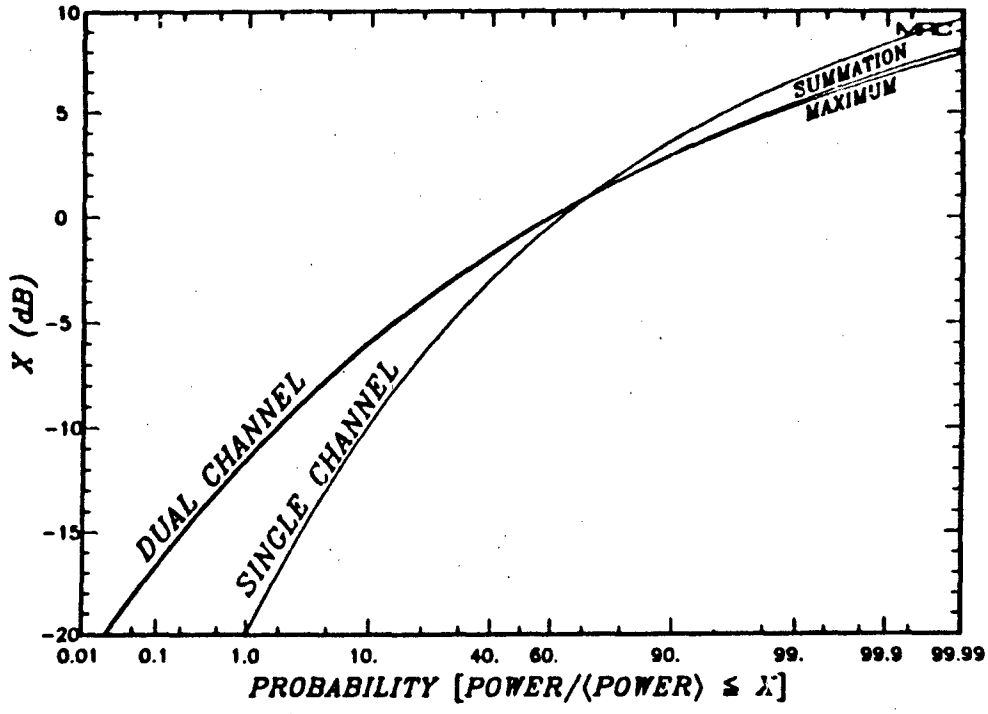

Figure 2. Cumulative distribution of the signal power used for demodulation in single and dual channel communication links.

example, the dual channel system has a probability of about 3×10^{-4} of fades of 20dB or greater while this probability is 10^{-2} for the single channel system.

2.5 AMPLITUDE MOMENTS

The expected values of the first 4 moments of the received amplitude z, where

$$z = |q(t)| \ , \qquad (2\text{-}36)$$

for one-way, monostatic, and bistatic cases, and for the combined amplitude defined in Equation 2-26 for the dual channel communications systems are needed for comparison with the simulation results. These are given in Table I and can be calculated directly from the moments of a Rayleigh distribution for all but dual channel maximum algorithm. In the latter case, Equation 2-29 is used to calculate the moments of z.

Table I. Moments of the amplitude of the received voltage.

Case	$E[z^n]$*			
	n = 1	n = 2	n = 3	n = 4
One-Way	$\sqrt{\pi/2}\,\sigma$	$2\sigma^2$	$3\sqrt{\pi/2}\,\sigma^3$	$8\sigma^4$
Monostatic	$2\sigma^2$	$8\sigma^4$	$48\sigma^6$	$192\sigma^8$
Bistatic	$\pi\sigma^2/2$	$4\sigma^4$	$9\pi\sigma^6/2$	$64\sigma^8$
Dual Channel				
Summation Algorithm	$\sqrt{2\pi}\,\sigma$	$(4+\pi)\sigma^2$	$9\sqrt{2\pi}\,\sigma^3$	$4(10+3\pi)\sigma^4$
Maximum Algorithm	$(\sqrt{2\pi} - \sqrt{\pi/4})\,\sigma$	$3\sigma^2$	$3(\sqrt{2\pi} - \sqrt{\pi/16})\,\sigma^3$	$14\sigma^4$

* σ^2 is the variance of the underlying normal distributions.

SECTION 3
BINARY ERROR PROBABILITIES FOR TWO-WAY AND DUAL CHANNEL COMMUNICATION LINKS UNDER SLOW RAYLEIGH FADING CONDITIONS

Binary error probabilities of two-way and dual channel communication links are derived in this section for noncoherent M-ary frequency shift keying (M-ary FSK), coherent phase-shift keying (PSK), differentially encoded coherent PSK (DPSK), and differentially coherent binary PSK (DBPSK) under slow Rayleigh fading conditions. Perfect phase tracking will be assumed for the PSK demodulation techniques. In the two-way geometry, a signal is transmitted through an ionospheric channel to a transponder which then retransmits the signal through an independent ionospheric channel to a receiver which is not colocated with the original transmitter. It is assumed that the transponder is an ideal linear amplifier that is noiseless and that outputs a signal with identical statistics to the input signal. For a dual channel communication link, independent signals are obtained by the use of spatial diversity (e.g., separated receiver antennas or transmitter locations) or by other diversity techniques such as multiple transmission frequencies. The results of the previous section showed that the distributions of the combined signals for the two algorithms considered are essentially identical. Therefore, the binary error probabilities will be calculated only for the maximum algorithm which has the simpler mathematical form for the distribution of combined power.

The probability of bit error in an additive white Gaussian noise (AWGN) channel for a constant energy signal and for M-ary FSK modulation is[6]

$$P_{be}(E_b/N_o) = \frac{1}{2(M-1)} \sum_{k=2}^{M} (-1)^k \binom{M}{k} \exp\left[-\left(\frac{k-1}{k}\right)(\log_2 M)\frac{E_b}{N_o}\right] \qquad (3\text{-}1)$$

and is

$$P_{be}(E_b/N_o) = \begin{cases} (1/2)\ \mathrm{erfc}(\sqrt{E_b/N_o}) & \text{ideal coherent PSK} \\ \mathrm{erfc}(\sqrt{E_b/N_o})\ [1 - (1/2)\ \mathrm{erfc}(\sqrt{E_b/N_o})] & \text{ideal } \Delta\text{PSK} \\ (1/2)\ \exp(-E_b/N_o) & \text{DBPSK} \end{cases} \quad (3\text{-}2)$$

for PSK modulation where P_{be} represents the binary error rate at the demodulation output and E_b/N_o is the input modulation bit energy-to-noise density ratio. Under slow Rayleigh fading conditions, the probability of bit error must be averaged over the probability density function of the bit energy which for two-way links is given by the bistatic form of Equation 2-14 and for dual channel links is given by Equation 2-33 as

$$f(E_b) = \begin{cases} 2K_o[2\sqrt{E_b/\langle E_b\rangle}]/\langle E_b\rangle & \text{Two-way} \\ (3/\langle E_b\rangle)\ \exp(-3E_b/2\langle E_b\rangle)\ [1 - \exp(-3E_b/2\langle E_b\rangle] & \text{Dual Channel} \end{cases} \quad (3\text{-}3)$$

where $\langle E_b\rangle$ is the mean bit energy. The average probability of bit error is then

$$\langle P_{be}\rangle = \int_0^\infty P_{be}(E_b/N_o)\ f(E_b)\ dE_b\ . \quad (3\text{-}4)$$

For two-way slow Rayleigh fading, evaluation of Equation 3-4 for M-ary FSK and for DBPSK involves an integral of the form

$$I = \frac{2}{\langle E_b\rangle} \int_0^\infty \exp(-\alpha E_b/N_o)\ K_o[2\sqrt{E_b/\langle E_b\rangle}]\ dE_b \quad (3\text{-}5)$$

where

$$\alpha = \begin{cases} \left(\frac{k-1}{k}\right)\ (\log_2 M) & \text{M-ary FSK} \\ 1 & \text{DBPSK} \end{cases}$$

Upon changing variables ($u = 2\sqrt{E_b/\langle E_b\rangle}$), the integral reduces to

$$I = \int_0^\infty u \exp[-\alpha\langle E_b/N_o\rangle u^2/4]\, K_o(u)\, du \ . \tag{3-6}$$

This integral is given by Gradshteyn and Ryzhik[7] in terms of one of Whittaker's function which can be further reduced using the mathematical properties of confluent hypergeometric functions from Abramowitz and Stegun[8] to give

$$I = \frac{\exp[1/\alpha\langle E_b/N_o\rangle]\ E_1[1/\alpha\langle E_b/N_o\rangle]}{\alpha\langle E_b/N_o\rangle} \tag{3-7}$$

where E_1 is the exponential integral.

The average probability of bit error is then

$$\langle P_{be}\rangle = \frac{1}{2(M-1)(\log_2 M)\langle E_b/N_o\rangle} \sum_{k=2}^{M} (-1)^k \binom{M}{k} \frac{k}{k-1} \times \exp\left[\frac{k/(k-1)}{(\log_2 M)\ \langle E_b/N_o\rangle}\right] E_1\left[\frac{k/(k-1)}{(\log_2 M)\ \langle E_b/N_o\rangle}\right] \tag{3-8}$$

for M-ary FSK demodulation and is

$$\langle P_{be}\rangle = \frac{\exp[1/\langle E_b/N_o\rangle]\ E_1[1/\langle E_b/N_o\rangle]}{2\ \langle E_b/N_o\rangle} \tag{3-9}$$

for DBDSK demodulation. The mean probability of bit error cannot to the authors knowledge be obtained in closed form for ideal coherent PSK or ΔPSK modulation. However, by using the same change of variables that was

used to derive Equation 3-6, the mean probability of bit error for these cases can be rewritten as

$$\langle P_{be} \rangle = \begin{cases} (1/2) \int_0^\infty u\, K_0(u)\, \mathrm{erfc}[\sqrt{E_b/N_o}\, u/2]\, du & \text{ideal PSK} \\ \int_0^\infty u\, K_0(u)\, \mathrm{erfc}[\sqrt{\langle E_b/N_o \rangle}\, u/2]\, \{1 - (1/2)\, \mathrm{erfc}[\sqrt{\langle E_b/N_o \rangle}\, u/2]\}\, du & \text{ideal } \Delta\text{PSK} \end{cases} \tag{3-10}$$

Both integrals of Equation 3-10 have well behaved integrands and are easily evaluated numerically.

For dual channel links under slow Rayleigh fading conditions, the average bit error probability with M-ary FSK demodulation can be evaluated directly to give

$$\langle P_{be} \rangle = \frac{1}{2(M-1)} \sum_{k=2}^{M-1} (-1)^k \binom{M}{k} \times \frac{9}{[3+(k-1)(\log_2 M)\langle E_b/N_o \rangle/k]\,[3+2(k-1)(\log_2 M)\langle E_b/N_o \rangle/k]} \tag{3-11}$$

Similarly, with DBPSK demodulation,

$$\langle P_{be} \rangle = \frac{9/2}{(3+\langle E_b/N_o \rangle)(3+2\langle E_b/N_o \rangle)} \quad . \tag{3-12}$$

The evaluation of Equation 3-4 for ideal PSK and ideal ΔPSK involves integrals of the form

$$I = \int_0^\infty \mathrm{erfc}(\sqrt{x})\, e^{-\alpha x}\, dx = (2/\alpha)\, (1 - 1/\sqrt{1+\alpha}) \tag{3-13}$$

and

$$I = \int_0^\infty \operatorname{erfc}^2(\sqrt{x})\ e^{-\alpha x}\ dx \qquad (3\text{-}14)$$

$$= \frac{1}{\alpha}\left[1 - \frac{4}{\pi}\ \frac{\tan^{-1}\sqrt{1+\alpha}}{\sqrt{1+\alpha}}\right]$$

where the first integral is given by Gradshteyn and Ryzhik and the second integral can be integrated by parts to reduce it to a form given by Gradshteyn and Ryzhik. The mean probability of bit error for ideal PSK then becomes

$$\langle P_{be}\rangle = \frac{1}{2} + \frac{1/2}{\sqrt{1+3/\langle E_b/N_o\rangle}} - \frac{1}{\sqrt{1+3/(2\langle E_b/N_o\rangle)}}$$

and for ideal ΔPSK it becomes

$$\langle P_{be}\rangle = \frac{1}{2} + \frac{[1-(2/\pi)\ \tan^{-1}\sqrt{1+3/\langle E_b/N_o\rangle}]}{\sqrt{1+3/\langle E_b/N_o\rangle}} \qquad (3\text{-}16)$$

$$- \frac{2[1-(2/\pi)\ \tan^{-1}\sqrt{1+3/2\langle E_b/N_o\rangle}]}{\sqrt{1+3/2\langle E_b/N_o\rangle}}\ .$$

The probabilities of bit error for one-way or single channel communication links, for two-way links, and for dual channel links under slow Rayleigh fading conditions are shown in Figures 3 through 8 for non-coherent M-ary FSK with M equal to 2, 4, and 6, ideal coherent PSK, ΔPSK, and DBPSK demodulation respectively. The probability of bit error for an AWGN channel is also shown for each of the techniques. Note that an ideal coherent PSK dual channel system is not achievable in practice because of

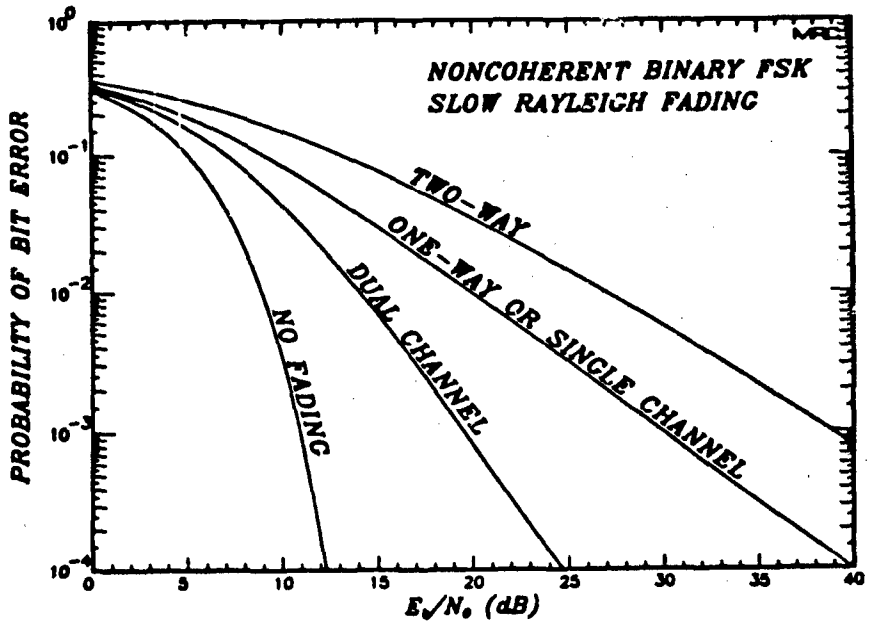

Figure 3. Theoretical performance of noncoherent binary FSK demodulation in an AWGN channel and under slow Rayleigh fading conditions.

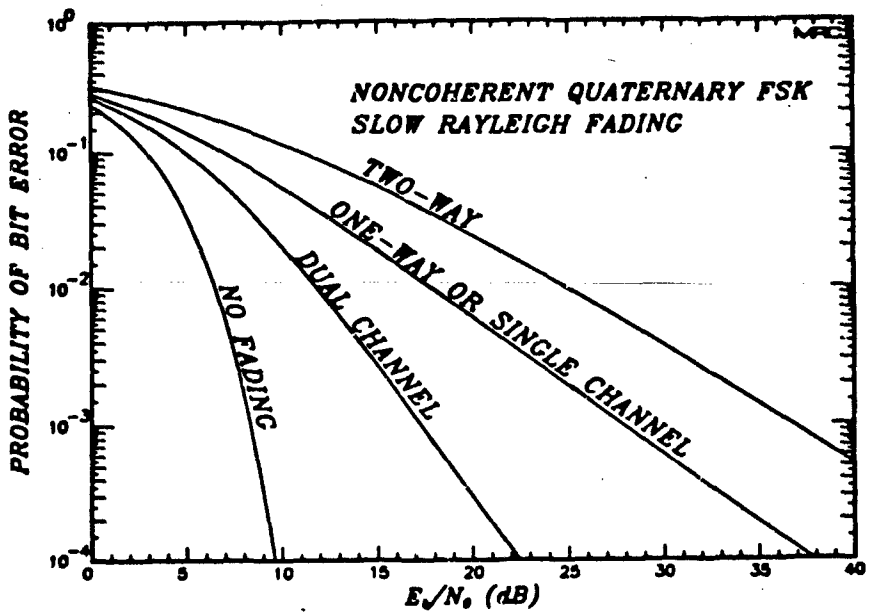

Figure 4. Theoretical performance of noncoherent quaternary FSK demodulation in an AWGN channel and under slow Rayleigh fading conditions.

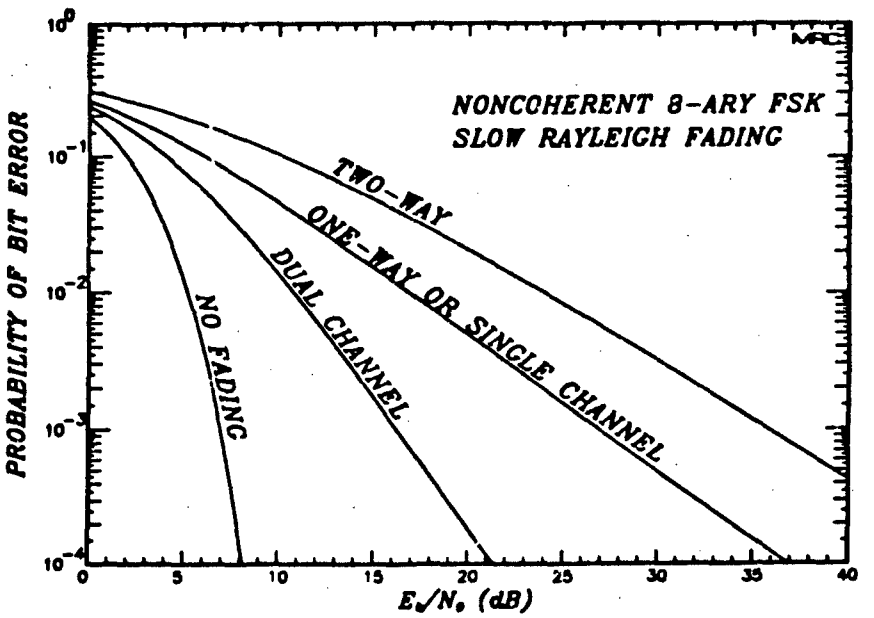

Figure 5. Theoretical performance of noncoherent 8-ary FSK demodulation in an AWGN channel and under slow Rayleigh fading conditions.

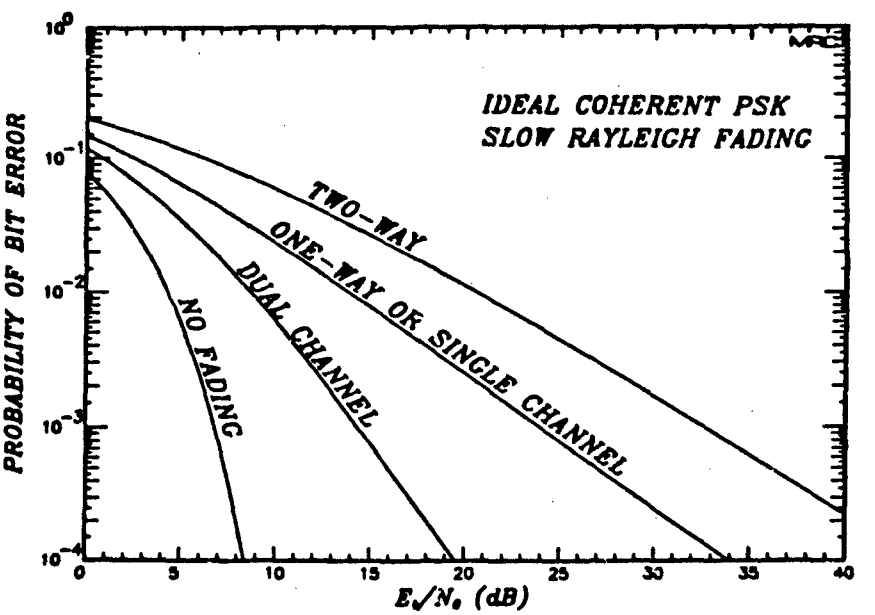

Figure 6. Theoretical performance of ideal coherent PSK demodulation in an AWGN channel and under slow Rayleigh fading conditions.

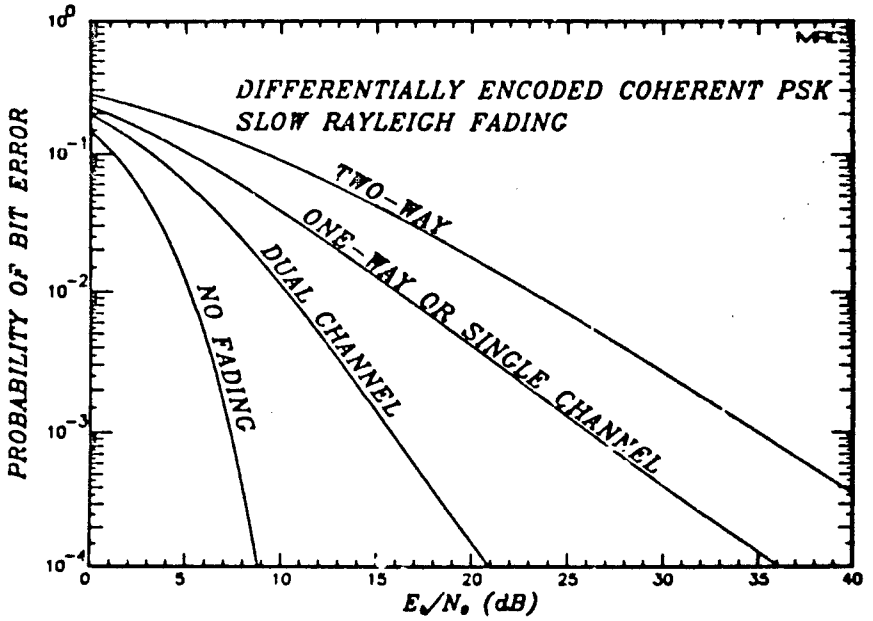

Figure 7. Theoretical performance of ideal coherent ΔPSK demodulation in an AWGN channel and under slow Rayleigh fading conditions.

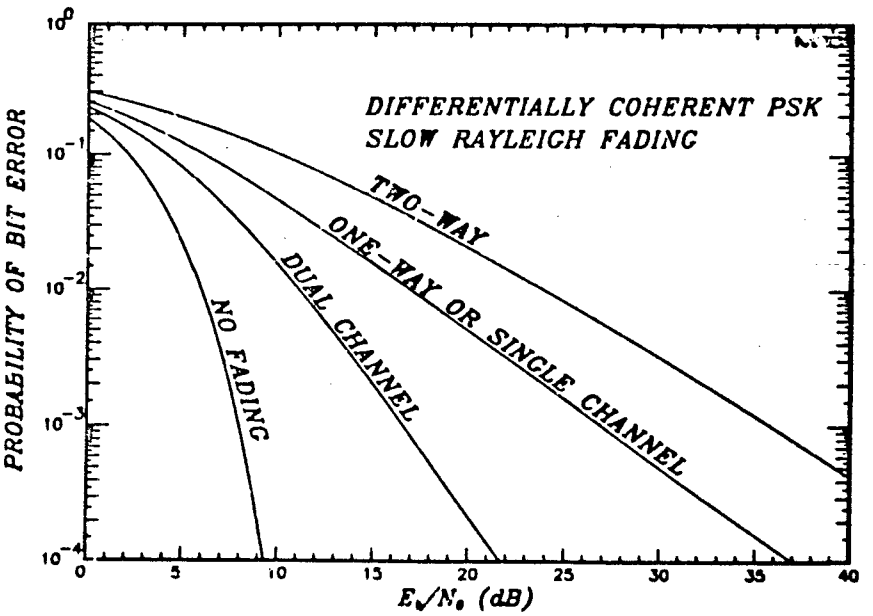

Figure 8. Theoretical performance of differentially coherent binary PSK demodulation in an AWGN channel and under slow Rayleigh fading conditions.

the π phase ambiguity. As can be seen from the figures, the mean probability of bit error for a given bit energy-to-noise density ratio is higher for a two-way link than it is for a one-way link because of the increased probability of occurrence of deep fades in the two-way geometry. However, the mean probability of bit error for a given bit energy-to-noise density ratio is lower for a dual channel link than it is for a single channel link because of the decreased probability of occurrence of deep fades in the dual channel link. At a bit error probability of 10^{-3}, the two-way link requires between 8.5 dB and 9.5 dB more bit energy-to-noise density than does the one-way link for all demodulation techniques considered. Conversely, the dual channel link requires between 9.5 dB and 11 dB less bit energy-to-noise density than does the single channel link to achieve a 10^{-3} bit error probability.

SECTION 4
LEVEL CROSSING PROBLEM

The main point of this study is a statistical characterization of the zero crossings of a random process z'(t) defined as

$$z'(t) = z(t) - \ell \tag{4-1}$$

where ℓ is an arbitrary amplitude level. This problem was first treated in detail by Rice[9] for the case that z(t) is a normally distributed random variable. The purpose of this section is to extend the results of Rice to the cases where z(t) is the amplitude of q(t) defined in Equation 2-9. For one-way, monostatic, or bistatic cases, an interesting statistic of the zero crossing problem that can be calculated in closed form is the mean number $\langle N(\ell,T)\rangle$ of crossings of the level ℓ in the time interval T. From the mean number of level crossings, the mean duration and separation of fades and flares can also be calculated in closed form.

It can be shown that[9]

$$\langle N(\ell,T)\rangle = \int_{t'}^{t'+T} dt \int_{-\infty}^{\infty} d\dot{z}\ |\dot{z}|\ f(\ell,\dot{z};t) \tag{4-2}$$

where $f(z,\dot{z};t)$ is the joint probability density function of z and its time derivative $\dot{z}$ at time t. For the stationary processes considered here, $f(z,\dot{z};t)$ is independent of t and

$$\langle N(\ell,T)\rangle = T \int_{-\infty}^{\infty} |\dot{z}| f(\ell,\dot{z}) d\dot{z} \quad . \tag{4-3}$$

4.1 ONE-WAY PROPAGATION

The first step in evaluating Equation 4-3 is to calculate the joint probability density function of the components of the one-way received voltage and their time derivatives. The joint probability density function of the in-phase and the quadrature phase components of the received one-way voltage, denoted by x and y respectively, is given by Equation 2-2. Rice has shown that if x and y are normally distributed and stationary with zero means, then $\dot{x}$ and $\dot{y}$ are normally distributed and stationary with zero means and variances given by

$$\sigma^2_{\dot{x}} = \sigma^2_{\dot{y}} = -\sigma^2\ddot{\rho}(0) = 2\sigma^2\Delta^2/\tau_1^2 \qquad (4\text{-}4)$$

where $\rho(\tau)$ is the second time derivative of the autocorrelation function of the one way voltage. In addition, $\dot{x}$ and $\dot{y}$ are independent of both x and y. For arbitrary power spectral densities, it is then required that $\rho(0)$ be finite. The implications of this requirement are discussed in more detail in Appendix A. The scaling factor Δ^2 is unity for a Gaussian PSD and is calculated for a $f^{-\mu}$ PSD in the Appendix. Thus the joint probability density function of x, $\dot{x}$, y, and $\dot{y}$ is

$$f(x,\dot{x},y,\dot{y}) = \frac{\exp\{-[x^2+y^2+\tau_1^2(\dot{x}^2+\dot{y}^2)/2\Delta^2]/2\sigma^2\}}{(2\pi\sigma^2)^2\,(2\Delta^2/\tau_1^2)} \quad . \qquad (4\text{-}5)$$

The joint probability density function of the amplitude r of the one-way received voltage and of $\dot{r}$ can now be obtained from Equation 4-5 by changing variables. Letting

$$x = r\cos\theta \qquad (4\text{-}6)$$

$$y = r\sin\theta$$

where θ is the phase of the received voltage, the time derivatives of x and y become

$$\begin{aligned} \dot{x} &= \dot{r}\cos\theta - r\dot{\theta}\sin\theta \\ \dot{y} &= \dot{r}\sin\theta + r\dot{\theta}\cos\theta \end{aligned} \tag{4-7}$$

so that

$$x^2 + y^2 = r^2$$

$$\dot{x}^2 + \dot{y}^2 = \dot{r}^2 + r^2\dot{\theta}^2 \quad . \tag{4-8}$$

Equation 4-5 can be then be rewritten in terms of r, $\dot{r}$, θ, and $\dot{\theta}$ as

$$f(x,\dot{x},y,\dot{y})\, dx d\dot{x} dy d\dot{y} = f(r,\dot{r},\theta,\dot{\theta})\, \left|\det(J)\right| dr d\dot{r} d\theta d\dot{\theta} \tag{4-9}$$

where the determinant of the Jacobian J of the coordinate transformation is

$$\det(J) = \det \begin{bmatrix} \partial x/\partial r & \partial \dot{x}/\partial r & \partial y/\partial r & \partial \dot{y}/\partial r \\ \partial x/\partial \dot{r} & \partial \dot{x}/\partial \dot{r} & \partial y/\partial \dot{r} & \partial \dot{y}/\partial \dot{r} \\ \partial x/\partial \theta & \partial \dot{x}/\partial \theta & \partial y/\partial \theta & \partial \dot{y}/\partial \theta \\ \partial x/\partial \dot{\theta} & \partial \dot{x}/\partial \dot{\theta} & \partial y/\partial \dot{\theta} & \partial \dot{y}/\partial \dot{\theta} \end{bmatrix} \tag{4-10}$$

$$= \det \begin{bmatrix} \cos\theta & -\dot{\theta}\sin\theta & \sin\theta & \dot{\theta}\cos\theta \\ 0 & \cos\theta & 0 & \sin\theta \\ -r\sin\theta & -\dot{r}\sin\theta - r\dot{\theta}\cos\theta & r\cos\theta & \dot{r}\cos\theta - r\dot{\theta}\sin\theta \\ 0 & -r\sin\theta & 0 & r\cos\theta \end{bmatrix}$$

$$= r^2 \quad .$$

The joint probability density function of r and $\dot{r}$ is given by integrating Equation 4-9 over θ and $\dot{\theta}$:

$$f(r,\dot{r})dr d\dot{r} = \int_0^{2\pi} d\theta \int_{-\infty}^{\infty} d\dot{\theta}\, f(r,\dot{r},\theta,\dot{\theta})\, dr d\dot{r} \qquad (4\text{-}11)$$

$$= \frac{r^2 \exp\left[-\left(r^2+\tau_1^2\,\dot{r}^2/2\Delta^2\right)/2\sigma^2\right] dr d\dot{r}}{(2\pi\sigma^2)^2\,(2\Delta^2/\tau_1^2)}$$

$$\times \int_0^{2\pi} d\theta \int_{-\infty}^{\infty} d\dot{\theta}\, \exp(-\tau_1^2 r^2 \dot{\theta}^2/4\Delta^2\sigma^2)$$

$$= \frac{r\,\exp(-r^2/2\sigma^2)}{\sigma^2}\, dr \cdot \frac{\exp(-\tau_1^2\dot{r}^2/4\Delta^2\sigma^2)}{\sqrt{4\pi\Delta^2\sigma^2/\tau_1^2}}\, d\dot{r} \quad .$$

It can be seen from Equation 4-11 that the probability density function of r is Rayleigh; the probability density function of $\dot{r}$ is Gaussian with zero mean and $2\Delta^2\sigma^2/\tau_1$ standard deviation; and because $f(\dot{r},r)$ is separable into a function of r times a function of $\dot{r}$, r and $\dot{r}$ are independent.

The mean number of crossing in the time interval T for the one-way case can now be easily evaluated from Equations 4-3 and 4-11. Using Equation 2-12 to write σ in terms of the mean received power, the mean number of crossing becomes

$$\langle N(L,T)\rangle = \Delta(T/\tau_0)\,\sqrt{8L/\pi\langle S\rangle}\; e^{-L/\langle S\rangle} \qquad (4\text{-}12)$$

where $L = \ell^2$ is the power of the level ℓ and where τ_0 is equal to τ_1 in this case. The effect of arbitrary power spectral densities is then to scale the mean number of level crossings in the one-way propagation by the quantity Δ. Noting that two crossings are required for a fade (flare) below (above) the level ℓ, the expected number of fades (flares) per unit time is $\langle N(L,T)\rangle/2T$.

4.2 MONOSTATIC PROPAGATION

For the monostatic case, the amplitude z of the received voltage is equal to r^2 so that x and y as functions of z and the phase θ are

$$\begin{aligned} x &= z^{1/2} \cos\theta \\ y &= z^{1/2} \sin\theta \quad . \end{aligned} \tag{4-13}$$

Using this transformation, the calculation of $f(z,\dot{z})$ is then identical to the one-way case. In this case, the time derivatives or x and y become

$$\begin{aligned} \dot{x} &= z^{-1/2}\, \dot{z}\, \cos\theta/2 - z^{1/2}\, \dot{\theta}\, \sin\theta \\ \dot{y} &= z^{-1/2}\, \dot{z}\, \sin\theta/2 + z^{1/2}\, \dot{\theta}\, \cos\theta \end{aligned} \tag{4-14}$$

so that

$$\begin{aligned} x^2+y^2 &= z \\ \dot{x}^2+\dot{y}^2 &= \dot{z}^2/4z + z\dot{\theta}^2 \quad . \end{aligned} \tag{4-15}$$

Again the change of variables requires the evaluation of the determinant of the Jacobian, defined in Equation 4-10 by replacing r with z, which gives

$$\det(J) = \det \begin{bmatrix} z^{-1/2}\cos\theta/2 & -z^{-3/2}\,\dot{z}\cos\theta/4 - z^{-1/2}\,\dot{\theta}\sin\theta/2 & z^{-1/2}\sin\theta/2 & z^{-3/2}\,\dot{z}\sin\theta/4 + z^{-1/2}\,\dot{\theta}\cos\theta/2 \\ 0 & z^{-1/2}\cos\theta/2 & 0 & z^{-1/2}\sin\theta/2 \\ -z^{1/2}\sin\theta & z^{-1/2}\,\dot{z}\sin\theta/2 - z^{1/2}\,\dot{\theta}\cos\theta & z^{1/2}\cos\theta & z^{-1/2}\,\dot{z}\cos\theta/2 - z^{1/2}\,\dot{\theta}\sin\theta \\ 0 & -z^{1/2}\sin\theta & 0 & z^{1/2}\cos\theta \end{bmatrix}$$

$$= 1/4 \tag{4-16}$$

The joint probability density function of z and $\dot{z}$ can now be written as

$$f(z,\dot{z})dzd\dot{z} = (1/4)\int_0^{2\pi} d\theta \int_{-\infty}^{\infty} d\dot{\theta}\; f(z,\dot{z},\theta,\dot{\theta})dzd\dot{z} \tag{4-17}$$

$$= \frac{\exp[-(z+\tau_1^2\,\dot{z}^2/8\Delta^2 z)/2\sigma^2]}{4(2\pi\sigma^2)^2(2\Delta^2/\tau_1^2)} \int_0^{2\pi} d\theta \int_{-\infty}^{\infty} d\dot{\theta}\; \exp(-\tau_1^2 z\dot{\theta}^2/4\Delta^2\sigma^2)dzd\dot{z}$$

$$= (\tau_1/8\Delta\sigma^3\sqrt{\pi z})\;\exp[-(z+\tau_1^2\dot{z}^2/8\Delta^2 z)/2\sigma^2]dzd\dot{z}\quad .$$

Because Equation (4-17) is not separable into a function of z times a function of $\dot{z}$, z and $\dot{z}$ are statistically dependent.

The mean number of crossings for the monostatic case of the level L per time interval T is easily evaluated from Equations 4-3 and 4-17 as

$$\langle N(L,T)\rangle = \delta\Delta(T/\tau_0)\,[32L/\pi^2\langle S\rangle]^{1/4}\;\exp[-\sqrt{2L/\langle S\rangle}] \tag{4-18}$$

where τ_0 is equal to $\delta\tau_1/\sqrt{2}$ for two-way propagation and σ is again written in terms of the mean power using Equation 2-12.

4.3 BISTATIC PROPAGATION

For the bistatic propagation case, the amplitude z of the received voltage q(t) from Equation 2-9 can be written as

$$z = st \tag{4-19}$$

where s and t are the amplitudes of the two independent bistatic path voltages $p_1(t)$ and $p_2(t)$. The joint probability density function of s, $\dot{s}$, t, and $\dot{t}$ is then

$$f(s,\dot{s},t,\dot{t}) = f(s,\dot{s})\, f(t,\dot{t}) \tag{4-20}$$

where $f(s,\dot{s})$ and $f(t,\dot{t})$ are both given by Equation 4-11 assuming that each path has the same PSD and decorrelation time. The more general problem where the PSD and/or the decorrelation time of the two paths differ is considered in Appendix B.

In this case it is convenient to use Equation 4-19 to write $f(s,\dot{s},t,\dot{t})$ in terms of a new set of variables z, $\dot{z}$, s, and $\dot{s}$. The Jacobian of this transformation is

$$J = \begin{bmatrix} \partial s/\partial z & \partial \dot{s}/\partial z & \partial t/\partial z & \partial \dot{t}/\partial z \\ \partial s/\partial \dot{z} & \partial \dot{s}/\partial \dot{z} & \partial t/\partial \dot{z} & \partial \dot{t}/\partial \dot{z} \\ \partial s/\partial s & \partial \dot{s}/\partial s & \partial t/\partial s & \partial \dot{t}/\partial s \\ \partial s/\partial \dot{s} & \partial \dot{s}/\partial \dot{s} & \partial t/\partial \dot{s} & \partial \dot{t}/\partial \dot{s} \end{bmatrix} \tag{4-21}$$

where the old variables (s, $\dot{s}$, t, and $\dot{t}$) in terms of the new variables (s, $\dot{s}$, z, and $\dot{z}$) are

$$\begin{aligned} s &= s \\ \dot{s} &= \dot{s} \\ t &= z/s \\ \dot{t} &= \dot{z}/s - z\dot{s}/s^2 \end{aligned} \tag{4-22}$$

so that the determinant of the Jacobian becomes

$$\det(J) = s^{-2} \quad . \tag{4-23}$$

The joint probability density function of z and $\dot{z}$ is then obtained by integrating $f(s,\dot{s},z,\dot{z})$ over s and $\dot{s}$ as

$$f(z,\dot{z}) = (\tau_1^2/4\pi\Delta^2\sigma^6) \int_0^\infty ds \int_{-\infty}^{\infty} d\dot{s}\; zs^{-2}$$

$$x\ \exp\{-[s^2 + z^2/s^2 + \tau_1^2(\dot{s}^2 + \dot{z}^2 s^{-2} + z^2\dot{s}^2 s^{-4} - 2z\dot{z}\dot{s}/s^3)/2\Delta^2]/2\sigma^2\} \qquad (4\text{-}24)$$

The $\dot{s}$ integral can be performed in closed form to give

$$f(z,\dot{z}) = (\tau_1 z/2\sqrt{\pi}\Delta\sigma^5) \int_0^\infty ds\ (s^4+z^2)^{-1/2}$$

$$x\ \exp\{-[s^2 + z^2/s^2 + \tau_1^2 s^2\dot{z}^2(s^4+z^2)^{-1}/2\Delta^2]/2\sigma^2\} \qquad (4\text{-}25)$$

The mean number of crossings of the level L requires an integral of Equation 4-25 over $\dot{z}$ which can be obtained in closed form. Upon changing variables in the remaining integral to $u = s/\sigma$; using Equation 2-12 to write σ in terms of the mean power; and noting that τ_0 is equal to $\delta\tau_1/\sqrt{2}$ in the bistatic geometry when the two paths have the same decorrelation time; the mean number of crossings becomes

$$\langle N(L,T)\rangle = \delta\Delta(T/\tau_0)\sqrt{8L/\langle S\rangle\pi} \int_0^\infty \sqrt{1+4L/\langle S\rangle u^4}\ \exp[-(1+4L/\langle S\rangle u^4)u^2/2]\ du \qquad (4\text{-}26)$$

The remaining integral is easy to evaluate using numerical techniques because the exponential term in the integrand is $\exp(-2L/\langle S\rangle u^2)$ for $u \ll 1$ and is $\exp(-u^2/2)$ for $u \gg 1$. Hence the integrand goes exponentially to zero at both limits of the integral.

4.4 MEAN DURATION AND SEPARATION OF FADES AND FLARES

The mean numbers of level crossings per received decorrelation time are plotted in Figure 9 versus the ratio L/<S> in dB for the one-way, monostatic, and bistatic propagation cases and for a Gaussian PSD for which δ and Δ are both unity. These results show the higher frequency of deep fades in the two-way monostatic or bistatic propagation cases versus the one-way propagation case. They also show that for levels between +5 dB and about -12 dB relative to the mean power, the bistatic case has a higher frequency of level crossings than does the monostatic case.

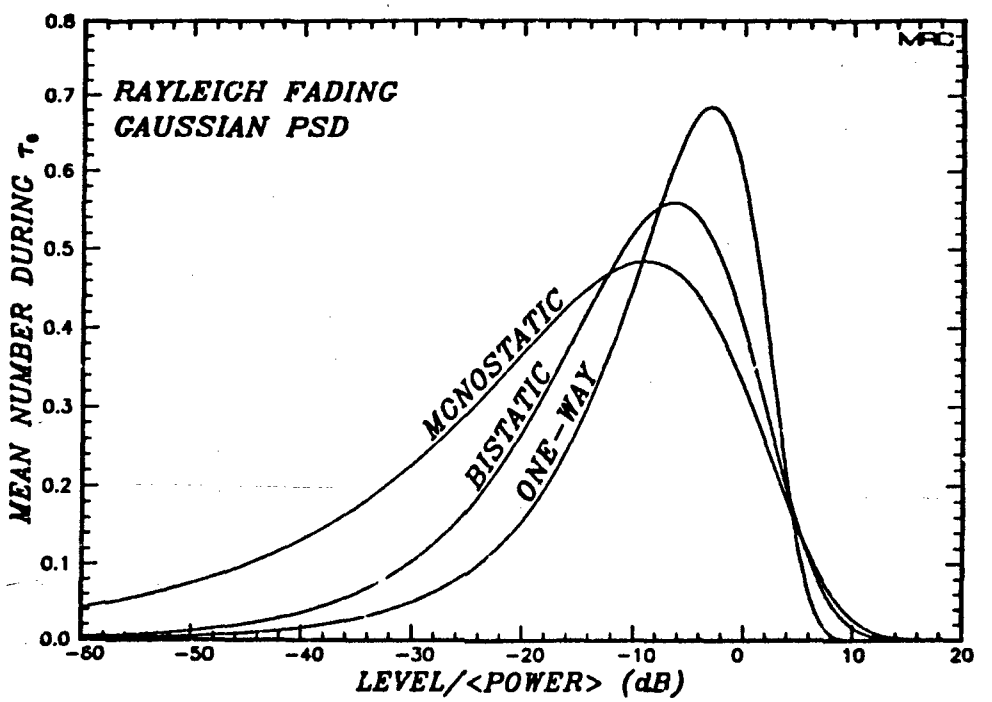

Figure 9. Mean number of level crossings in one decorrelation time τ_o.

The mean duration $\langle t_D \rangle$ of fades or flares can be obtained directly from the mean number of level crossings by noting that [10]

$$\begin{aligned} (1/2)\ \langle N(L,\tau_o)\rangle\ \langle t_{D,fade}\rangle/\tau_o &= F(L) \\ (1/2)\ \langle N(L,\tau_o)\rangle\ \langle t_{D,flare}\rangle/\tau_o &= 1 - F(L) \end{aligned} \qquad (4\text{-}27)$$

where $F(L)$ is the probability that the received power is less than or equal to L (Equation 2-11) and $(1/2)\ \langle N(L,\tau_o)\rangle/\tau_o$ is the mean number of fades or flares per unit time. In addition, the mean separation $\langle t_S \rangle$ fades or flares is

$$\langle t_{S,fade} \rangle = \langle t_{S,flare} \rangle = 2\tau_o/\langle N(L,\tau_o)\rangle \qquad (4\text{-}28)$$

or just twice the mean interval between level crossings.

The scaling of the mean duration and separation of fades or flares from the Gaussian values $\langle t_D \rangle_G$ and $\langle t_S \rangle_G$ is

$$\begin{aligned} \langle t_D \rangle &= \frac{1}{\delta\Delta}\ \langle t_D \rangle_G \\ \langle t_S \rangle &= \frac{1}{\delta\Delta}\ \langle t_S \rangle_G \end{aligned} \qquad (4\text{-}29)$$

where again δ is unity for one-way propagation. Under Rayleigh fading conditions, the PSD will be bounded by the Gaussian form in the strong scatter, fast fading limit with $1/\delta\Delta \equiv 1$ and by an f^{-3} PSD in the slow fading limit. An f^{-4} spectrum lies between these two limits and is of particular interest since it is frequently used for system specification and testing.[11] For an f^{-4} PSD, the values of $1/\delta\Delta$ that are calculated in Appendix A are 0.66 for one-way propagation and 0.74 for two-way propagation when both of the one-way paths have the same decorrelation time.

The mean duration of fades below an arbitrary level L for a Gaussian PSD is shown in Figure 10 and the mean duration of flares above the level L for a Gaussian PSD is shown in Figure 11. The monostatic case

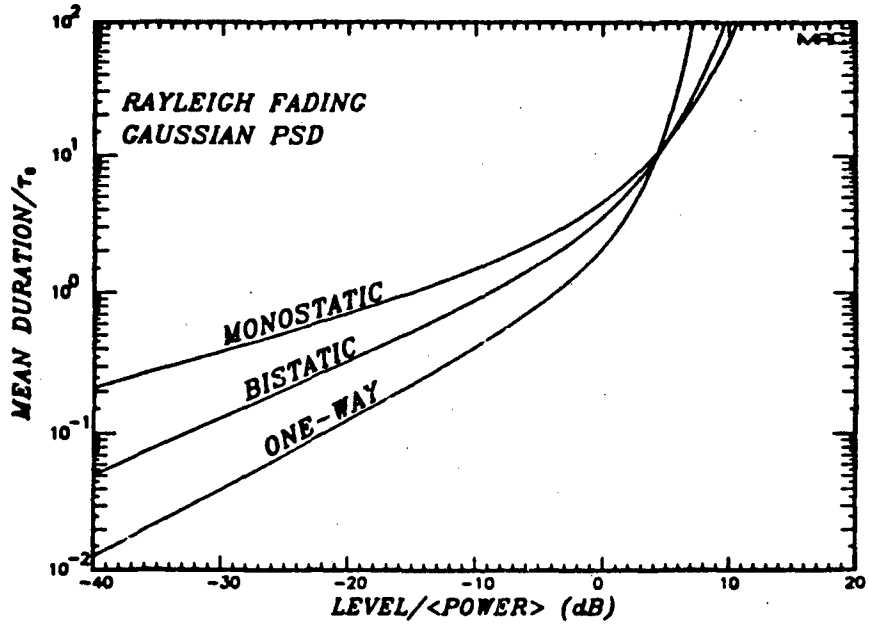

Figure 10. Mean duration of fades below an arbitrary level.

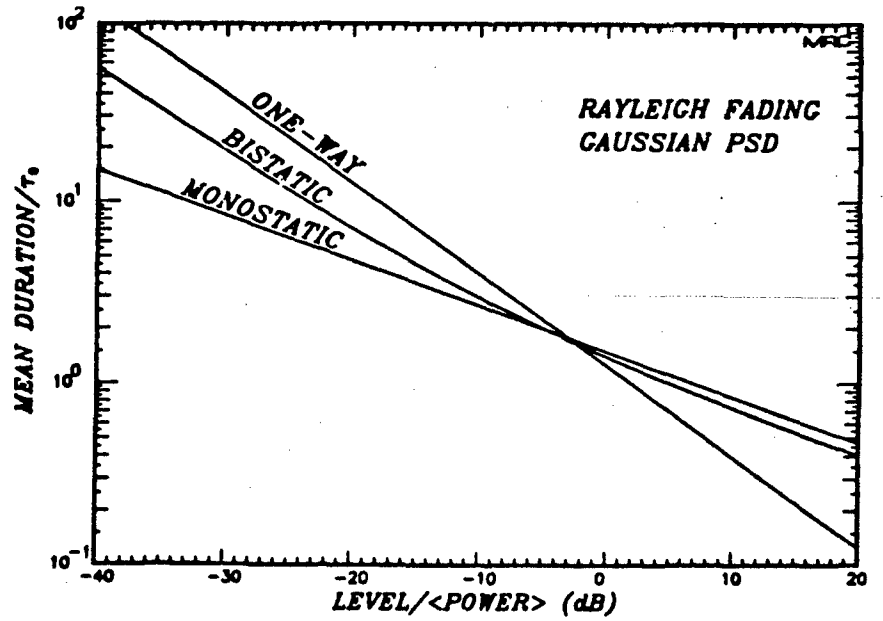

Figure 11. Mean duration of flares above an arbitrary level.

has the longest mean duration of fades for any level L and the one-way case has the shortest mean duration of fades. However, above levels of about -3 dB relative to the mean power, the monostatic case also has the longest mean duration of flares while the one-way case has the shortest mean duration of flares. The situation is reversed at levels below -3 dB. That is, the one-way case has the longest mean time above levels which are 3 dB or more below the mean power. The bistatic mean duration of fades or flares lies between the other two cases except in the cross-over region (-10 dB to -3 dB) of the mean duration of flares.

The mean separation of fades or flares for the Gaussian PSD is shown in Figure 12. The monostatic case has shortest mean separation of

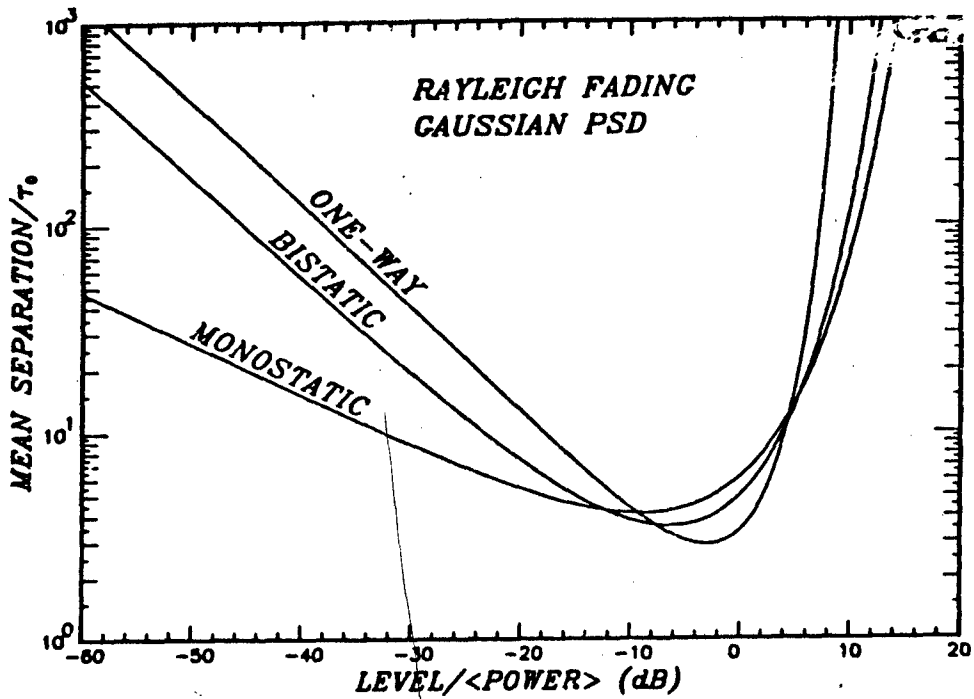

Figure 12. Mean separation of fades or flares.

fades or flares for levels 11 dB or more below the mean power and for levels 8 dB or more above the mean power. For levels between -9 dB and 2 dB relative to the mean power, the one-way case has the shortest mean separation of fades or flares. Except where the curves cross over, the bistatic mean separation of fades or flares lies between the other two cases.

Using these results, qualitative information can be obtained on the difference between mean performance effects of a Rayleigh fading environment on one-way versus two-way communication links or monostatic versus bistatic space based radars. In the communication link case, a comparison of the one-way and bistatic propagation cases shows that the mean duration of fades is longer for the two-way link; that the mean duration of flares above the mean power is longer for the two-way link; and that for levels between -9 dB and 2 dB relative to the mean power, the one-way link has shorter mean separations between fades or flares while the one-way link has longer mean separations between fades or flares for levels outside of the -9 dB to 2 dB range. By comparing the monostatic and bistatic propagation cases it can be seen that the mean duration of fades is longer for the monostatic radar; that the mean duration of flares above the mean power is also longer for the monostatic radar; and that the bistatic radar has shorter mean separations of fades or flares for levels between -11 dB and 3 dB relative to the mean power while the monostatic radar has longer mean separations of fades or flares outside of the -11 dB to 3 dB range.

SECTION 5
GENERATION OF THE RECEIVED VOLTAGES AND DATA GATHERING

The probability density functions of the durations and separations of fades or flares are unobtainable by analytic methods for even the simplest case of a one-way communication link. However, the desired statistics are easily calculated using Monte-Carlo methods by generating either one or two random sequences of the one-way voltage p(t) with Gaussian correlation and then using Equation 2-9 to generate the sequences of the received voltage q(t). It is then an easy matter to find the statistics of the duration separation of fades or flares relative to a given level that exist in the amplitudes z(t). The sequences generated are limited to be less than or equal to 8192 samples because of the fast Fourier transform routine that is utilized. Thus this process is repeated multiple times in order to collect sufficient data.

The method of generating the sequences is described in detail elsewhere[12] and is briefly reviewed here. The desired Gaussian autocorrelation is equivalent to a Gaussian PSD S(f) where

$$S(f) = \int_{-\infty}^{\infty} \rho(t)\, \exp(-i2\pi ft)dt$$

$$= \tau_1 \sqrt{\pi}\, \exp(-\pi^2 \tau_1^2 f^2). \qquad (5\text{-}1)$$

The voltage samples are first generated in frequency space using the discrete equivalent S_n of the PSD S(f) and are then discrete Fourier

transformed to the time domain. A total of $N=2^m$ (m is a positive integer less than a equal to 13) voltage samples are generated covering a total time of

$$T = N\Delta t \quad . \tag{5-2}$$

If there are n samples per one-way decorrelation time, then

$$\Delta t = \tau_1 / n \quad . \tag{5-3}$$

Because the spectral samples of a stationary random process are independent, N complex voltages ξ_j (j=0,1,..., N-1) are generated with Rayleigh distributed amplitudes and unifrmly distributed phases. Thus

$$\xi_j = \sqrt{-2\sigma^2 \ell n(u_{1,j})}\ \exp(i2\pi u_{2,j}), \qquad j = 0,1,\ldots,N-1 \tag{5-4}$$

where $u_{1,j}$ and $u_{2,j}$ are independent, uniformly distributed random variables on the interval $[0,1)$. The real and imaginary parts of ξ_j are independent, normally distributed random variables with zero means and σ^2 variances. The parameter σ is set by requiring that the average received power be unity in all cases. The frequency samples ξ_j are then weighted symmetrically by the discrete voltage spectral density $\sqrt{S_j}$ where

$$S_j = \Delta f\ S[(j-N/2)\Delta f], \qquad j = 0,1,\ldots,N-1, \tag{5-5}$$

and where the frequency sample spacing is

$$\Delta f = 1/T = 1/N\Delta t = n/N\tau_1 \quad . \tag{5-6}$$

Hence, the frequency voltages $\hat{x}_j$ are given by

$$\hat{x}_j = \xi_j \, (n\sqrt{\pi}/N)^{1/2} \exp[-\pi^2 n^2 (j-N/2)^2/(2N^2)] \quad . \qquad (5\text{-}7)$$

$$j = 0,1,\ldots,N-1$$

The one-way received voltage p_k is the discrete Fourier transform of $\hat{x}_j$:

$$p_k = \sum_{j=0}^{N-1} \hat{x}_j \exp(i2\pi jk/N), \qquad k = 0,1,\ldots,N-1. \qquad (5\text{-}8)$$

In order to show that the samples p_k have the correct correlation properties, the autocorrelation of p_k can be written as

$$\langle p_k \, p_\ell^* \rangle = \sum_{j=0}^{N-1} \sum_{m=0}^{N-1} \langle \hat{x}_j \, \hat{x}_m^* \rangle \exp[i2\pi(jk-\ell m)/N] \quad . \qquad (5\text{-}9)$$

However, because the frequency samples $\hat{x}_j$ are independent,

$$\langle x_j \, x_m^* \rangle = \begin{cases} \langle \xi_j \xi_j^* \rangle S_j & \text{if } j = m \\ 0 & \text{if } j \neq m \end{cases} \qquad (5\text{-}10)$$

where

$$\langle \xi_j \, \xi_j^* \rangle = 2\sigma^2 \quad . \qquad (5\text{-}11)$$

Therefore

$$\langle p_k \, p_\ell^* \rangle = 2\sigma^2 \sum_{j=0}^{N-1} S_j \exp[i2\pi j(k-\ell)/N] = 2\sigma^2 \, \rho(k-\ell) \qquad (5\text{-}12)$$

where $\rho(k-\ell)$ is the discrete autocorrelation function which is equal to the discrete Fourier transform of S_j.

The first 100 decorrelation times of the received or combined power for the one-way, monostatic, bistatic, and dual channel summation algorithm, and dual channel maximum algorithm cases are plotted in Figures 13 a,b,c,d,e respectively for sequences generated with 10 amplitude samples per one-way decorrelation time. From the figures, it can be seen that during the time plotted the one-way received power has one fade more than -25 dB below the mean power and none more than -30 dB below the mean power; the monostatic received power has ten fades more than -30 dB below the mean power; and the bistatic received power has two fades more than -30 dB below the mean power. The dual channel combined power sequences have no fades more than 20 dB below the mean power. The summation algorithm sequence has seven fades which are more than 10 dB below the mean power but none of those fades reaches 15 dB below the mean. The maximum algorithm has eight fades which fall more than 10 dB below the mean power and two that exceed 15 dB below the mean power.

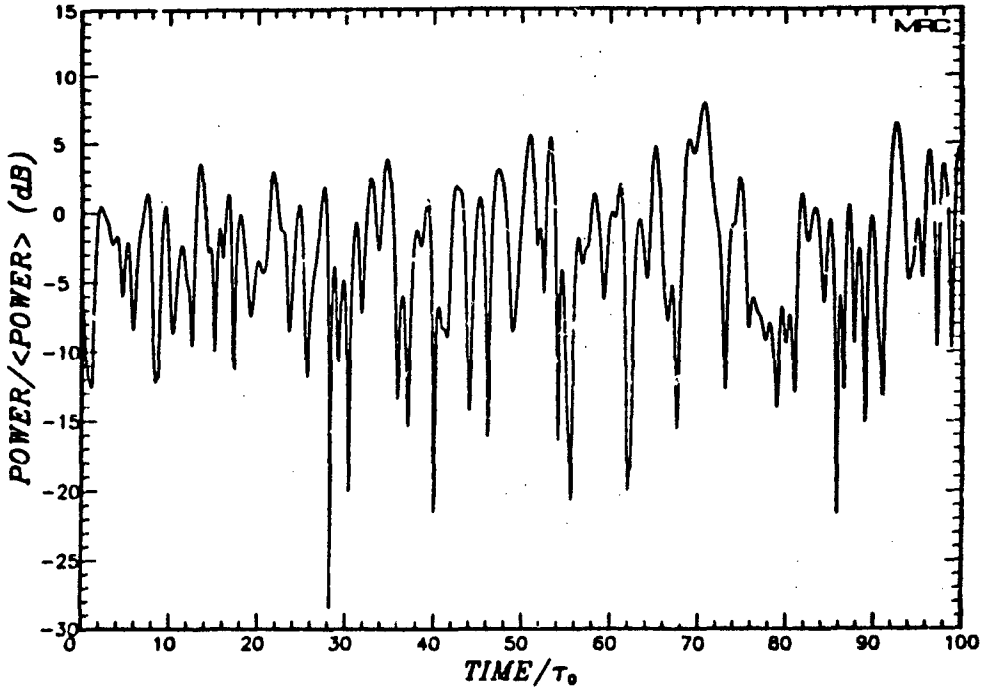

Figure 13a. Example of the received power for the one-way case.

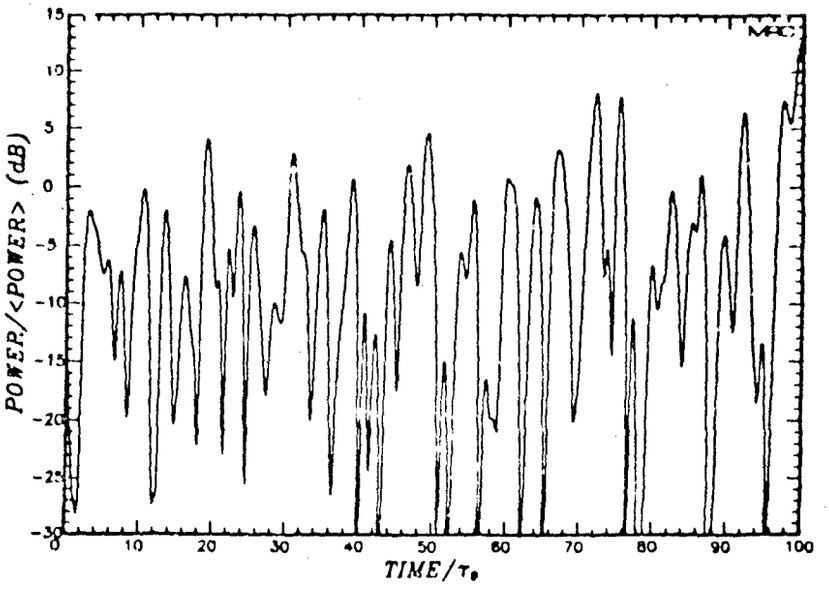

Figure 13b. Example of the received power for the monostatic case.

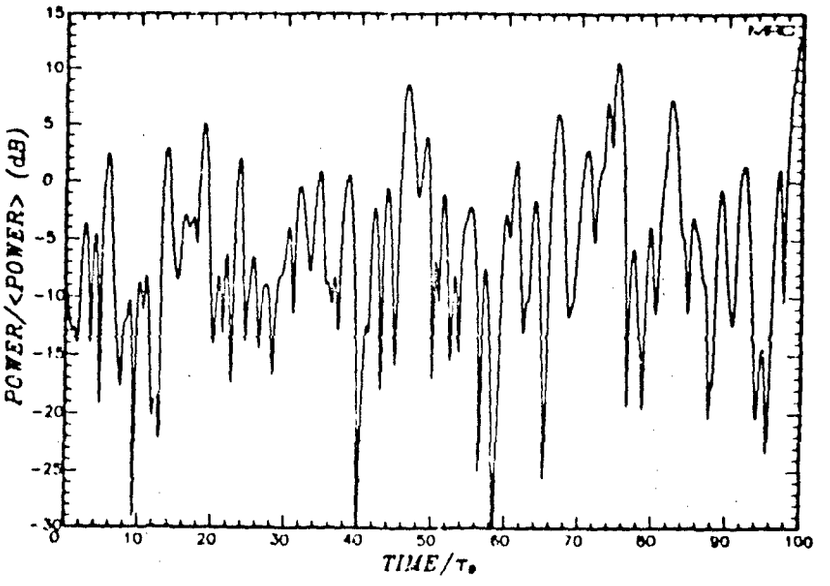

Figure 13c. Example of the received power for the bistatic case.

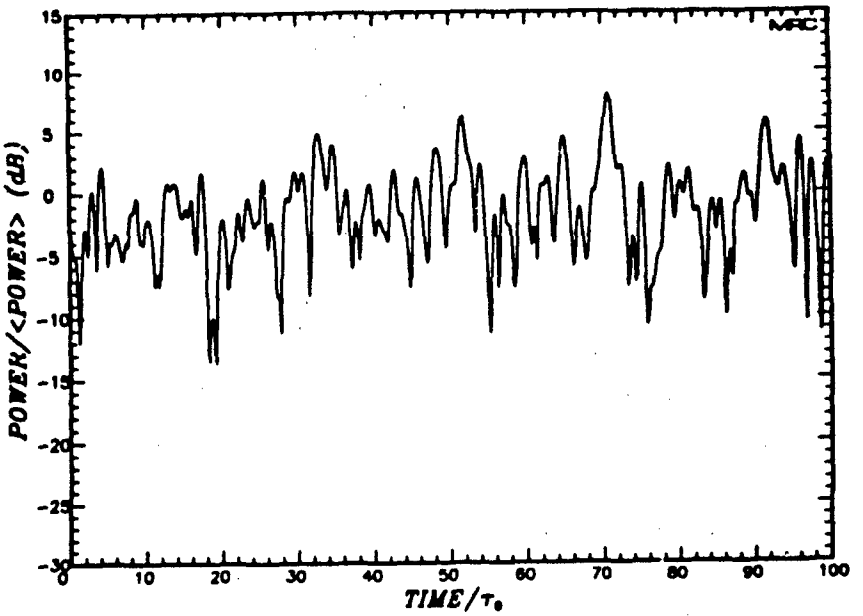

Figure 13d. Example of the combined power for identically distributed dual channels (summation algorithm).

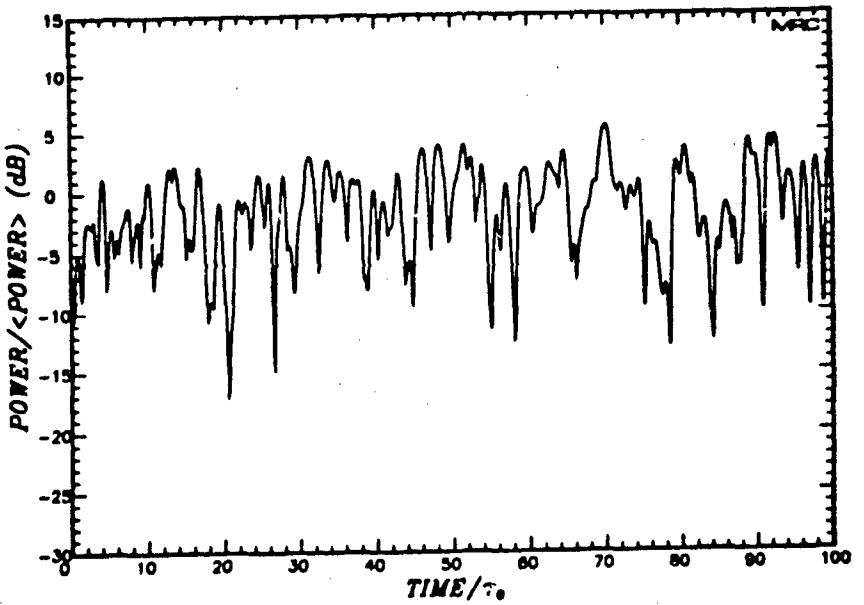

Figure 13e. Example of the combined power for identically distributed dual channels (maximum algorithm).

The phase of the one-way received voltage,

$$\theta(t) = \tan^{-1}\{\mathrm{Im}[p(t)]/\mathrm{Re}[p(t)]\} \qquad (5\text{-}13)$$

is shown in Figure 14 where it can be observed that the most rapid changes in the phase occur when the received power is in a deep fade. The autocorrelation of the one-way voltage shown in Figure 13a is plotted in Figure 15 along with the Gaussian form. Although the autocorrelation of one sequence is a random variate and therefore has a distribution about its mean, the average autocorrelation of twenty sequences, plotted in Figure 16, shows close agreement with the desired Gaussian form.

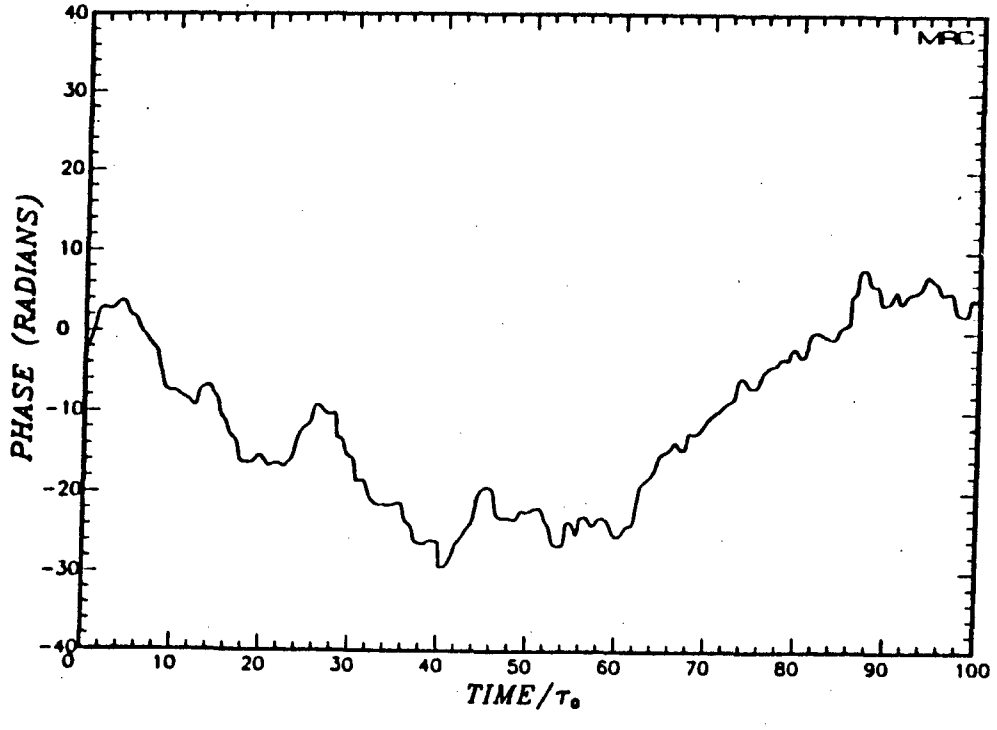

Figure 14. Phase of the voltage for the one-way received power shown in Figure 13a.

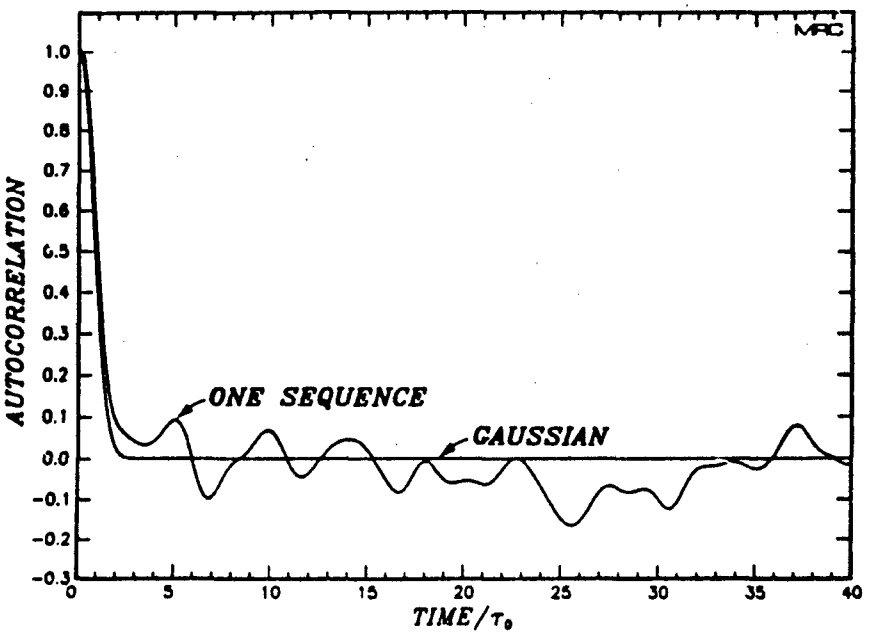

Figure 15. Autocorrelation of one random sequence of the one-way received voltage and the desired Gaussian form.

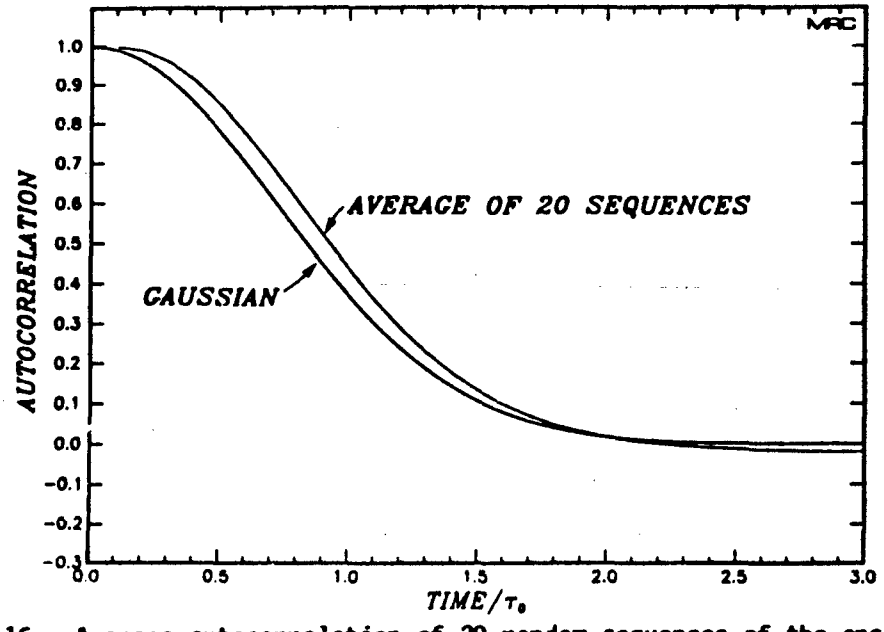

Figure 16. Average autocorrelation of 20 random sequences of the one-way received voltage and the desired Gaussian form.

The statistics of the duration and separation of fades or flares is gathered by stepping through the random sequences and comparing the received power with the desired level. Because of the finite length of the voltage sequences, some boundary effects exist. For example, when a new sequence is generated the first fade (flare) below (above) some level L can be recorded only after encountering the first amplitude above (below) L. Similarly, a fade or flare must end before the end of the sequence to be included in the data. Also, except when the sequence ends during a fade or flare, the number of intervals between fades or flares in a sequence will be one less than the number of occurrences of fades or flares. Histograms are generated of the samples of duration and separation from which median values are calculated. In addition, statistics are collected on the amplitudes z(t) and on the number of crossings of the level L.

The total number of received voltage samples generated, which is equal to the number of voltages per sequence times the number of sequences generated, is selected in order to achieve about 10^4 fades or flares. The mean number of occurrences per sequence is $\langle N(L,\tau_1)\rangle/2(N/n)$ where N/n is the number of decorrelation times per sequence. The number of samples n per decorrelation time has been selected so that the mean duration of a fade or flare is roughly greater than 10 samples in order to collect meaningful duration data. Thus for very deep fades with correspondingly short durations, 20 or more samples per decorrelation time are required to obtain good statistics on the fade duration. Consequently, the number of decorrelation times per sequence is reduced and the required number of sequences that must be generated is increased. Because of these considerations, the minimum level relative to the mean power for fades has been limited to -15 dB and the maximum level for flares has been limited to +5 dB.

SECTION 6
SIMULATION RESULTS

The results from the Monte Carlo simulation with a Gaussian PSD are presented in this section for the one-way, monostatic, and bistatic cases, and for the dual channel communication link cases. First, the moments of the amplitude z for each of the cases are compared with the expected values given in Table I (Page 24) in order to verify that the simulated received voltages have the desired amplitude statistics. Then the correlation properties of the received voltages are verified by comparing the mean number of level crossings and the mean duration and mean separation of fades and flares with the results calculated in Section 4. Finally, the mean, median, and standard deviation of the duration and interval between fades or flares are presented in tabular form. A comparison is made with multiple phase screen calculation results in Appendix C Plots of the probability density function and the cumulative probability distribution are shown for the one-way case in Appendix D.

The first four moments of the amplitude z of the received voltage normalized to the expected values are snown in Table II for the various propagation cases given in Table I. The largest deviation of the amplitude moments from the expected values occur in the monostatic and bistatic cases while the one-way amplitude moments vary by at most 4.3 percent from the expected values.

The statistics of one-way, monostatic, and bistatic fades and flares are summarized in Tables III, IV, and V respectively. The mean,

median, and standard deviation, normalized to τ_0 of fade or flare duration and separation are shown for various levels along with the mean-to-standard deviation (μ/σ) ratios.

Table II. Moments of the received voltages from the Monte Carlo simulation.

Case	$\langle Z^n \rangle / E[Z^n]$*				No. of Amplitude Samples
	n = 1	n = 2	n=3	n = 4	
One-Way	1.007	1.017	1.029	1.043	344064
Monostatic	1.010	1.028	1.049	1.071	524288
Bistatic	0.995	0.989	0.985	0.983	524288
Dual Channel Communication					
Summation Algorithm	1.000	1.001	1.002	1.003	524288
Maximum Algorithm	0.997	0.995	0.993	0.992	524288

*$\langle Z^n \rangle$ denotes simulation results for 0 dB fading.

$E[Z^n]$ denotes expected values given in Table I.

Close agreement is seen between the analytic results of Section 4 and the simulation results for the mean number of level crossings and the mean duration and separation of fades and flares. The close agreement of the analytic and simulation mean values confirms that the simulated received voltage has both the proper amplitude statistics and correlation properties because the mean number of level crossings depends depends on both the first and second order statistics of the received voltage.

The mean-to-standard deviation ratios of the data range from 1.1 to 1.8 with most in the range from 1.2 to 1.5. As a point of comparison, a Rayleigh distribution has

$$\mu/\sigma = (4/\pi - 1)^{-1/2} \approx 1.913 \quad . \tag{6-1}$$

Table III. Statistics of one-way scintillation.

Flares	Fades	L/<S> (dB)	n++	<N(L,τ0)> Analytic†	<N(L,τ0)> Simulation	Duration of Fades/Flares No+	Duration of Fades/Flares <tD>/τ0††	Duration of Fades/Flares Mean*	Duration of Fades/Flares Std. Dev.*	Duration of Fades/Flares Median*	Duration of Fades/Flares μ/σ	Separation of Fades/Flares No+	Separation of Fades/Flares <tS>/τ0†††	Separation of Fades/Flares Mean*	Separation of Fades/Flares Std. Dev.*	Separation of Fades/Flares Median*	Separation of Fades/Flares μ/σ
X		5	30	0.120	0.118	9786	0.705	0.708	0.410	0.60	1.73	9205	16.7	16.0	14.3	11.6	1.12
X		3	20	0.307	0.305	9869	0.887	0.893	0.550	0.75	1.62	9738	6.53	6.47	5.09	4.90	1.27
X		0	10	0.587	0.586	15344	1.25	1.25	0.857	0.90	1.46	15301	3.41	3.41	1.98	2.80	1.72
	X	0	10	0.587	0.584	10028	2.15	2.14	1.76	1.50	1.22	10018	3.41	3.41	1.95	2.80	1.75
	X	-3	20	0.684	0.681	10030	1.15	1.16	0.920	0.80	1.26	9987	2.92	2.93	1.59	2.50	1.84
	X	-5	20	0.654	0.651	9990	0.829	0.823	0.630	0.55	1.31	9944	3.06	3.06	1.87	2.55	1.64
	X	-10	30	0.457	0.459	12432	0.417	0.417	0.308	0.30	1.35	12255	4.38	4.34	3.48	3.27	1.25
	X	-15	50	0.275	0.274	11483	0.226	0.225	0.167	0.16	1.35	10989	7.27	7.00	6.24	5.10	1.12

* Normalized to τ_0

\+ Number of samples of the duration or separation

++ Number of voltage samples per τ_0

† Equation 4-12

†† Equation 4-27

††† Equation 4-28

Table IV: Statistics of monostatic scintillation.

Flares	Fades	L/<S> (dB)	n**	<N(ε,τ0)>		Duration of Fades/Flares						Separation of Fades/Flares					
				Analytic†	Simulation	No*	<t0>/τ0††	Mean*	Std. Dev.*	Median*	μ/σ	No*	<tS>/τ0†††	Mean*	Std. Dev.*	Median*	μ/σ
X		5	20	0.145	0.146	10539	1.12	1.13	0.682	0.92	1.65	10305	13.8	13.5	11.4	10.04	1.18
X		3	20	0.216	0.218	10216	1.2[illegible]	1.27	0.799	1.06	1.58	10075	9.24	9.07	7.14	6.86	1.27
X		0	10	0.326	0.326	12087	1.49	1.51	0.993	1.13	1.52	12035	6.13	6.11	4.10	4.81	1.49
	X	0	10	0.326	0.326	12047	4.64	4.60	3.99	3.25	1.15	12035	6.13	6.11	4.10	4.81	1.49
	X	-3	20	0.415	0.414	9817	3.05	3.01	2.53	2.12	1.19	9789	4.82	4.79	2.83	3.96	1.70
	X	-5	20	0.455	0.453	9674	2.42	2.39	1.95	1.70	1.22	9641	4.40	4.40	2.43	3.75	1.81
	X	-10	20	0.482	0.482	10452	1.49	1.47	1.13	1.06	1.30	10405	4.15	4.13	2.36	3.47	1.75
	X	-15	30	0.440	0.442	9888	1.01	0.997	0.740	0.71	1.35	9799	4.55	4.48	2.92	3.64	1.52

* Normalized to τ_0

\+ Number of samples of the duration or separation

** Number of voltage samples per τ_0

† Equation 4-18

†† Equation 4-27

††† Equation 4-28

Table V: Statistics of bistatic scintillation.

Flares	Fades	L/<S> (dB)	n**	<N(t,τ0)> Analytic†	<N(t,τ0)> Simulation	Duration of Fades/Flares No*	<tD>/τ0††	Mean*	Std. Dev.*	Median*	μ/σ	Separation of Fades/Flares No*	<tS>/τ0†††	Mean*	Std. Dev.*	Median*	μ/σ
X		5	20	0.148	0.147	10628	1.00	1.00	0.597	0.85	1.68	10398	13.5	13.4	11.6	9.83	1.15
X		3	20	0.245	0.248	9599	1.14	1.15	0.718	0.92	1.59	9486	8.16	7.99	6.42	5.94	1.24
X		0	10	0.400	0.393	14564	1.40	1.41	0.929	1.13	1.51	14522	5.00	5.08	3.38	3.96	1.50
	X	0	10	0.400	0.392	14541	3.60	3.66	3.27	2.55	1.12	14519	5.00	5.08	3.39	3.96	1.50
	X	-3	20	0.514	0.511	9990	2.16	2.15	1.82	1.49	1.18	9876	3.89	3.89	2.22	3.32	1.75
	X	-5	20	0.552	0.549	9848	1.63	1.63	1.36	1.13	1.20	9815	3.63	3.62	2.01	3.11	1.80
	X	-10	30	0.521	0.522	10060	0.896	0.892	0.754	0.61	1.18	9982	3.84	3.82	2.55	3.15	1.50
	X	-15	30	0.399	0.400	10024	0.536	0.528	0.450	0.33	1.17	9912	5.02	4.95	3.97	3.78	1.25

* Normalized to τ_0

\+ Number of samples of the duration or separation

** Number of voltage samples per one-way decorrelation time τ_1

† Equation 4-26

†† Equation 4-27

††† Equation 4-28

Thus the durations and separation have narrower distributions about their means than does a Rayleigh distribution.

The statistics of dual channel fades are summarized in Table VI. In this case, no analytic expressions are available for the mean quantities. When comparing the summation algorithm (denoted by SUM in the table) with the maximum algorithm (denoted by MAX), the mean durations and separations of fades are slightly larger for the summation algorithm at all levels shown while the mean number of level crossings is slightly smaller. In comparison with the single channel one-way communication link data, the dual channel has on the average shorter fade durations which for deep fades below -10 dB occur much farther apart. Fades -10 dB below the mean power in the dual channel system occur only about 1/3 as often as they occur in the single channel system and they are only 2/3 as long.

Table VI: Statistics of dual channel fades.

Sum	Max	L/<S> (dB)	n++	<N(L,τ0)>	Duration of Fades					Separation of Fades				
				Simulation	No+	Mean*	Std. Dev.*	Median*	μ/σ	No+	Mean*	Std. Dev.*	Median*	μ/σ
	X	0	10	0.662	17339	1.83	1.60	1.30	1.14	17311	3.01	1.78	2.50	1.69
	X	-3	20	0.674	10599	0.821	0.663	0.60	1.24	10546	2.96	1.94	2.45	1.53
	X	-5	30	0.508	9843	0.556	0.437	0.433	1.27	9712	3.90	2.98	3.03	1.31
	X	-10	30	0.143	10230	0.271	0.196	0.20	1.38	9716	13.3	12.5	9.43	1.06
X		0	10	0.633	16581	1.88	1.57	1.30	1.20	16559	3.15	1.81	2.60	1.74
X		-3	20	0.622	10436	0.859	0.653	0.65	1.32	10376	3.20	1.99	2.65	1.61
X		-5	30	0.462	9707	0.590	0.421	0.467	1.40	9573	4.28	3.35	3.23	1.28
X		-10	30	0.129	12896	0.286	0.194	0.233	1.47	12175	14.6	13.9	10.3	1.05

*Normalized to τ_0

+Number of samples of the duration or separation

++Number of voltage samples per τ_0

SECTION 7
RESULTS AND CONCLUSIONS

The major results of this study are:

- Binary error rates under slow Rayleigh fading conditions for various frequency-shift keying and phase-shift keying demodulation techniques have been calculated for two-way and dual channel communication links.

- Analytic expressions have been derived for the mean number of level crossings and the mean duration and separation of fades and flares for one-way, monostatic, and bistatic propagation with Rayleigh amplitude statistics and arbitrary power spectral densities.

- The probability density functions and cumulative distributions of the duration and separation of fades and flares for one-way propagation, Rayleigh amplitude statistics, and a Gaussian power spectral density are compiled in Appendix D.

The key conclusions of this study are:

- Under slow Rayleigh fading conditions, a bistatic communication link through a satellite transponder requires about 9 dB more bit energy-to-noise density than does a one-way link to achieve a bit error rate of 10^{-3} while a dual channel communication link requires about 10 dB less bit energy-to-noise density to achieve a 10^{-3} bit error rate.

- Relative to monostatic space based radar systems, bistatic radars have shorter mean fade durations and longer mean separations of deep fades more than 10 dB below the mean power.

- Fades in dual channel communication links which are more than 10 dB below the mean power are, on the average, two-thirds as long and occur about one third as often as fades 10 dB below the mean power in single channel links.

REFERENCES

1. Knepp, D. L., Multiple Phase-Screen Propagation Analysis for Defense Satellite Communications Systems, DNA 4424T, MRC-R-332, Mission Research Corporation, September 1977.

2. Wittwer, L. A., The Propagation of Satellite Signals Through Turbulent Media, AFWL-TR-77-183, Air Force Weapons Laboratory, January 1978.

3. Fante, R. L., "Some New Results on Propagation of Electromagnetic Waves in Strongly Turbulent Media," IEEE Trans. Antennas and Propagation, Vol. AP-23, pp. 382-385, May 1975.

4. Knepp, D. L. and R. A. Dana, The Effects of Scintillation on Spaced Based Radar Performance, MRC-R-682, Mission Research Corporation, March 1982.

5. Marcum, J. I., "A Statistical Theory of Target Detection by Pulsed Radar," IRE Trans. Information Theory. Vol IT-6, pp 145-268, April 1960.

6. Bogusch, R. L., M. J. Barrett, D. L. Knepp, and B. E. Sawyer, Signal Propagation Effects on Selected Satellite Systems, MRC-R-405, Mission Research Corporation, July 1978.

7. Gradshteyn, I. S. and I. M. Ryzhik, Table of Integrals, Series, and Products, Academic Press, New York, 1965.

8. Abramowitz, M. and I. A. Stegun (editors), Handbook of Mathematical Functions, Dover Publications, Inc., New York, 1965.

9. Rice, S. O., in N. Wax (editor), "Mathematical Analysis of Random Noise," in Selected Papers on Noise and Stochastic Processes, Dover Publications, Inc., New York, 1954.

10. Rice, S. O., "Distribution of the Duration of Fades in Radio Transmission: Gaussian Noise Model," The Bell System Technical Journal, Vol. 37, pp. 581-635, May 1958.

11. Boqusch, R. L., Satellite Link Criterion (Volume I), MRC-R-626, Mission Research Corporation, February 1982.

12. Mitchell, R. L., Radar Signal Simulation, Artech House, Inc., Dedham, Massachusetts, 1976.

13. Shkarofsky, I. P., "Generalized Turbulence Space-Correlation and Wave-number Spectrum-function Pairs," Canadian J. Phys., Vol. 46, pp. 2133-2153, 1968.

APPENDIX A
SCALING FACTORS FOR $f^{-\mu}$ POWER SPECTRAL DENSITIES

It was shown in Section 4 that the mean number of level crossings and the mean duration and separation of fades or flares for an arbitrary power spectral density (PSD) can be obtained from the mean values for a Gaussian PSD by simple scaling factors. It is the purpose of this Appendix to calculate the scaling factors for general $f^{-\mu}$ power spectral densities and to sketch the formalism for calculating the scaling factors for arbitrary power spectral densities.

In order to make these calculations as simple as possible, it is assumed in bistatic geometries that the two one-way paths have identical first and second order statistics. It is an easy matter to generalize these results to a bistatic geometry with different second order statistics on each path (i.e., to geometries where the PSD and/or the decorrelation time of the two paths differ).

A.1 GENERAL RESULTS

Before calculating the scaling factors, some general results need to be established. The autocorrelation function of the complex voltage $\rho(\tau)$ is related to the PSD $S(f)$ by the Fourier transform pair

$$\rho(\tau) = \int_{-\infty}^{\infty} S(f) e^{i2\pi f\tau} d\tau \qquad \text{(A-1)}$$

$$S(f) = \int_{-\infty}^{\infty} \rho(\tau) e^{-i2\pi f\tau} d\tau \qquad \text{(A-2)}$$

For a Gaussian autocorrelation function

$$\rho(\tau) = \exp[-(\tau/\tau_1)^2] \qquad \text{(A-3)}$$

it is well know that the PSD is also Gaussian (c.f. Equation 5-1).

The scale factor Δ, defined in Equation 4-4, is proportional to the second time derivative of $\rho(\tau)$ evaluated at zero time delay. Differentiating Equation A-1 twice gives

$$\rho(o) = -4\pi^2 \int_{-\infty}^{\infty} f^2 S(f) df \qquad \text{(A-4)}$$

which for a Gaussian PSD reduces to $-2/\tau_1^2$. The scale factor Δ for an arbitrary PSD is then

$$\Delta^2 = 2\pi^2 \tau_1^2 \int_{-\infty}^{\infty} f^2 S(f) df \ . \qquad \text{(A-5)}$$

Convergence of the integral in Equation A-5 requires that S(f) approach zero faster than f^{-3} for large f.

The other scale factor δ, defined in Equation 2-26, relates the two-way decorrelation time to the one-way decorrelation time. It was shown in general in Section 7 that for two-way geometries

$$\rho_{\text{two-way}}(\tau) = \rho^2_{\text{one-way}}(\tau) \ . \qquad \text{(A-6)}$$

The one-way decorrelation time τ_1 is defined by

$$\rho_{\text{one-way}}(\tau_1) = 1/e \ . \tag{A-7}$$

The decorrelation time of the received voltage in a two-way propagation geometry, τ_0, is then calculated from the equation

$$\rho_{\text{one-way}}(\tau_0) = 1/\sqrt{e} \ . \tag{A-8}$$

Again for a Gaussian PSD, τ_0 is just $\tau_1/\sqrt{2}$ so that in general

$$\delta = \sqrt{2}\tau_0/\tau_1 \ . \tag{A-9}$$

A.2 $f^{-\mu}$ ($\mu > 3$) POWER SPECTRAL DENSITIES

A simple form for the PSD with an $f^{-\mu}$ frequency dependence is

$$S(f) = \frac{S_0}{(f^2 + f_0^{\,2})^{\mu/2}} \tag{A-10}$$

where the coefficient S_0 is given by the normalization condition

$$\rho(0) = \int_{-\infty}^{\infty} S(f)df = 1 \tag{A-11}$$

which reduces to

$$S_0 = \frac{f_0^{\,\mu-1}\,\Gamma(\mu/2)}{\Gamma(1/2)\,\Gamma[(\mu-1)/2]} \ . \tag{A-12}$$

Note that Equation A-10 is valid only for $\mu > 3$ because of the requirement that $\ddot{\rho}(0)$ be finite. A second more general form with an inner scale which is valid for $\mu \leq 3$ is considered later in this appendix. The autocorrelation function corresponding to the PSD of Equation A-10 is

$$\rho(\tau) = \frac{(2\pi f_0 \tau)^{(\mu-1)/2} \; K_{(\mu-1)/2}\,(2\pi f_0 \tau)}{2^{(\mu-3)/2}\; \Gamma[(\mu-1)/2)]} \tag{A-13}$$

where K_ν is the νth order K Bessel function. The one-way and two-way decorrelation times can now be calculated by solving the transcendental equations

$$\frac{x^{(\mu-1)/2} \; K_{(\mu-1)/2}\,(x)}{2^{(\mu-3)/2}\; \Gamma[(\mu-1)/2]} = \frac{1}{e} \tag{A-14}$$

$$\frac{y^{(\mu-1)/2} \; K_{(\mu-1)/2}\,(y)}{2^{(\mu-3)/2}\; \Gamma[(\mu-1)/2]} = \frac{1}{\sqrt{e}} \tag{A-15}$$

for x and y where

$$x = 2\pi f_0 \tau_1 \tag{A-16}$$

$$y = 2\pi f_0 \tau_0 \; . \tag{A-17}$$

The scale factor δ is simply

$$\delta = \sqrt{2}\, y/x \tag{A-18}$$

which is only a function of μ. The scale factor Δ is given by evaluating Equations A-5 and using Equation A-16 to write f_o in terms of x and τ_1. This results in

$$\Delta^2 = \frac{\Gamma[(\mu-3)/2]\ x^2}{4\ \Gamma[(\mu-1)/2]} \qquad \text{(A-19)}$$

which is again only a function of μ and is therefore independent of the decorrelation time and of the level of the fades or flares.

The scale factor δ is plotted in Figure A-1 for $3 < \mu < 10$ where it can be seen that δ approaches unity as μ increases. Recall that δ and Δ are both unity for a Gaussian PSD. The scaling for the mean duration and separation of fades or flares, $1/\delta\Delta$ (c.f., Equation 4-29), is shown in Figure A-2 for one-way ($\delta \equiv 1$) and two-way propagation. For $\mu = 4$, the scale factors are as follows:

$$\delta = 0.8946$$

$$1/\delta\Delta = \begin{cases} 0.6589 & \text{one-way} \\ 0.7365 & \text{two-way} \end{cases} \qquad \text{(A-20)}$$

Note that $1/\delta\Delta$ changes rapidly between f^{-4} and f^{-3} where $1/\delta\Delta$ is zero.

A.3 $f^{-\mu}$ POWER SPECTRAL DENSITIES WITH AN INNER SCALE

The PSD of Equation A-10 can be used for $\mu > 3$ only. A more general form has been given by Shkarofsky[13] as

$$S(f) = \frac{(2\pi f_o t_o)^{\mu/2}\ (t_o/f_o)^{1/2}\ K_{\mu/2}\left[2\pi t_o\sqrt{f^2 + f_o^2}\right]}{K_{(\mu-1)/2}\ (2\pi f_o t_o)\ \left[2\pi t_o\sqrt{f^2 + f_o^2}\right]^{\mu/2}} \qquad \text{(A-21)}$$

which depends on both an outer scale f_o and an inner scale t_o^{-1}. This PSD, which is shown schematically in Figure A-3, is valid for any μ. For

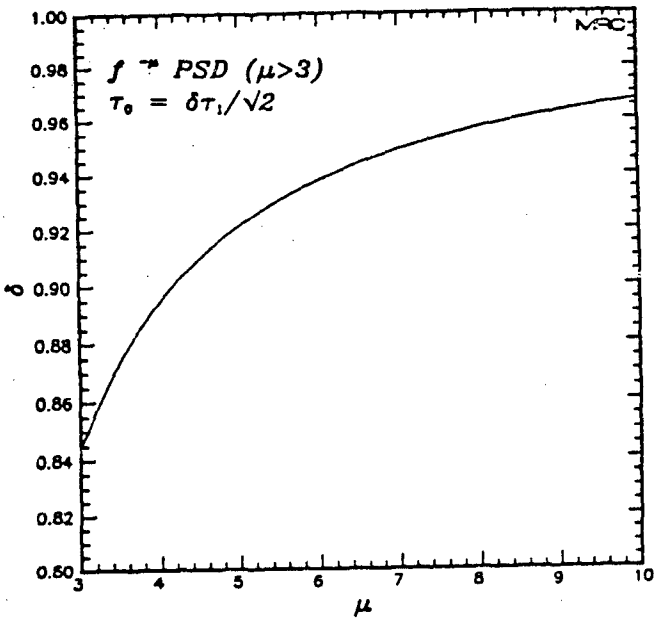

Figure A-1. τ_0 Scaling for $f^{-\mu}$ ($\mu > 3$) power spectral densities.

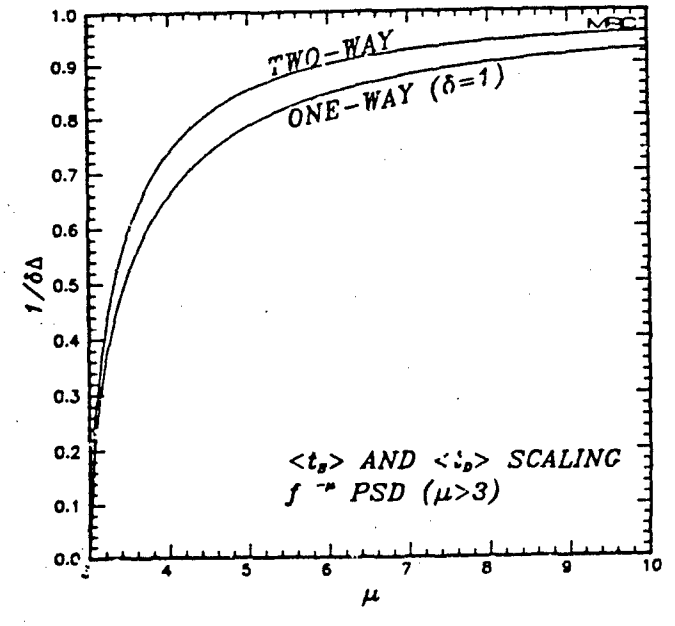

Figure A-2. Scaling of the mean separation and duration of fades and flares for $f^{-\mu}$ ($\mu > 3$) power spectral densities.

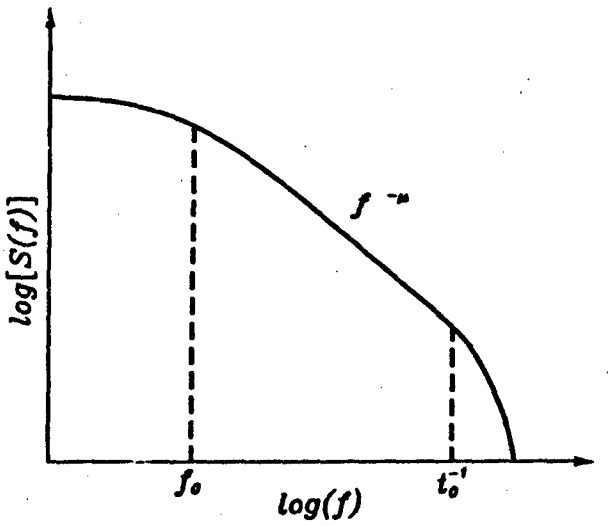

Figure A-3. Schematic diagram of the power spectral density with an inner and an outer scale.

frequencies in the range $f_0 << f << t_0^{-1}$, S(f) has an approximate $f^{-\mu}$ frequency dependence. Once μ has been fixed, the outer scale f_0 is determined by the decorrelation time. The other scale is left as a parameter. Because an f^{-3} PSD provides a slow scattering limit to Rayleigh fading environments, the subsequent discussion will consider only $\mu = 3$. Setting $\mu = 3$ in Equation A-21, the corresponding autocorrelation function is

$$\rho(\tau) = \frac{\sqrt{\beta^2 + (2\pi f_0 \tau)^2}\ K_1\left[\sqrt{\beta^2 + (2\pi f_0 \tau)^2}\right]}{\beta K_1(\beta)} \qquad \text{(A-22)}$$

where

$$\beta = 2\pi f_0 t_0 \quad . \qquad \text{(A-23)}$$

In this case, the one-way and two-way decorrelation times are computed by solving the equations

$$\frac{\sqrt{\beta^2 + x^2}\, K_1\left[\sqrt{\beta^2 + x^2}\right]}{\beta K_1(\beta)} = \frac{1}{e} \qquad \text{(A-24)}$$

$$\frac{\sqrt{\beta^2 + y^2}\, K_1\left[\sqrt{\beta^2 + y^2}\right]}{\beta K_1(\beta)} = \frac{1}{\sqrt{e}} \qquad \text{(A-25)}$$

for x and y where

$$x = 2\pi f_o \tau_1 \qquad \text{(A-26)}$$

$$y = 2\pi f_o \tau_o$$

and where x and y are now functions of the parameter β. Once x and y have been obtained, Equation A-18 is used to determine δ as a function of β. The scale factor Δ is determined by evaluating Equation A-5 which yields

$$\Delta^2 = \frac{K_o(\beta)x^2}{\beta K_1(\beta)} \quad . \qquad \text{(A-28)}$$

The scale factor δ and the scaling for the mean duration of fades and flares ($1/\delta\Delta$) are plotted in Figures A-4 and A-5 respectively with β in the range $10^{-10} \leq \beta \leq 1$. Note however, that as β approaches unity, the range of frequencies for which the PSD has an f^{-3} frequency dependence shrinks to zero. For $\beta \leq 10^{-3}$, Figure A-5 shows that $1/\delta\Delta$ is only weakly dependent on β, and for $\beta \leq 10^{-2}$, Figure A-4 shows that δ is independent of β.

All that remains to complete this discussion is to relate β to physical quantities. To this end, Equation A-26 is used to related f_o

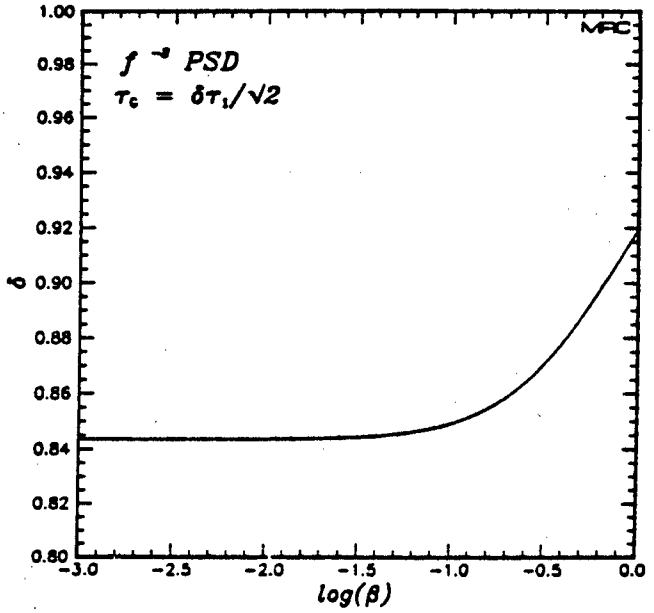

Figure A-4. τ_0 Scaling for an f^{-3} power spectral density.

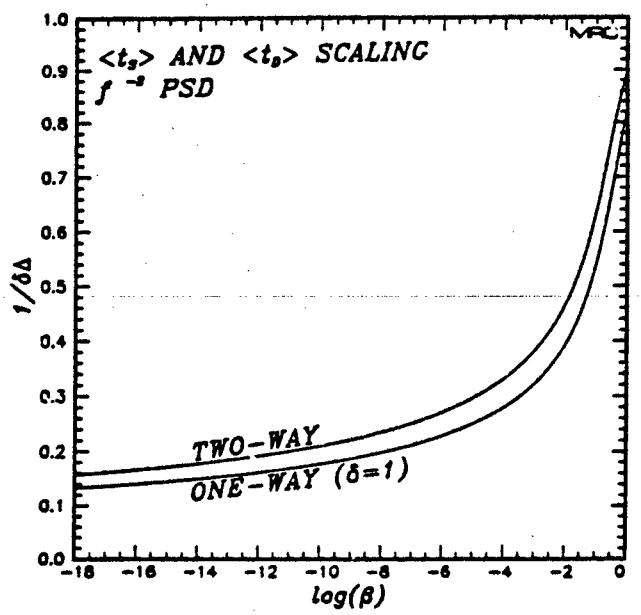

Figure A-5. Scaling of the mean separation and duration of fades and flares for an f^{-3} power spectral density.

to the decorrelation distance and the solution of Equation A-24. The inner scale t_o^{-1} can be estimated by noting that physically the PSD must go rapidly zero for frequencies that exceed the radio transmission frequency f_{RF}. The inner scale is then n/f_{RF} where n is a parameter which is the order of unity. The value of β is then determined by

$$\beta/x(\beta) = n/(\tau_1 f_{RF}) \qquad \text{(A-29)}$$

where $x(\beta)$ is the solution of Equation A-24 which is itself a function of β. This equation is easily inverted by plotting β versus $x(\beta)/\beta$ which is equal to $\tau_1 f_{RF}/n$. The results are shown on Figure A-6. Because $x(\beta)$ for $\beta \leq 10^{-2}$ is independent of β and constant at a value of 1.658, β is accurately given by

$$\beta = 1.658n/(\tau_1 f_{RF}), \quad \beta \leq 10^{-2} \; . \qquad \text{(A-30)}$$

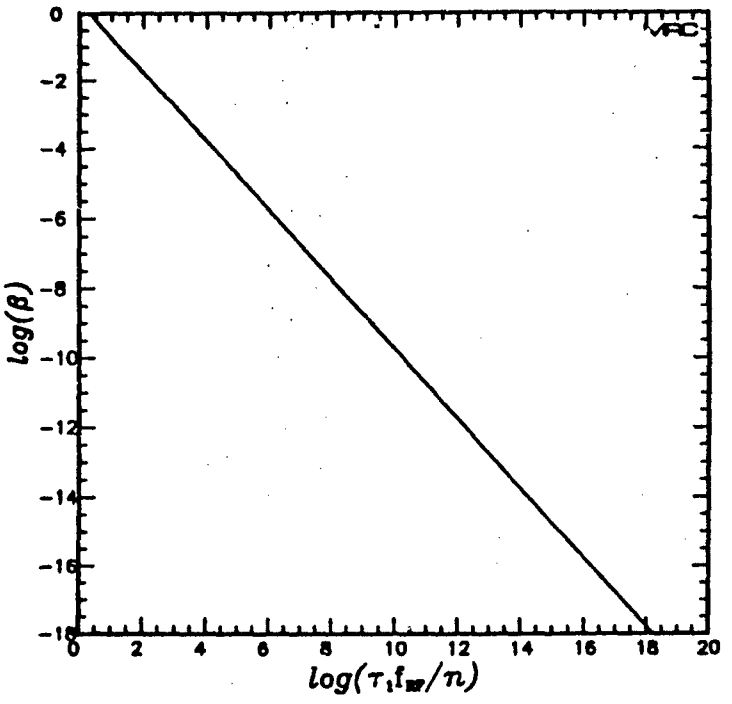

Figure A-6. β as a function of τ_1 and the transmission frequency f_{RF}.

The parameter β is a function of the decorrelation time and hence the scaling factors are also functions of τ_1.

The scaling factors for satellite systems with transmission frequencies in the range 250 MHz to 20 GHz are shown in Table VII for slow fading conditions. Typically, the one-way scaling factor $1/\Delta$ is 0.18 and the two-way scaling factor $1/\delta\Delta$ is 0.21.

Table VII. Slow fading (f^{-3} PSD) scaling factors for satellite systems.

f_{RF}(GHz)	τ_1 (sec)	log(β)*	δ	$1/\delta\Delta$	
				one-way	two-way
0.25	20	-9.5	0.844	0.182	0.216
1.2	10	-9.9	0.844	0.178	0.211
7.5	3	-10.1	0.844	0.176	0.209
20.0	2	-10.4	0.844	0.174	0.206

*n = 1

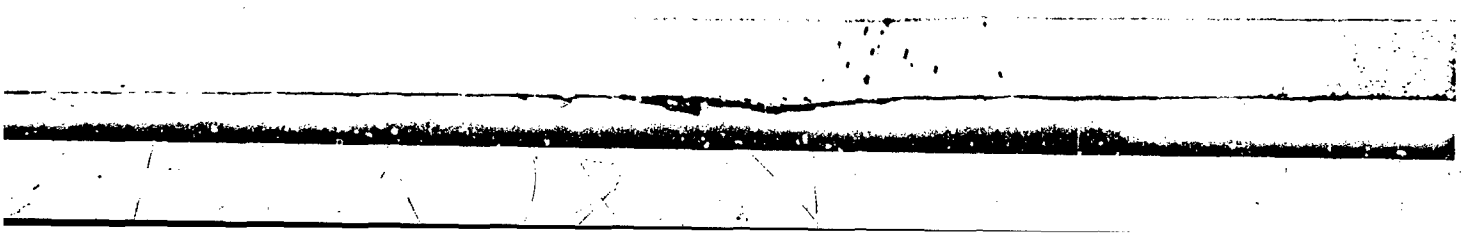

APPENDIX B
LEVEL CROSSING PROBLEM FOR BISTATIC PROPAGATION WITH INDEPENDENT SECOND ORDER STATISTICS

The mean number of level crossings is calculated in this Appendix for bistatic propagation where the second order statistics of the two paths are independent. The amplitudes of the one-way voltages of the two paths are assumed to be Rayleigh distributed and independent.

Let $\rho_1(\tau)$ and $\rho_2(\tau)$ denote the autocorrelation functions of the two paths. Both the power spectral densities, or equivalently the functional form of the autocorrelation functions, and the decorrelation times are allowed to differ. The calculation of the mean number of level crossings then follows the deviation of Section 4.

The joint probability density function of the amplitude and the time derivative of the amplitude for the i^{th} one-way propagation path is given by Equation 4-11 as

$$f(r,\dot{r}) = \frac{r\,\exp(-r^2/2\sigma^2)}{\sigma^2} \cdot \frac{\exp(-\tau_{1,i}\dot{r}^2/4\Delta_i^2\sigma^2)}{\sqrt{4\pi\Delta_i^2\sigma^2/\tau_{1,i}^2}} \qquad (B\text{-}1)$$

$$(i = 1 \text{ or } 2)$$

where Δ_i is defined in Equation 4-4 and $\tau_{1,i}$ is the one-way decorrelation time of the i^{th} path. The joint probability density function of

the amplitudes s and t of the two independent paths and of the time derivatives of s and t can be written as

$$f(s,\dot{s},t,\dot{t}) = \frac{ste^{-(s^2+t^2)/2\sigma^2}}{\sigma^4} \cdot \frac{\exp[-(\tau_{1,1}^2\dot{s}^2/\Delta_1^2+\tau_{1,2}^2\dot{t}^2/\Delta_2^2)/4\sigma^2]}{(4\pi\Delta_1\Delta_2\sigma^2/\tau_{1,1}\tau_{1,2})} \tag{B-2}$$

Using the same change of variables that was used in Section 4, the joint probability density function of the received amplitude z and the time derivative $\dot{z}$ becomes

$$f(z,\dot{z}) = (\tau_{1,1}\tau_{1,2}/4\pi\Delta_1\Delta_2\sigma^6) \int_0^\infty ds \int_{-\infty}^{\infty} d\dot{s}\ zs^{-2} \tag{B-3}$$

$$\times \exp\{-[s^2+z^2/s^2+\tau_{1,1}^2\dot{s}^2/2\Delta_1^2+\tau_{1,2}^2(\dot{z}^2s^{-2}+z^2\dot{s}^2s^{-4}-2z\dot{z}\dot{s}s^{-3})/2\Delta_2^2]/2\sigma^2\} .$$

Only the $\dot{s}$ integral can be performed in closed form which reduces Equation B-3 to

$$f(z,\dot{z}) = (\tau_{1,1}z/2\sqrt{\pi}\Delta_1\sigma^5) \int_0^\infty ds\ (\zeta s^4+z^2)^{-1/2}$$

$$\times \exp\{-[s^2+z^2s^{-2}+\tau_{1,2}^2\zeta s^2(\zeta s^4+z^2)^{-1}\dot{z}^2/2\Delta_1^2]/2\sigma^2\} \tag{B-4}$$

where

$$\zeta = \tau_{1,1}^2\Delta_2^2/(\tau_{1,2}^2\Delta_1^2) . \tag{B-5}$$

The mean number of level crossings is obtained by substituting Equation B-4 into Equation 4-3 and performing the integral over $\dot{z}$. After changing the variables in the remaining integral to $u = s/\sigma$, using Equation 2-12 to write σ^4 in terms of the mean received power $\langle S \rangle$, and using Equation 2-26 to write $\tau_{1,1}$ in terms of the decorrelation time of the received signal, the mean number of crossing of the power level L becomes

$$\langle N(L,T) \rangle = \delta a_1 (T/\tau_0) \left[\frac{16L/\pi \langle S \rangle}{1+(\tau_{1,1}/\tau_{1,2})^2} \right]^{1/2} \tag{B-6}$$

$$\times \int_0^\infty \sqrt{\zeta + 4L/\langle S \rangle u^4} \exp\{-[1+4L/\langle S \rangle u^4] u^2/2\} \, du$$

This expression reduces to Equation 4-26 when $\tau_{1,1} = \tau_{1,2}$ and $\Delta_1 = \Delta_2$.

APPENDIX C
MPS RESULTS

The first four moments of the amplitudes of the five MPS realizations that have been analyzed for this report are presented in Table VIII. Each realization consists of 16384 amplitude samples and the corresponding phases. The data have been normalized so that the average power is unity. Hence $\langle z^2 \rangle$ is identically one in each case. The other moments show close agreement with Rayleigh values.

Table VIII: Amplitude statistics of the MPS data.

Realization	$\langle z^n \rangle / E[z^n]$*			
	n = 1	n = 2	n = 3	n = 4
8091	1.001	1.000	1.001	1.005
8094	0.993	1.000	1.021	1.058
8143	0.998	1.000	1.001	1.000
8642	1.000	1.000	0.999	0.995
9069	0.994	1.000	1.013	1.034

*$\langle z^n \rangle$ denotes the average from 16384 MPS samples
$E[z^n]$ denotes the Rayleigh value

The realizations differ in the number of samples, n, per decorrelation time which varies from 72.8 for MPS 8091 to 3.35 for MPS 8143. In the latter case, the statistics of deep fade durations will be unreliable because almost all of the deep fades will last for just one sample. With this in mind, the means, medians, standard deviations, and mean-to-standard deviation ratios are presented in Tables IX through XIII for the five MPS realizations.

Table IX: Statistics of fades for the MPS 8091 realization.

L/<s> (dB)	n**	<N(L,τ_0)>	Duration of Fades					Separation of Fades				
			No*	Mean*	Std. Dev.*	Median*	μ/σ	No*	Mean*	Std. Dev.*	Median*	μ/σ
0	72.8	1.00	112	1.20	1.33	0.772	0.900	112	1.93	1.59	1.72	1.21
-3	72.8	1.22	137	0.645	0.693	0.453	0.930	136	1.64	1.28	1.34	1.28
-5	72.8	1.07	120	0.496	0.406	0.358	1.27	119	1.87	1.44	1.62	1.30
-10	72.8	0.736	83	0.249	0.251	0.178	0.993	82	2.71	2.22	2.17	1.22
-15	72.8	0.391	44	0.151	0.118	0.096	1.28	43	5.17	5.48	3.63	1.944

*Normalized to τ_0

*Number of samples of the duration or separation

**Number of voltage samples per τ_0

Table X: Statistics of fades for the MPS 8094 realization.

L/<s> (dB)	n**	<N(L,τ_0)>	Duration of Fades					Separation of Fades				
			No*	Mean*	Std. Dev.*	Median*	μ/σ	No*	Mean*	Std. Dev.*	Median*	μ/σ
0	19.3	0.737	312	1.75	1.63	1.24	1.07	311	2.71	1.92	2.28	1.41
-3	19.3	0.875	371	0.924	0.788	0.672	1.17	370	2.28	1.48	1.91	1.54
-5	19.3	0.862	365	0.655	0.539	0.466	1.21	364	2.32	1.64	1.91	1.41
-10	19.3	0.600	254	0.336	0.288	0.207	1.17	253	3.32	2.78	2.43	1.20
-15	19.3	0.383	162	0.172	0.129	0.103	1.2	261	5.19	5.17	3.72	1.00

*Normalized to τ_0

*Number of samples of the duration or separation

**Number of voltage samples per τ_0

Table XI: Statistics of fades for the MPS 8143 realization.

L/<S> (dB)	n**	<N(L,τ_0)>	Duration of Fades					Separation of Fades				
			No+	Mean*	Std. Dev.*	Median*	μ/σ	No+	Mean*	Std. Dev.*	Median*	μ/σ
0	3.35	0.631	1543	1.99	1.72	1.19	1.16	1542	3.17	1.89	2.39	1.67
-3	3.35	0.725	1775	1.09	0.874	0.598	1.25	1774	2.76	1.54	2.09	1.79
-5	3.35	0.688	1686	0.802	0.607	0.299	1.32	1685	2.90	1.80	2.09	1.61
-10	3.35	0.[illegible]	1051	0.460	0.290	0.299	1.58	1050	4.66	3.95	3.29	1.18
-15	3.35	0.184	452	0.355	0.146	0.299	2.44	451	10.7	10.3	7.15	1.04

*Normalized to τ_0

+Number of samples of the duration or separation

**Number of voltage samples per τ_0

Table XII: Statistics of fades for the MPS 8642 realization.

L/<S> (dB)	n**	<N(L,τ_0)>	Duration of Fades					Separation of Fades				
			No+	Mean*	Std. Dev.*	Median*	μ/σ	No+	Mean*	Std. Dev.*	Median*	μ/σ
0	3.48	0.565	1328	2.24	1.93	1.44	1.16	1372	3.54	2.14	2.87	1.65
-3	3.48	0.650	1529	1.21	0.998	0.574	1.21	1528	3.08	1.69	2.30	1.82
-5	3.48	0.615	1447	0.885	0.698	0.287	1.27	1446	3.25	2.02	2 58	1.61
-10	3.48	0.399	939	0.497	0.347	0.287	1.43	938	5.01	4.20	3.44	1.19
-15	3.48	0.172	404	0.371	0.209	0.287	1.78	403	11.6	12.0	7.18	0.967

*Normalized to τ_0

+Number of samples of the duration or separation

**Number of voltage samples per τ_0

Table XIII: Statistics of fades for the MPS 9069 realization.

L/<S> (dB)	n**	<N(L,τ0)>	Duration of Fades					Separation of Fades				
			No+	Mean*	Std. Dev.*	Median*	μ/σ	No+	Mean*	Std. Dev.*	Median*	μ/σ
0	10.5	0.554	433	2.30	2.44	1.34	0.943	432	3.61	2.60	2.77	1.39
-3	10.5	0.664	519	1.21	1.08	0.763	1.12	518	3.01	1.93	2.48	1.56
-5	10.5	0.616	481	0.923	0.801	0.572	1.15	480	3.24	2.28	2.48	1.42
-10	10.5	0.442	345	0.453	0.354	0.286	1.28	344	4.52	4.60	2.86	0.983
-15	10.5	0.261	204	0.259	0.184	0.095	1.41	203	7.67	8.93	4.86	0.859

*Normalized to τ_0

+Number of samples of the duration or separation

**Number of voltage samples per τ_0

The average and the standard deviation of the MPS scaling factors for the mean duration and separation of fades and flares have been calculated from the ratio of the mean number of level crossings for the MPS realizations to the mean number of level crossings for a Gaussian power spectral density. The mean scaling factor is calculated as

$$\langle 1/\Delta \rangle = \frac{1}{5} \sum_{\ell=1}^{5} \langle N(L_\ell, \tau_0) \rangle_G / \langle N(L_\ell, \tau_0) \rangle_{MPS} \qquad (C\text{-}1)$$

where L_ℓ, ℓ = 1 through 5, are the five levels of the tabulated MPS data. The mean duration and separation data are not included in the average because these values are more sensitive to the number of amplitude samples per decorrelation time and are not independent of the mean number

of level crossings. The results are shown in Table XIV. Realizations 8143, 8642, and 9069 all have average values of $1/\Delta$ of about unity which indicates that their power spectral densities are nearly Gaussian. The power spectral densities of the other two realizations can be estimated by using $\langle 1/\Delta \rangle$ and the one-way curve of Figure A-2 to find an effective $f^{-\mu}$ dependence. The power spectral density is then approximately $f^{-3.8}$ for MPS 8091 and is $f^{-4.7}$ for MPS 8094.

Table XIV: Average Scaling Factors ($1/\Delta$).

Realization	$\langle 1/\Delta \rangle$	Std. Dev. ($1/\Delta$)
8091	0.617	0.054
8094	0.763	0.030
8143	1.077	0.240
8642	1.180	0.238
9069	1.048	0.015

APPENDIX D

PROBABILITY DENSITY FUNCTIONS AND CUMULATIVE PROBABILITY DISTRIBUTIONS FOR ONE-WAY SCINTILLATION

The probability density function histograms and cumulative distributions of the duration and separation of fades or flares under Rayleigh fading conditions with a Gaussian power spectral density are presented here for oneway propagation. All levels are relative to the mean power. In a few cases noted on the figures, the data have been rebinned to give the probability density histograms a more continuous appearance. Otherwise, each interval of the histogram corresponds to one sample of the received voltage sequences. The mean (μ), median (M), standard deviation (σ), (all normalized to τ_0) and number of samples are indicated on the figures. For fades 15 dB below the mean power and flares 5 d3 above the mean power, the conflicting conditions of short durations, which requires a large number of samples per decorrelation time, and long intervals between events resulted in about 10 and 20 percent of the separation data respectively exceeding the separation histogram array size. However, because the moments were calculated from the raw data and less than 20 percent of the data were effected, the mean, standard deviation, and median values are uneffected by the improper array sizes.

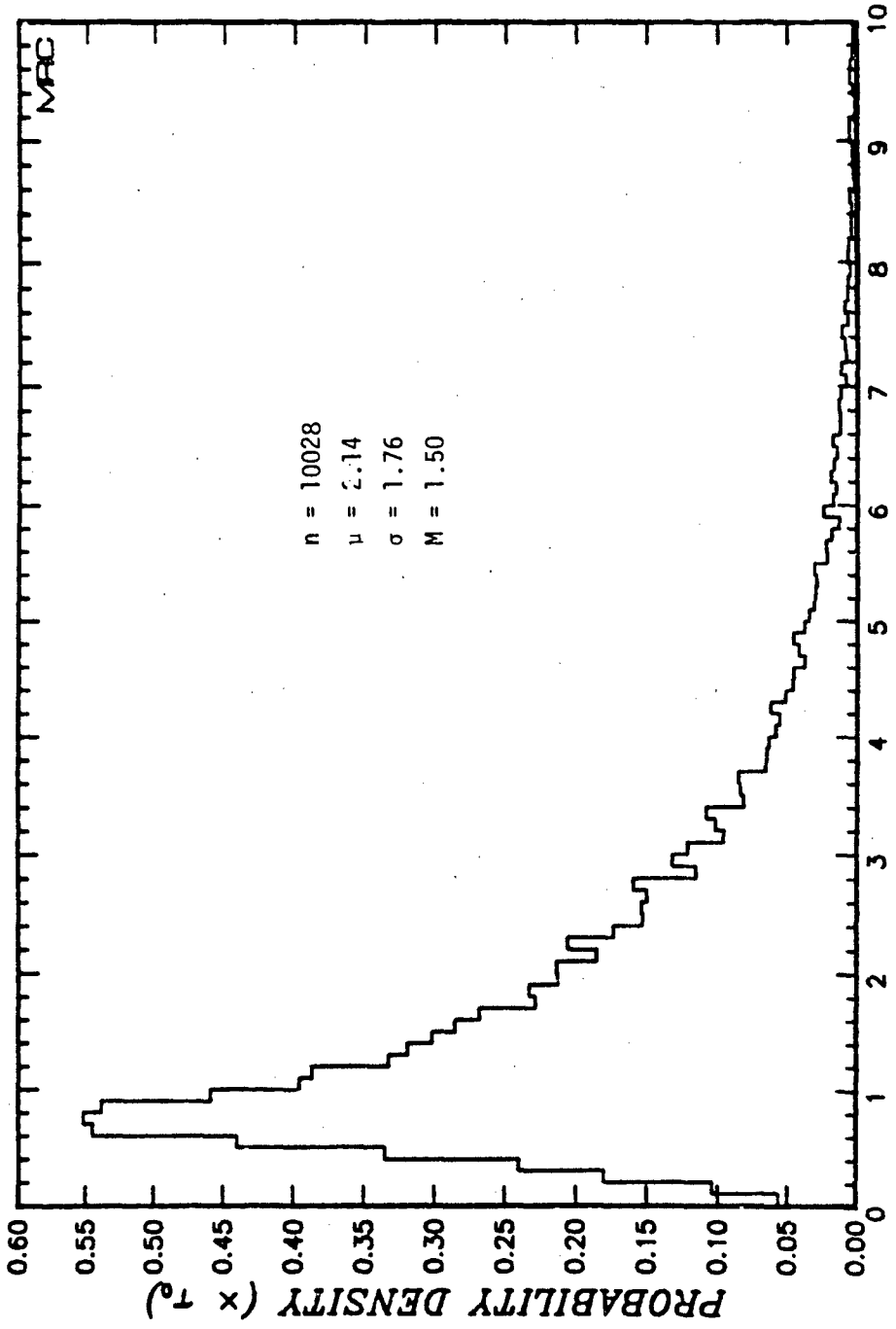

Figure D-1. Probability density function of the duration of fades below 0 dB.

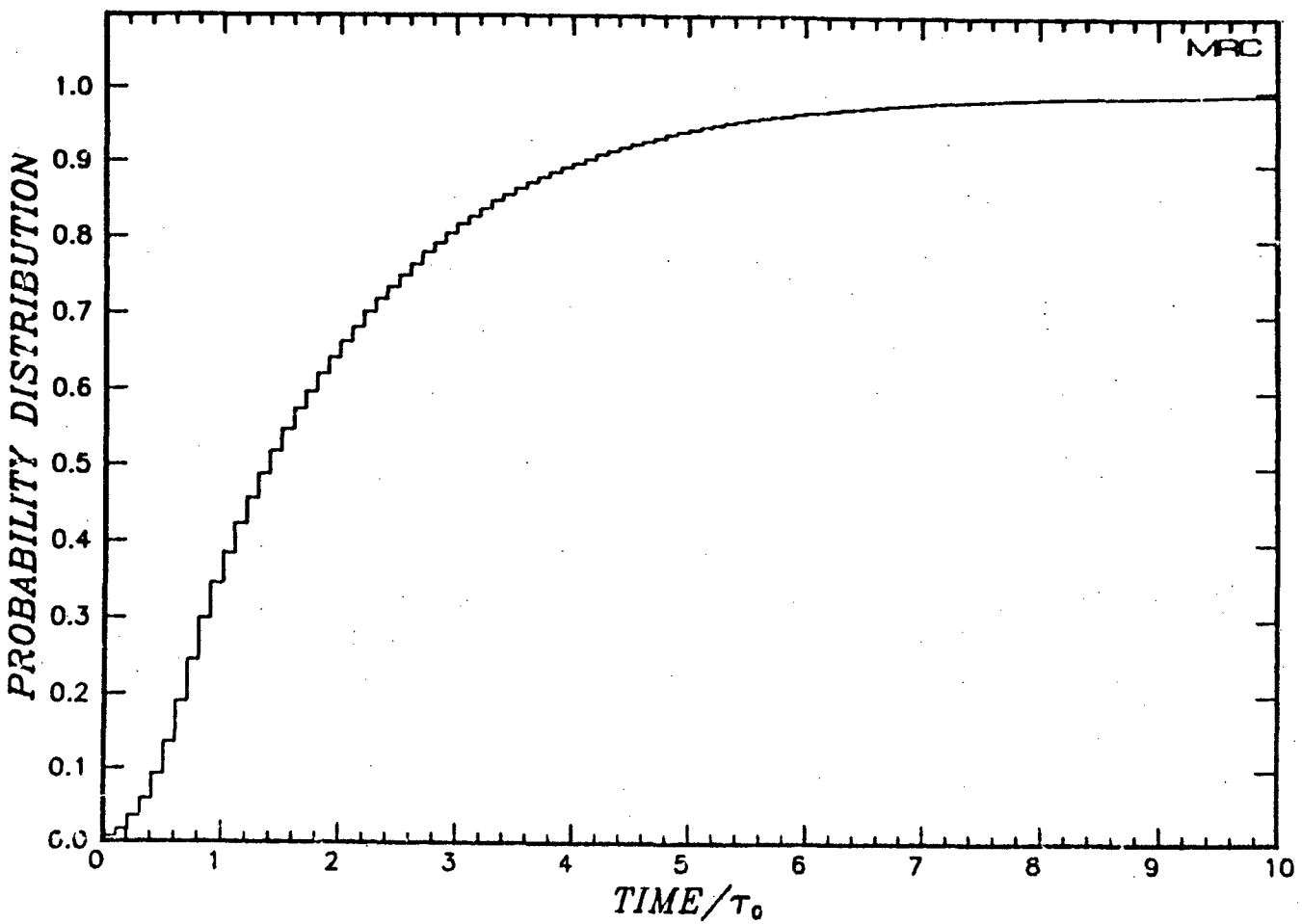

Figure D-2. Cumulative probability distribution of the duration of fades below 0 dB.

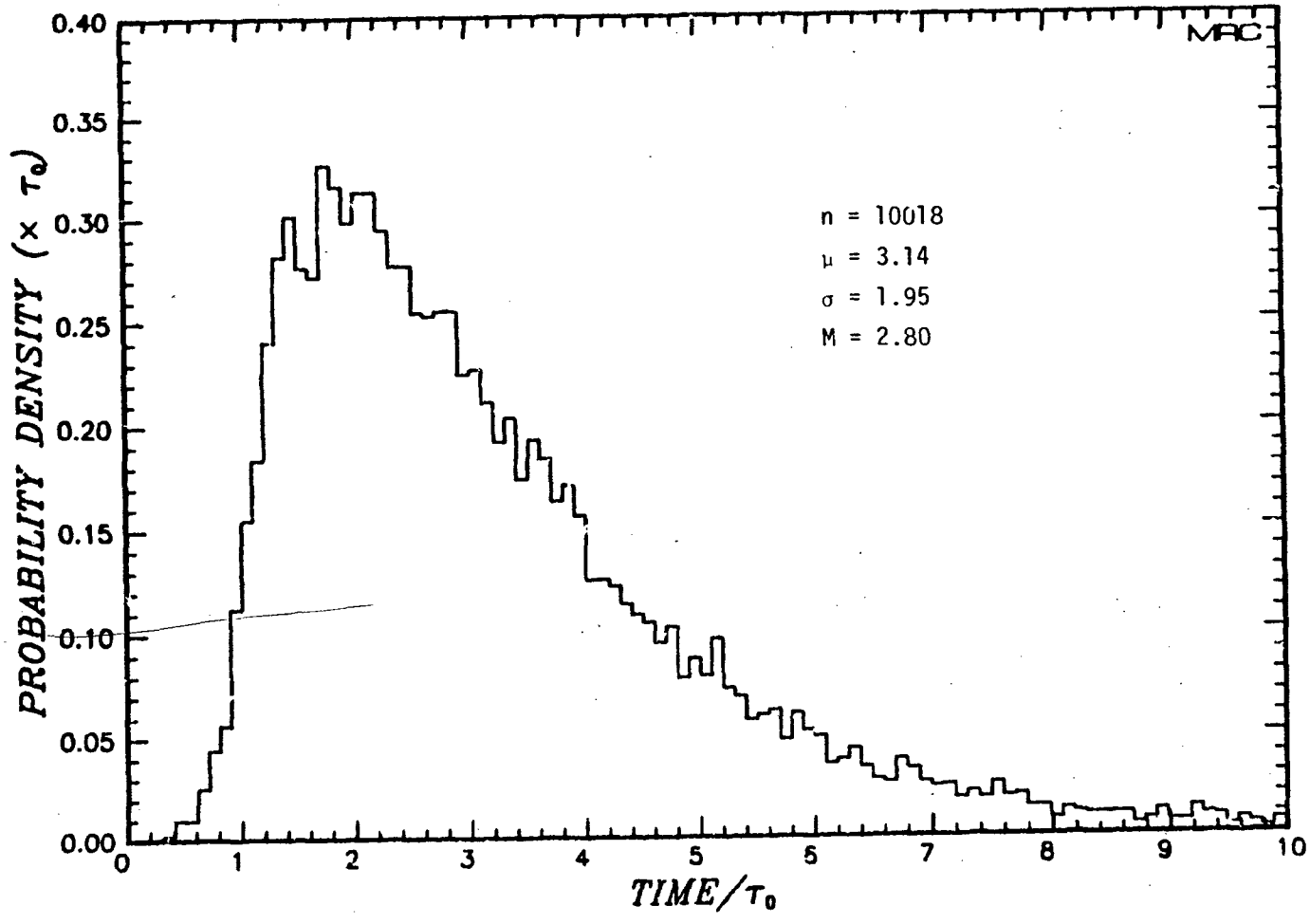

Figure D-3. Probability density function of the separation of fades below 0 dB.

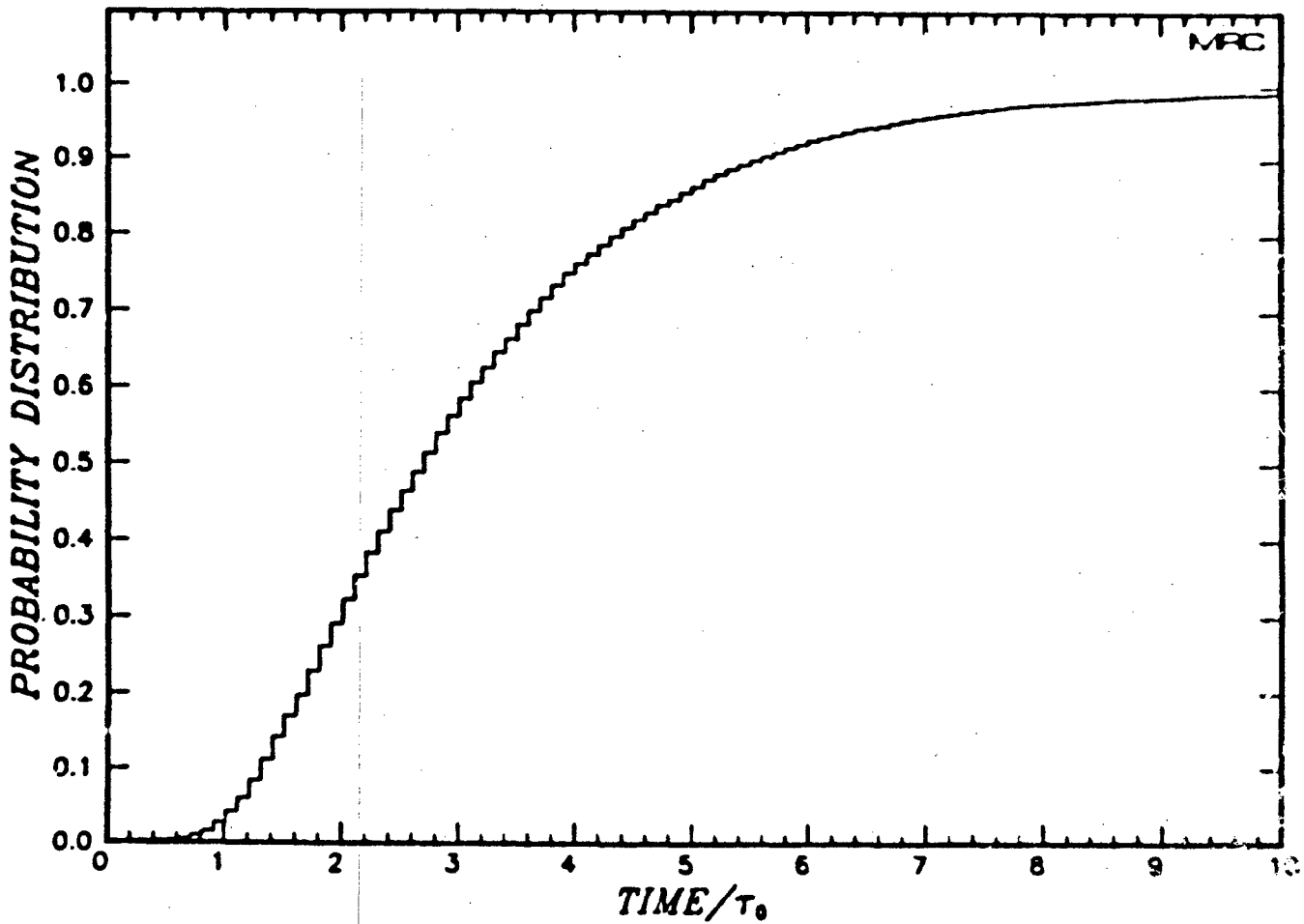

Figure D-4. Cumulative probability distribution of the separation of fades below 0 dB.

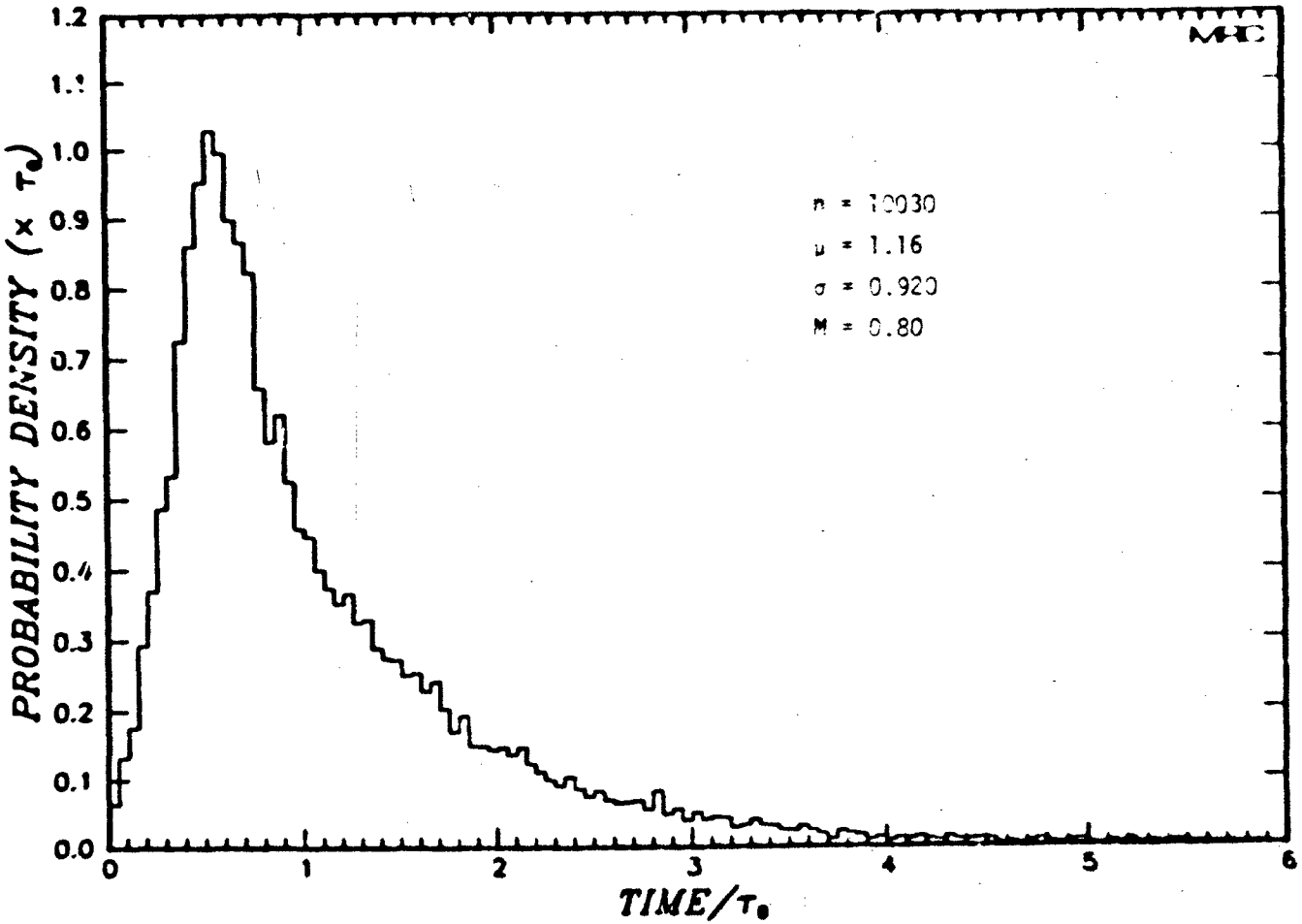

Figure D-5. Probability density function of the duration of fades below -3 dB.

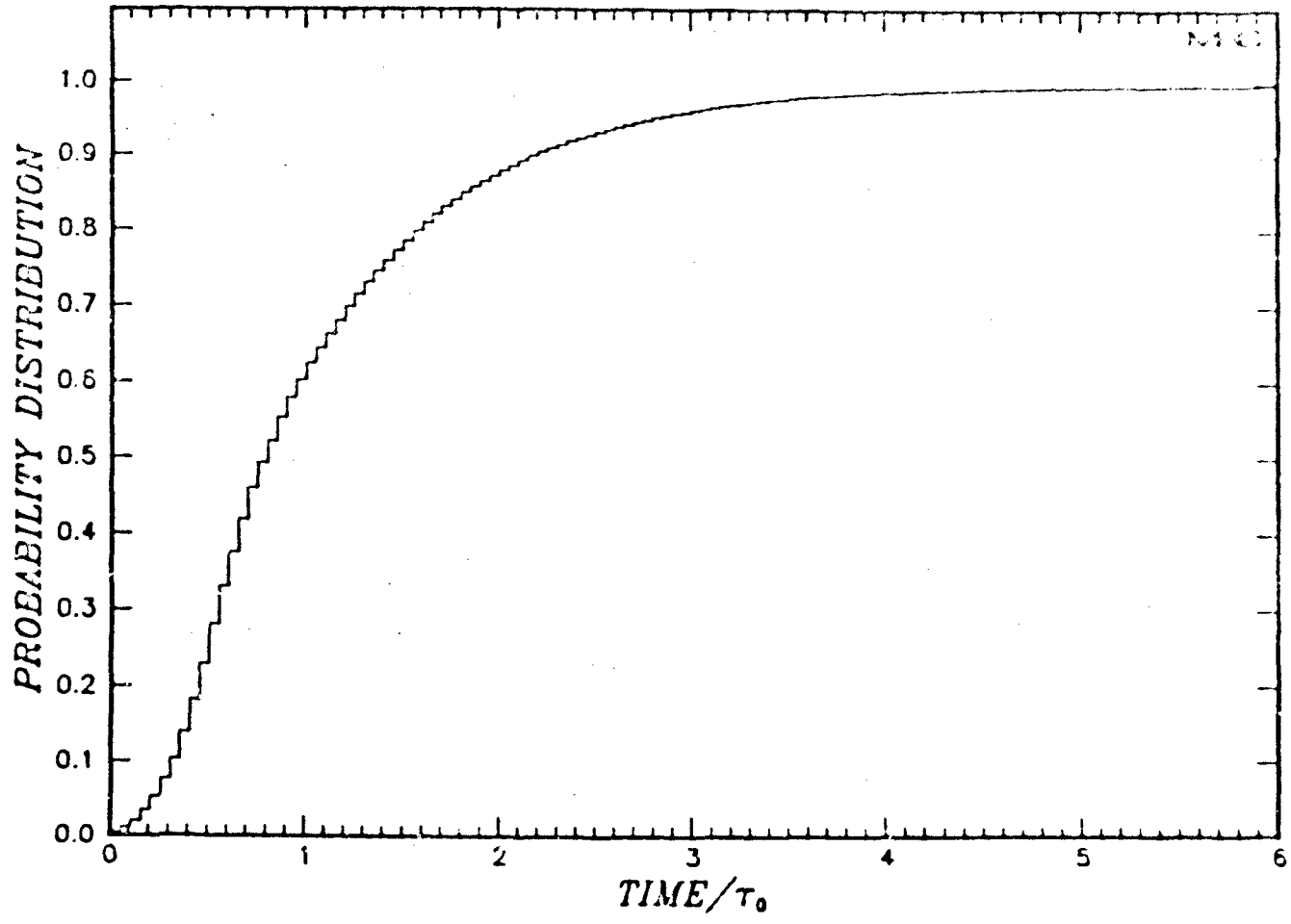

Figure D-6. Cumulative probability distribution of the duration of fades below -3 dB.

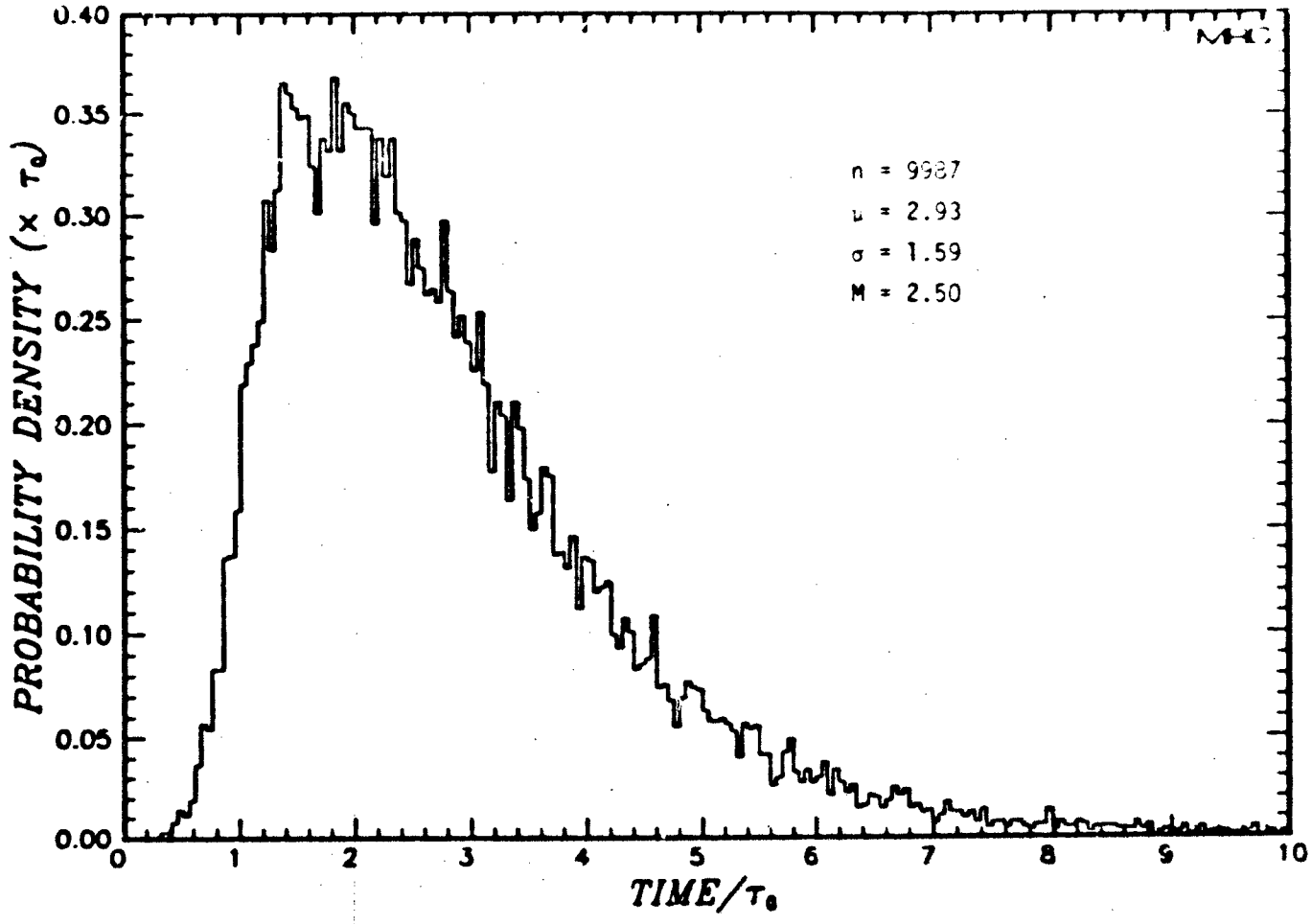

Figure D-7. Probability density function of the separation of fades below -3 dB.

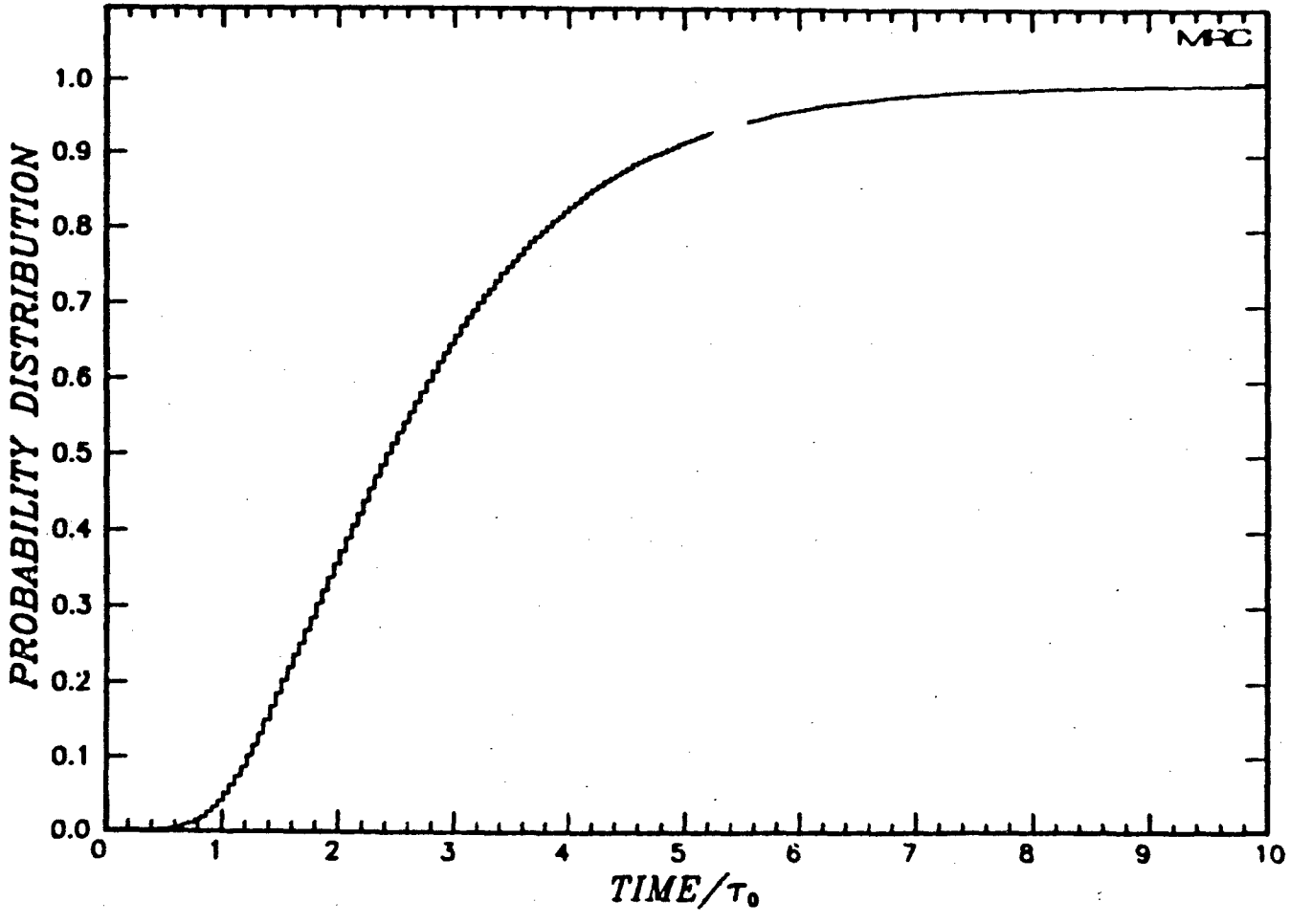

Figure D-8. Cumulative probability distribution of the separation of fades below -3 dB.

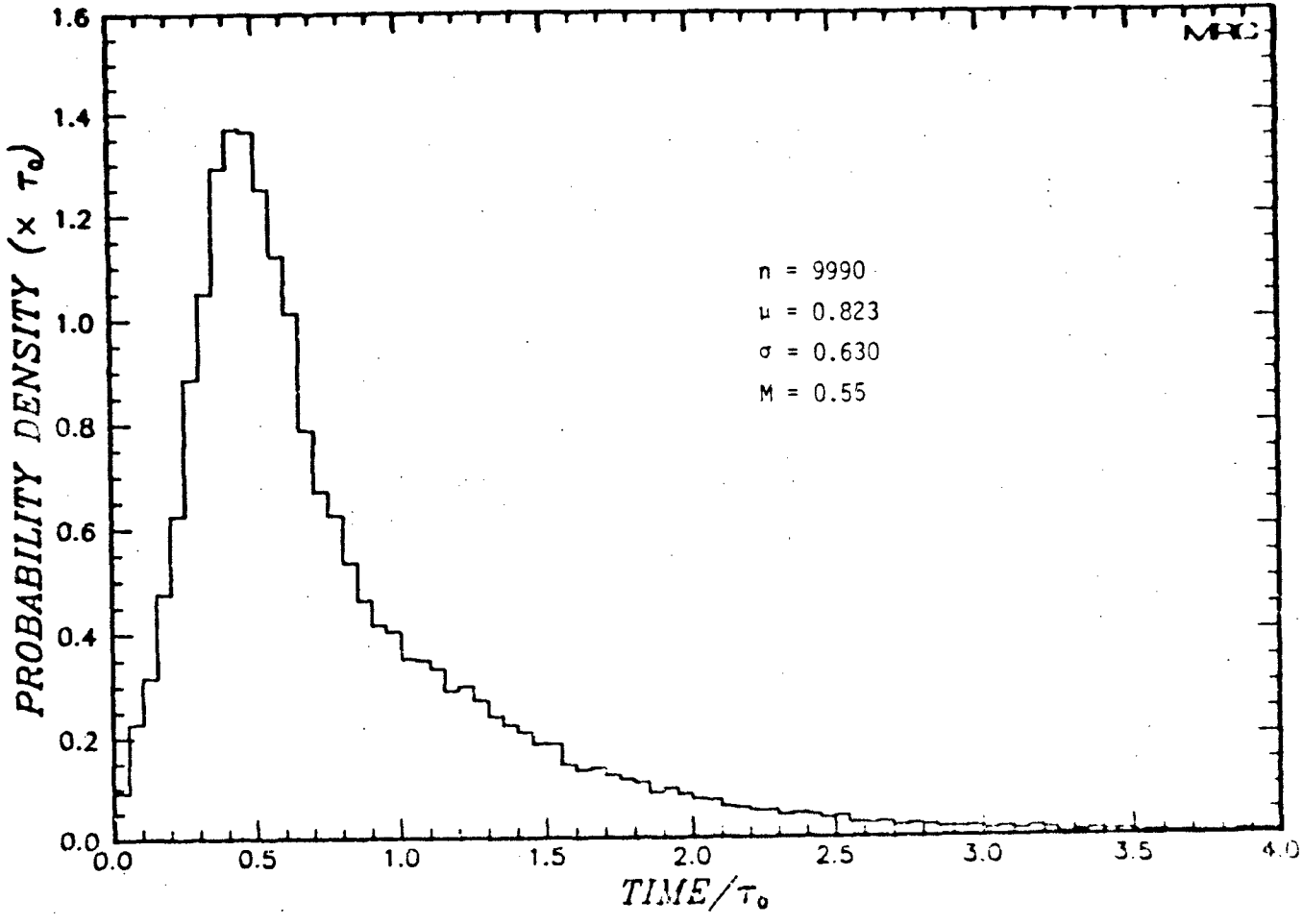

Figure B-9. Probability density function of the duration of fades below -5 dB.

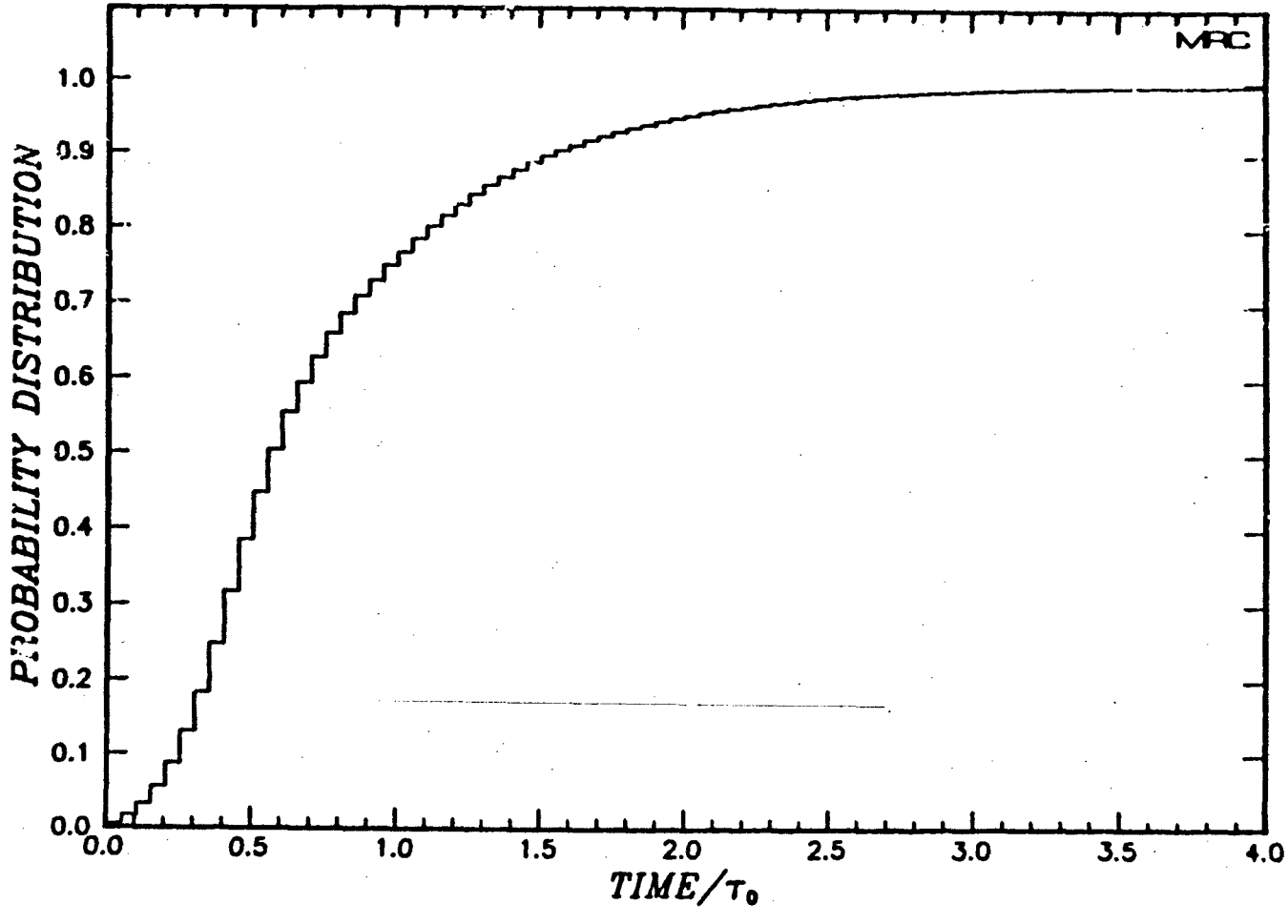

Figure D-10. Cumulative probability distribution of the duration of fades below -5 dB.

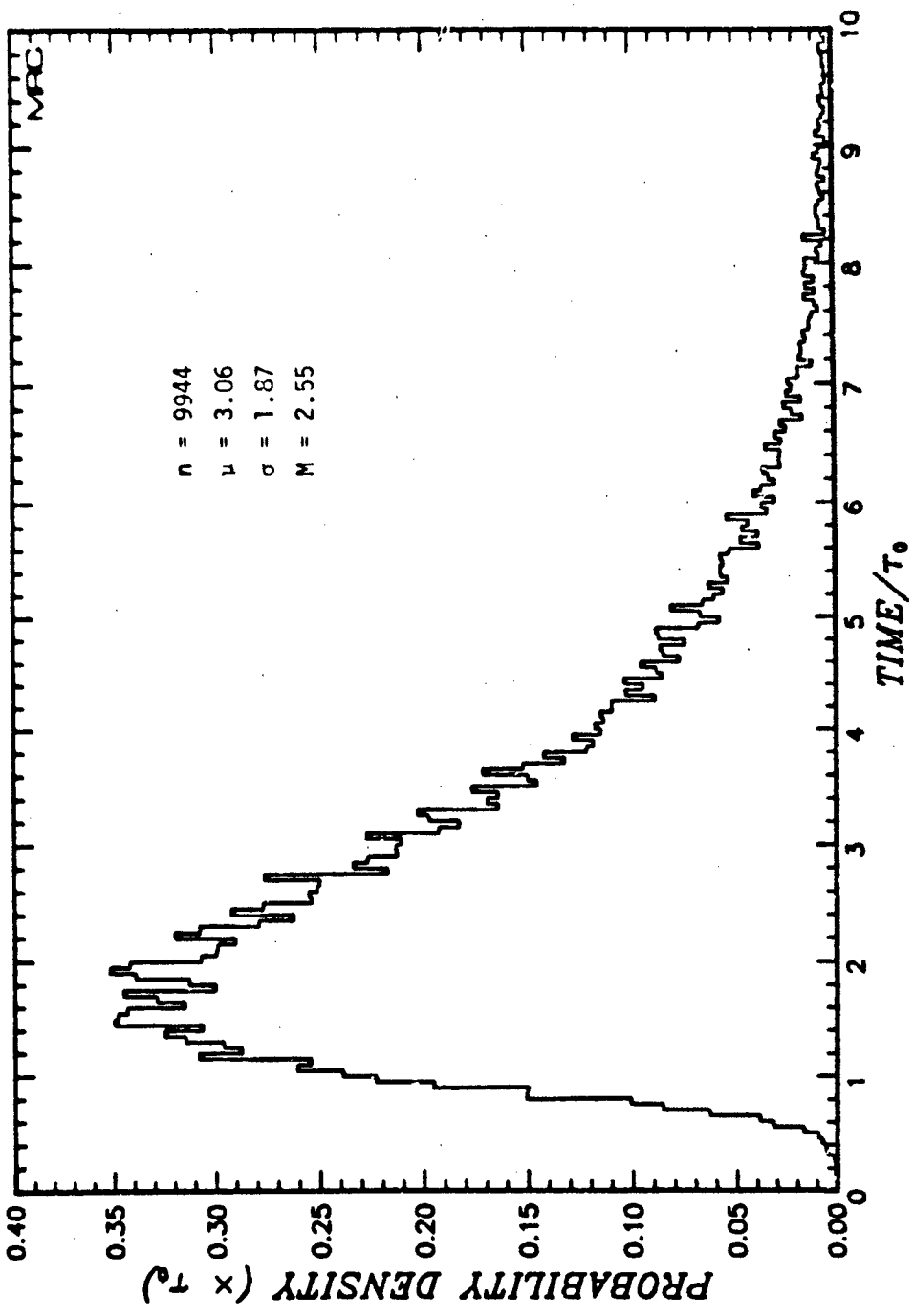

Figure D-11. Probability density function of the separation of fades below -5 dB.

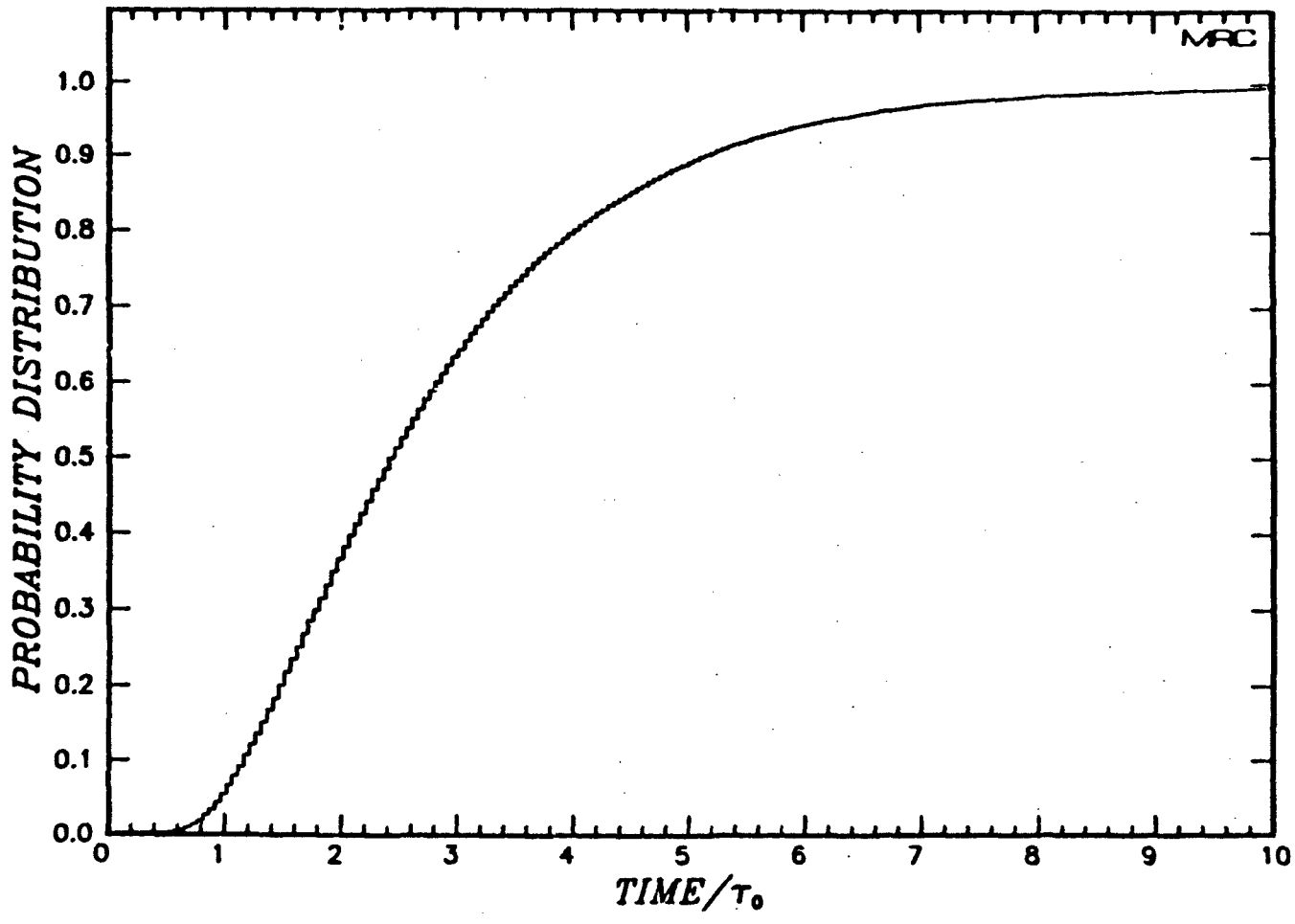

Figure D-12. Cumulative probability distribution of the separation of fades below -5 dB.

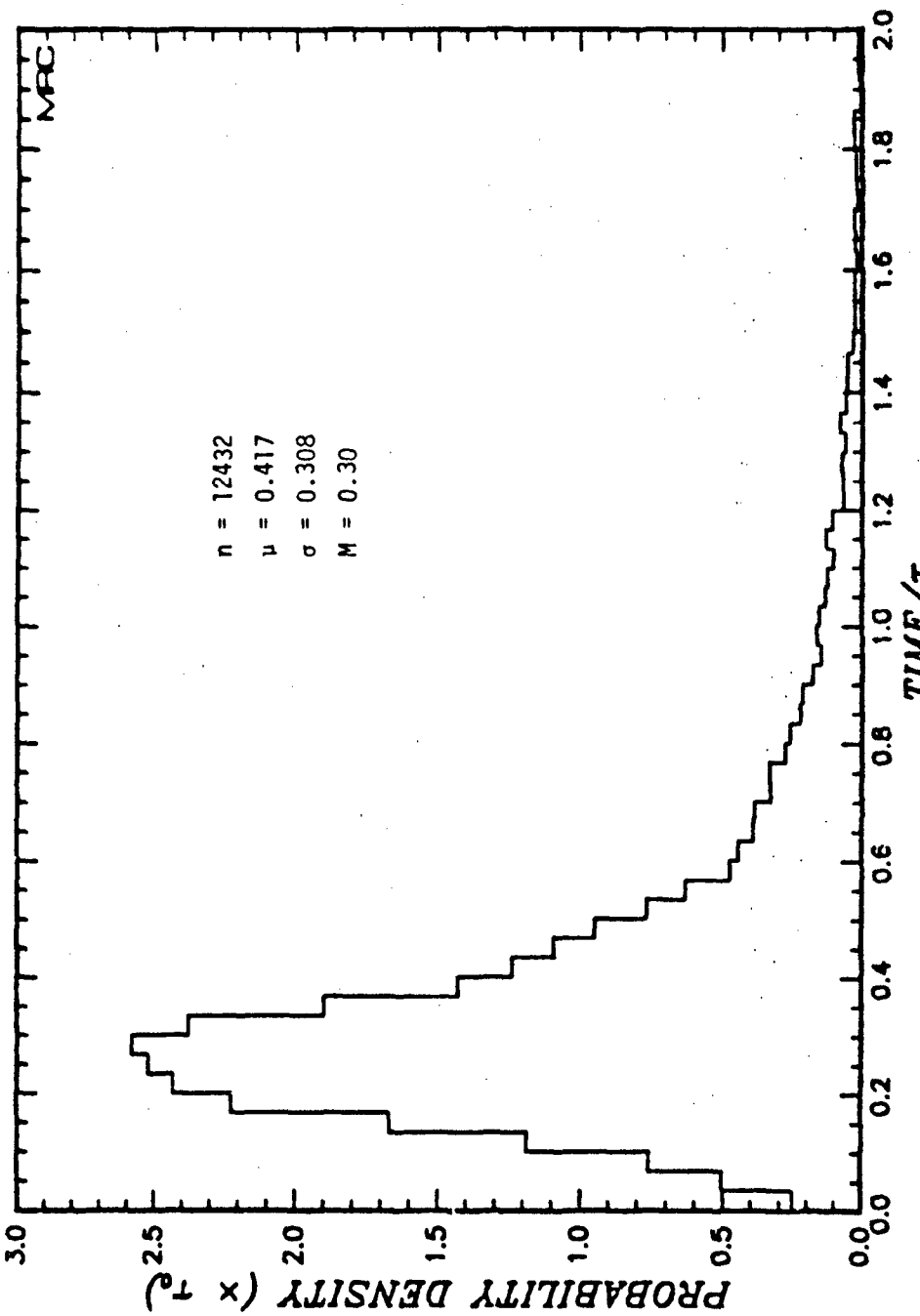

Figure D-13. Probability density function of the duration of the fades below -10 dB.

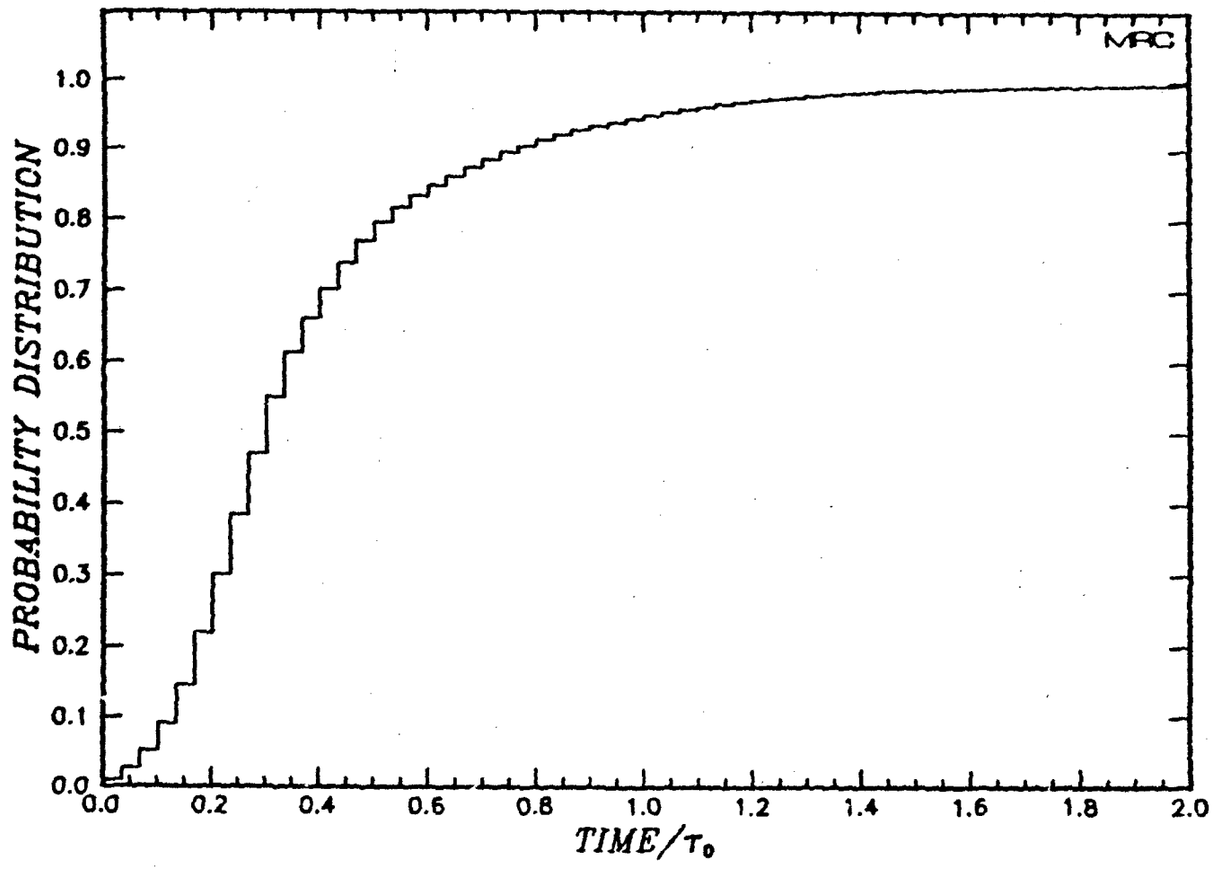

Figure D-14. Cumulative probability distribution of the duration of fades below -10 dB.

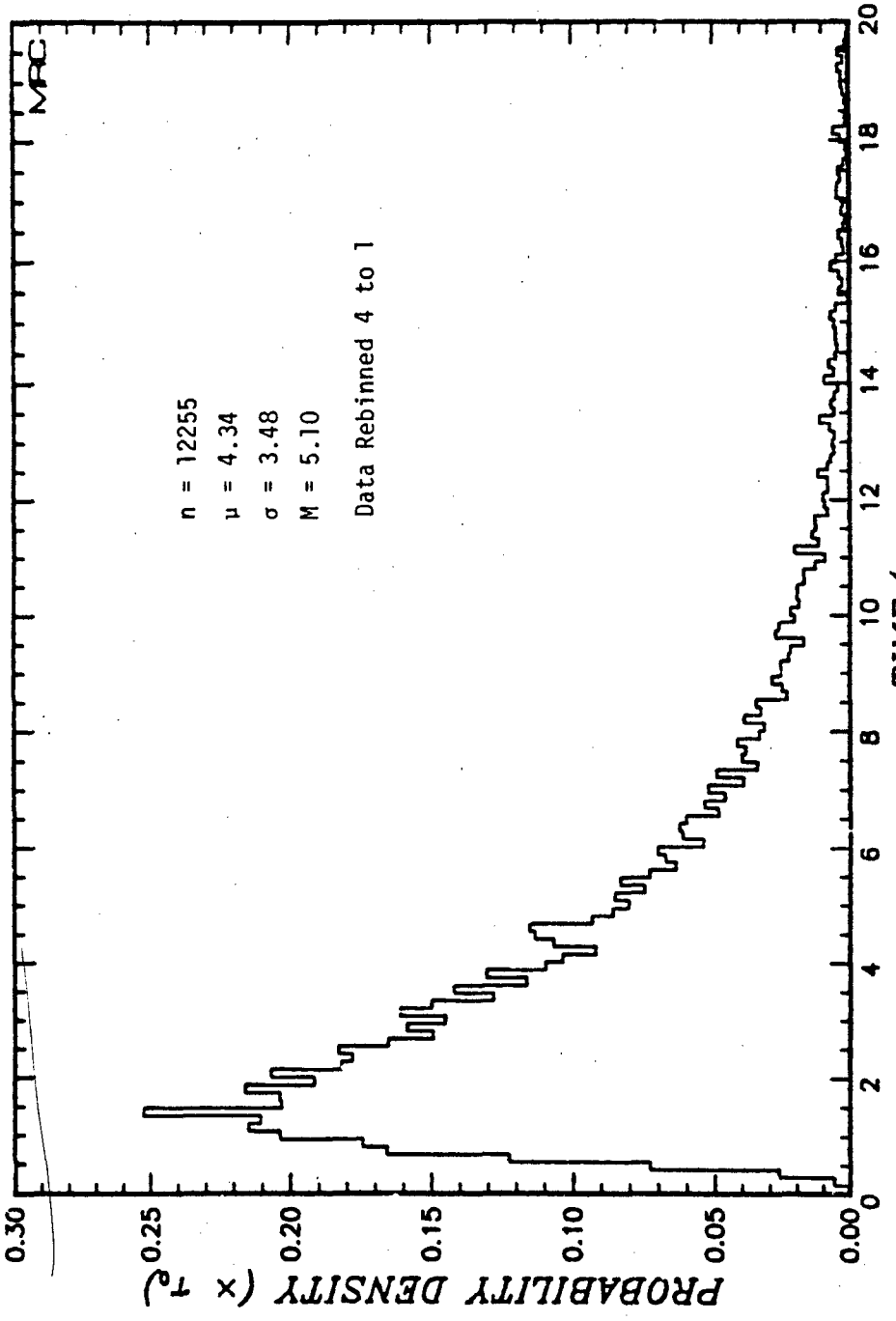

Figure D-15. Probability density function of the separation of fades below -10 dB.

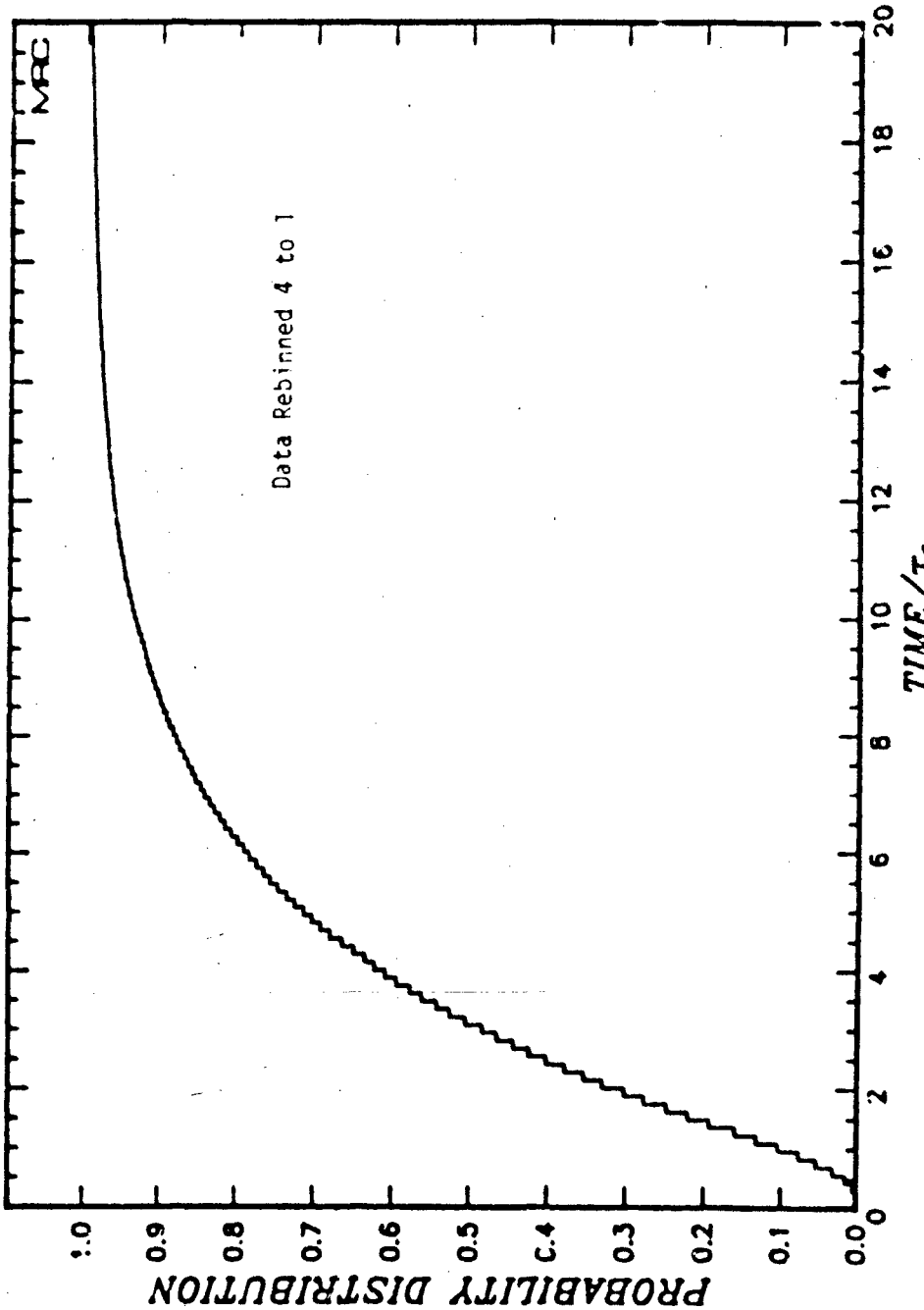

Figure D-16. Cumulative probability distribution of the separation of fades below -10 dB.

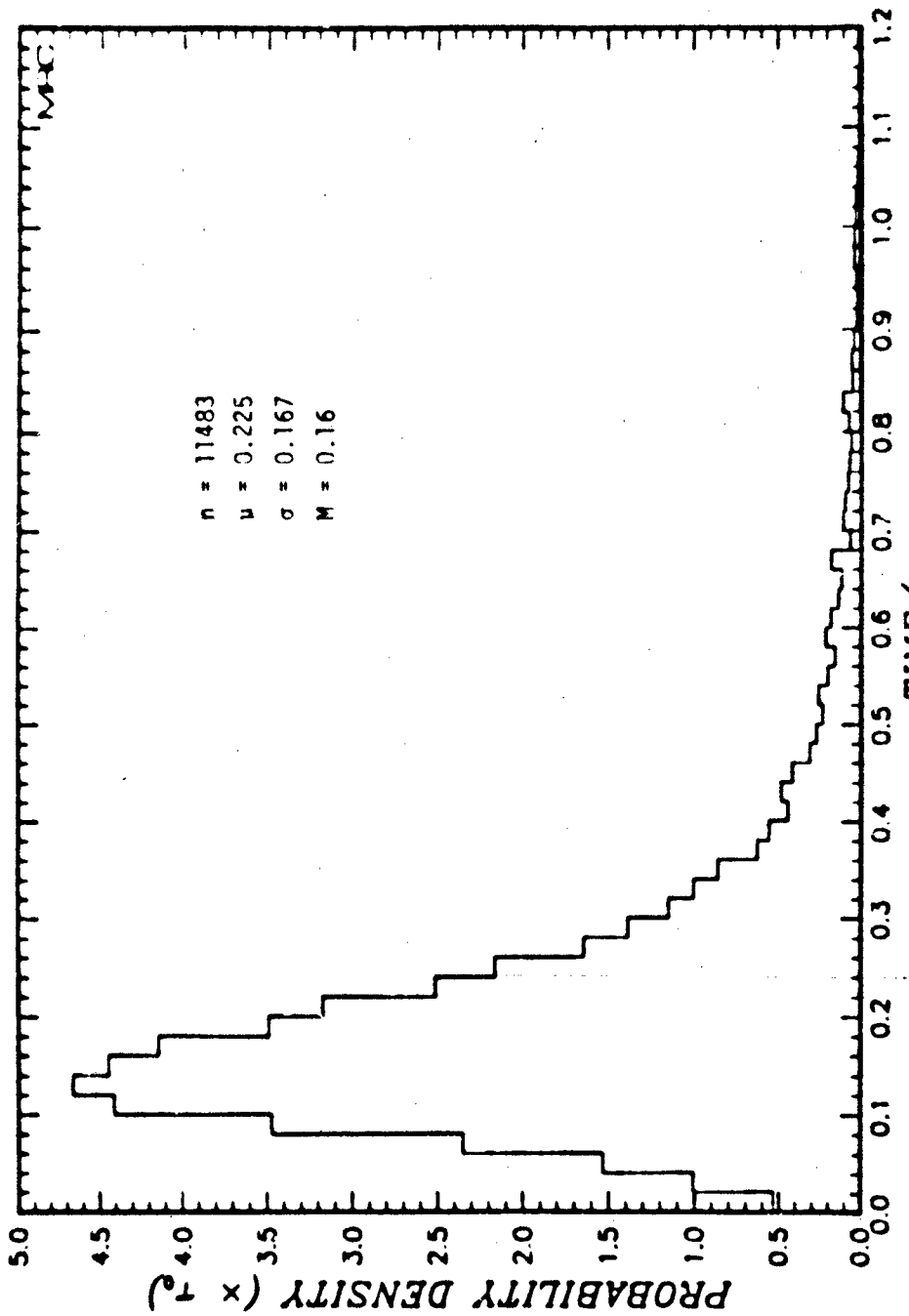

Figure D-17. Probability density function of the duration of fades below -15 dB.

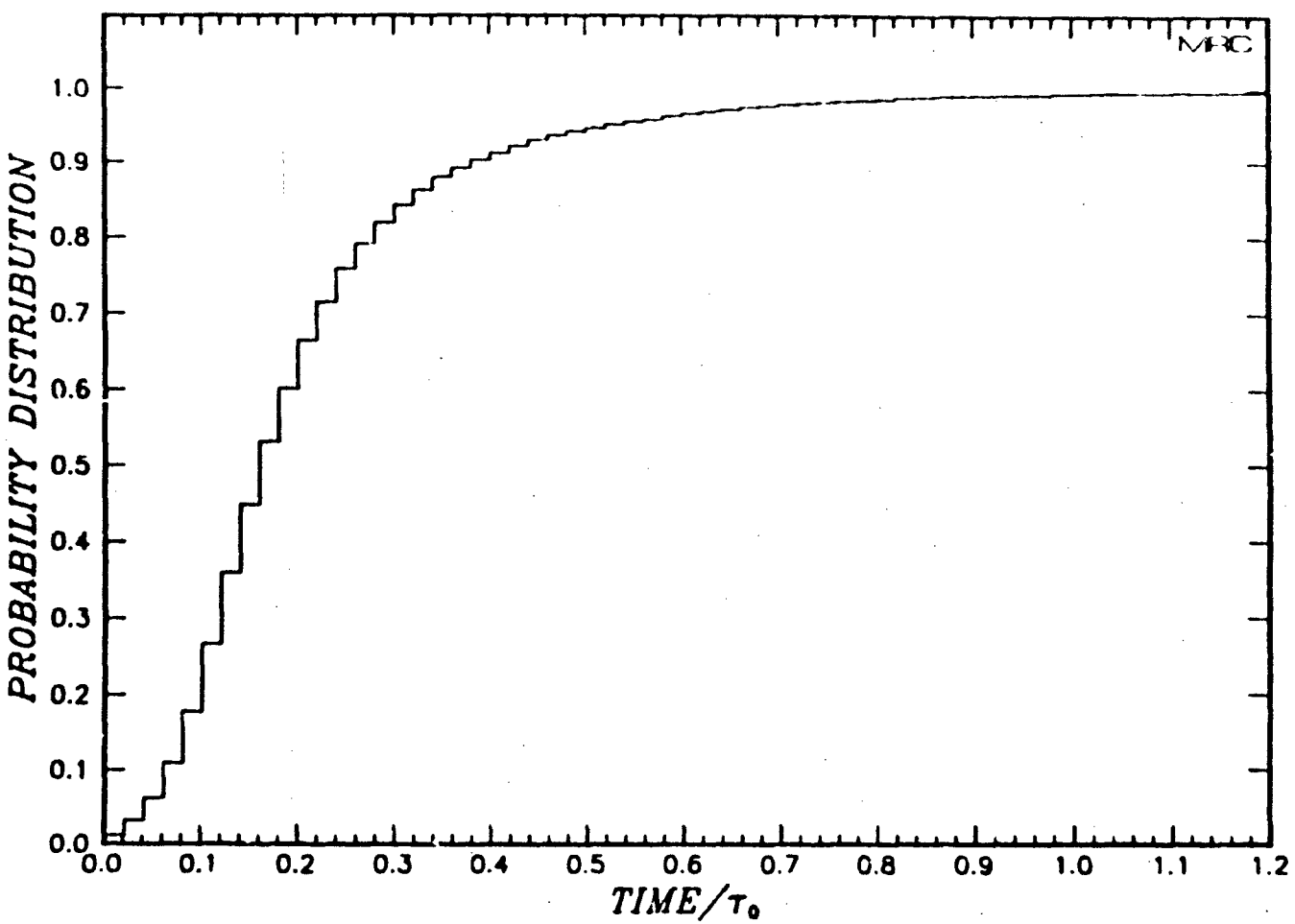

Figure D-18. Cumulative probability distribution of the duration of fades below -15 dB.

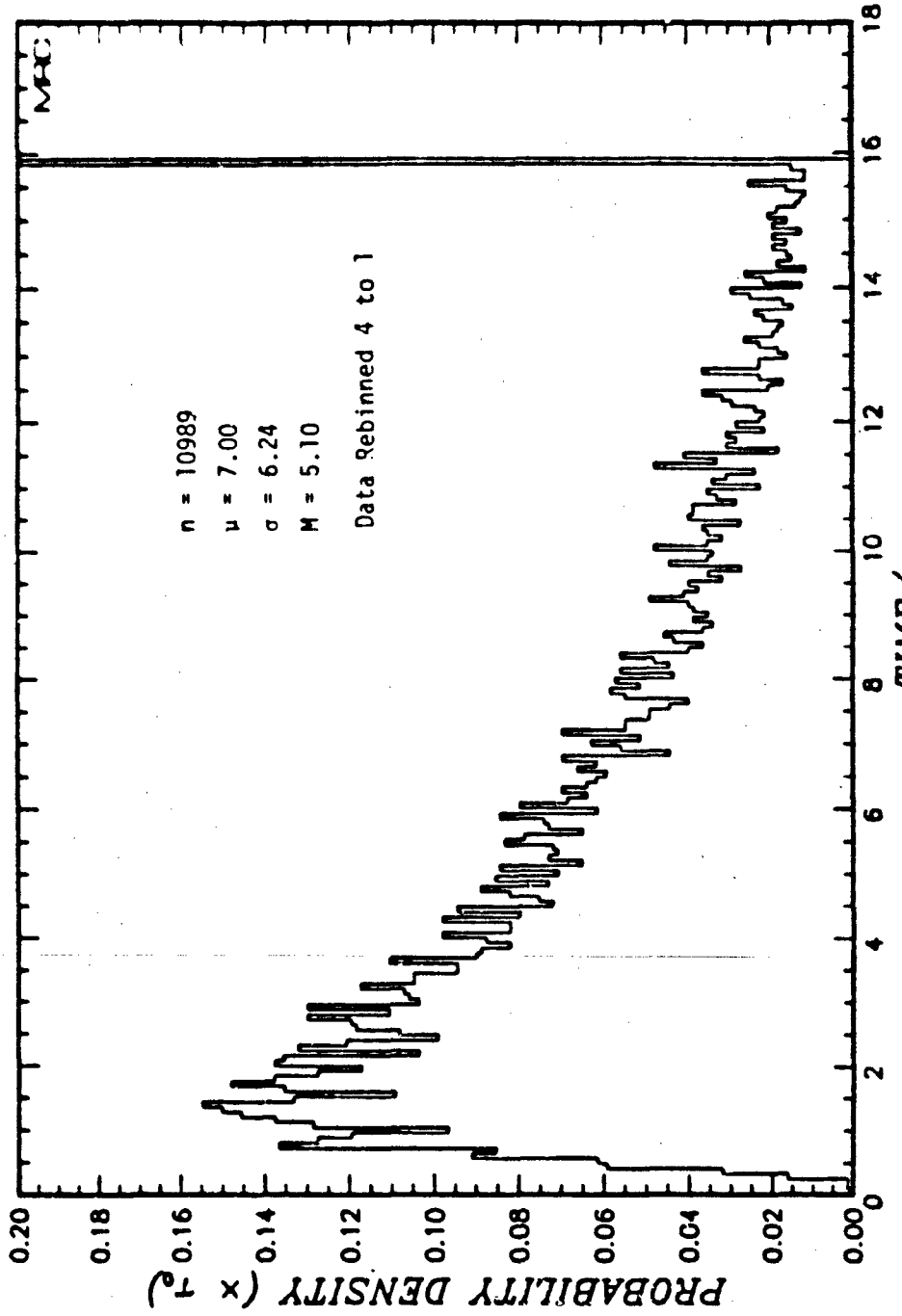

Figure D-19. Probability density function of the separation of fades below -15 dB.

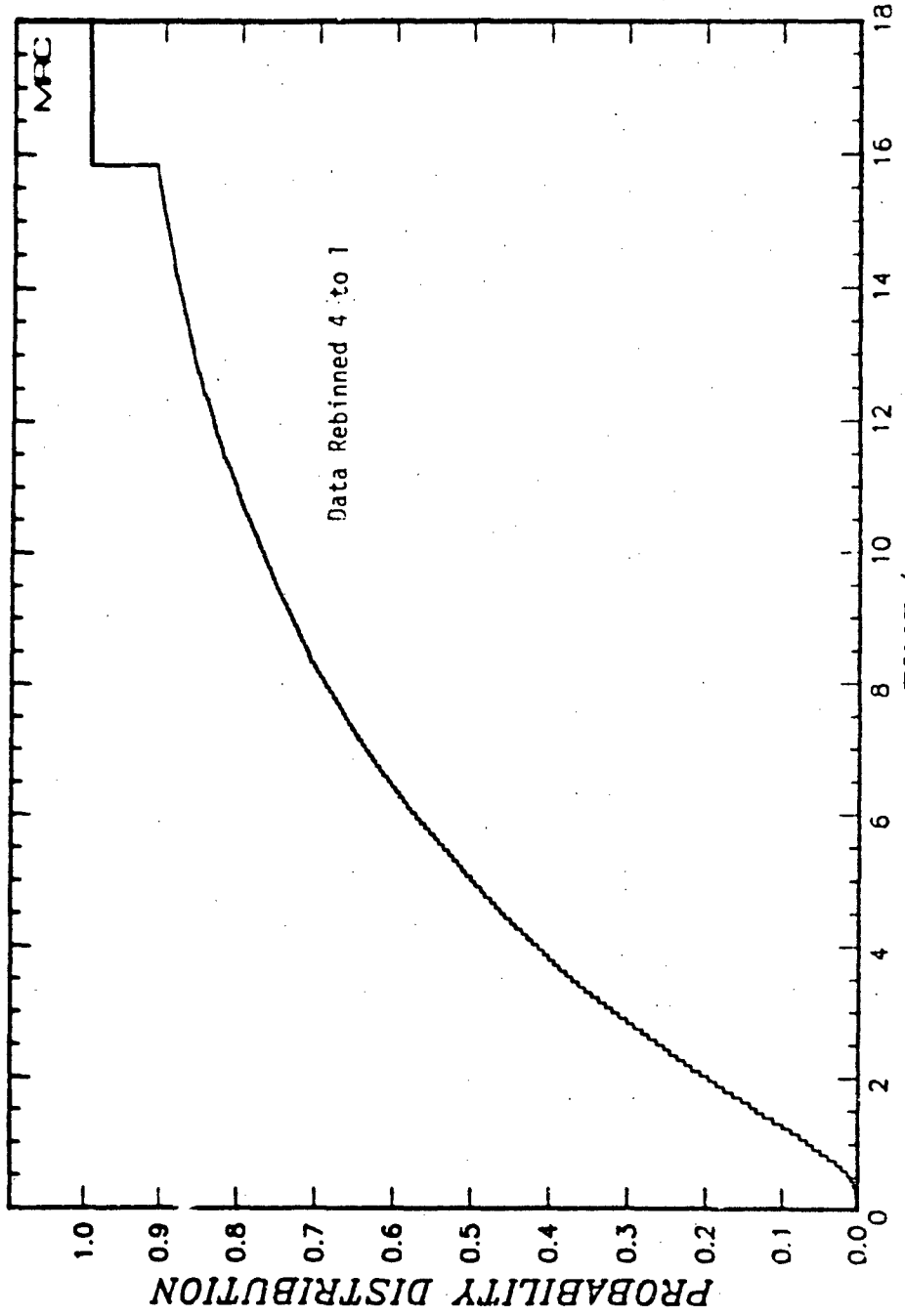

Figure D-20. Cumulative probability distribution of the separation of fades below -15 dB.

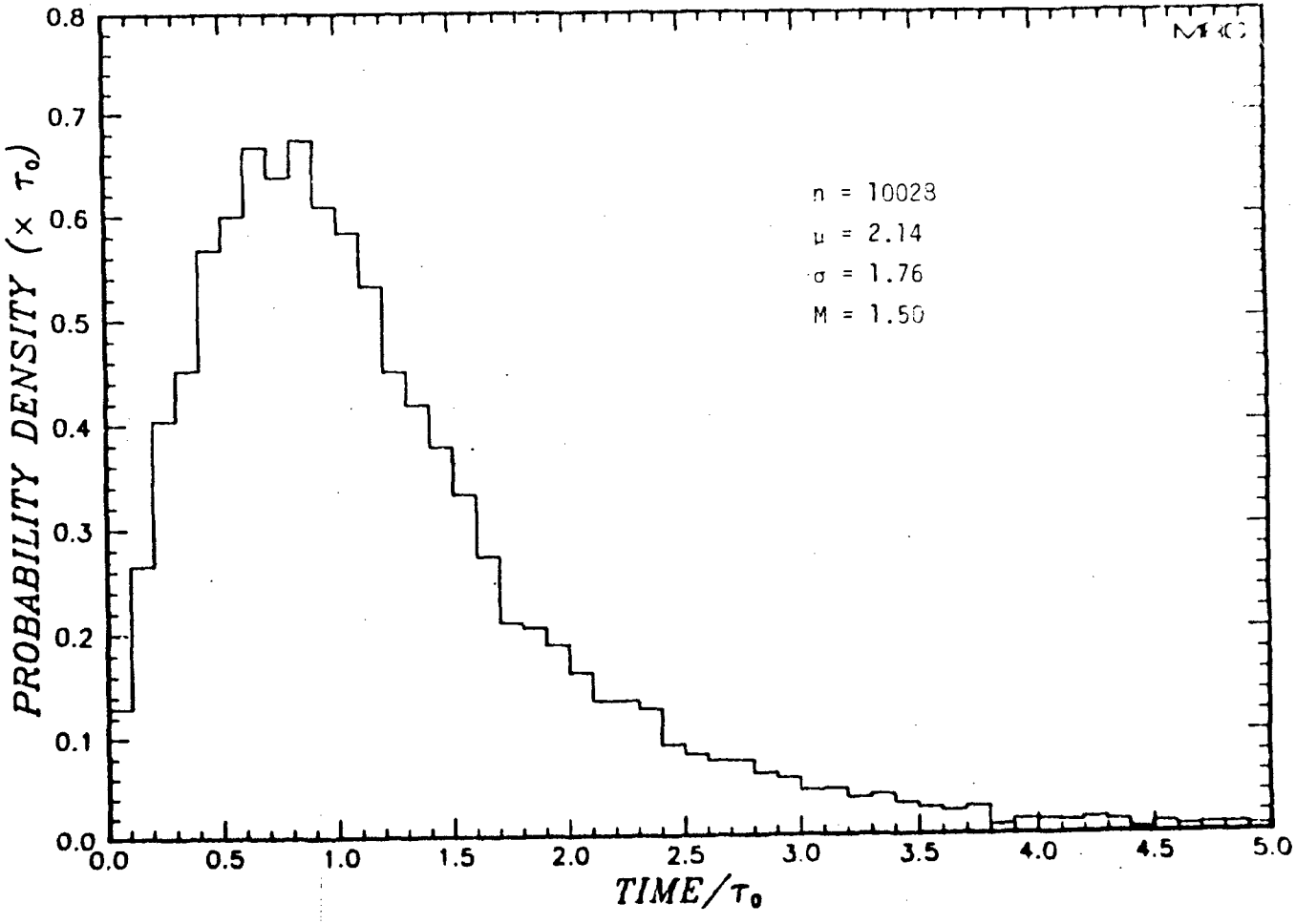

Figure D-21. Probability density function of the duration of flares above 0 dB.

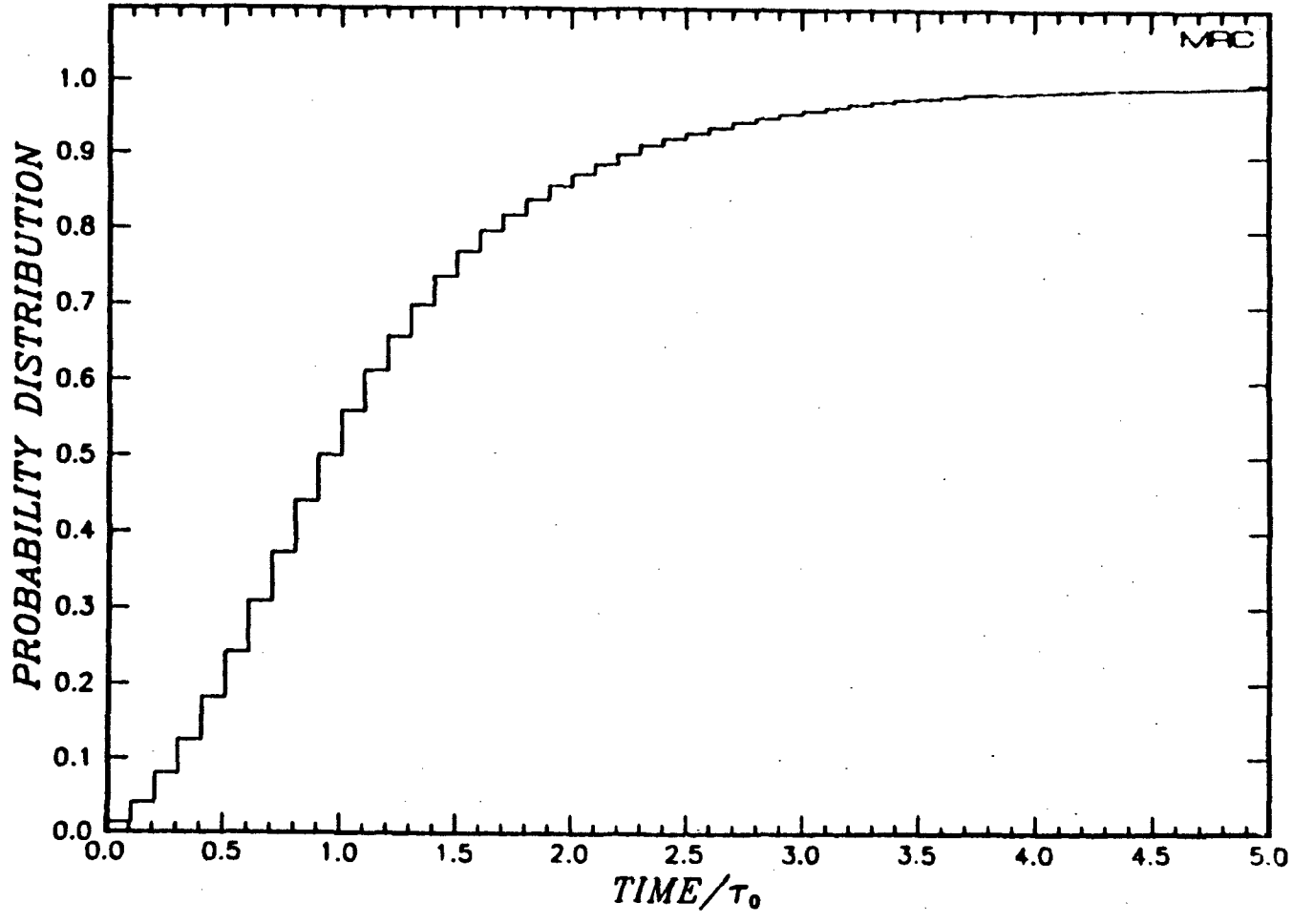

Figure D-22. Cumulative probability distribution of the duration of flares above 0 dB.

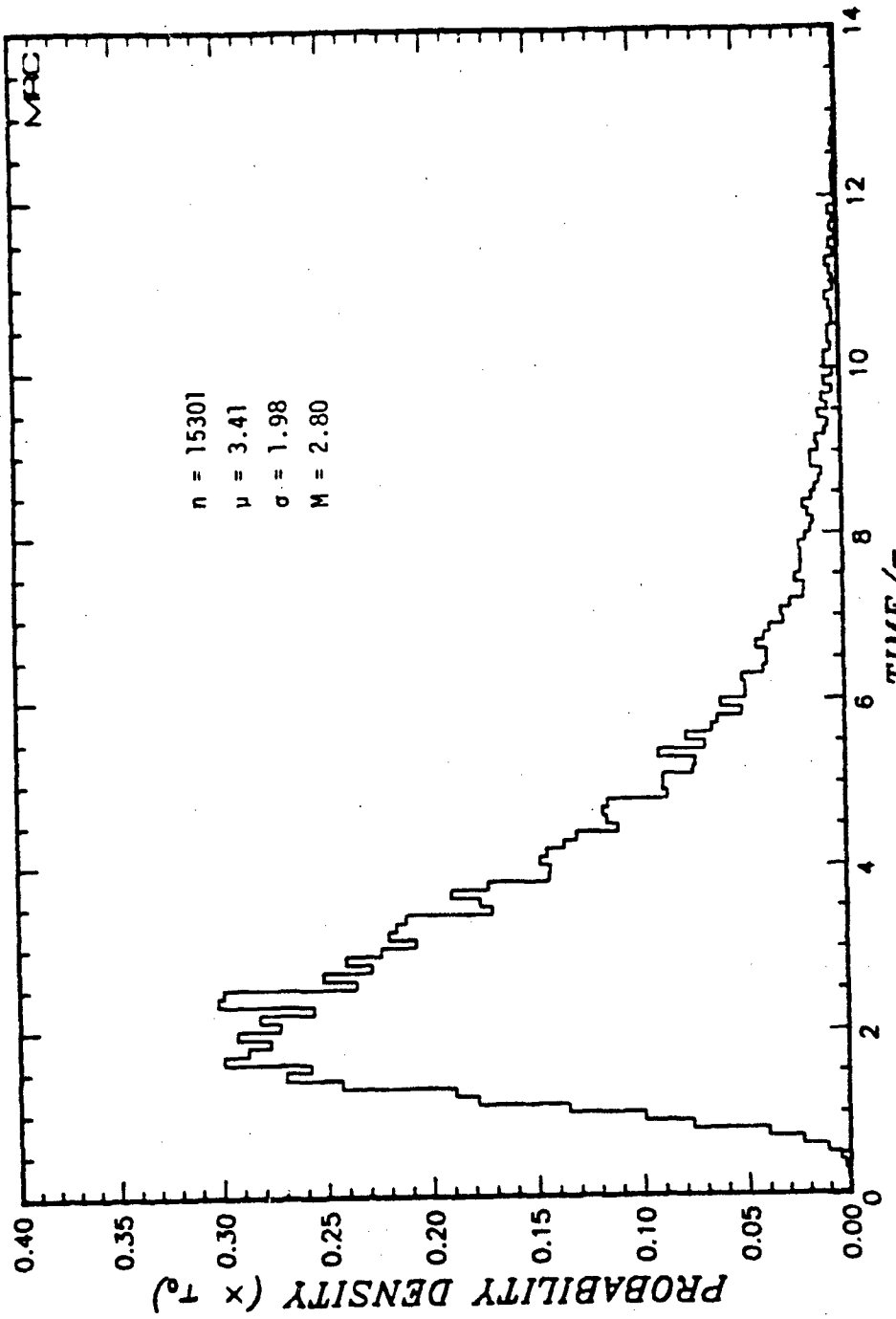

Figure D-23. Probability density function of the separation of flares above 0 dB.

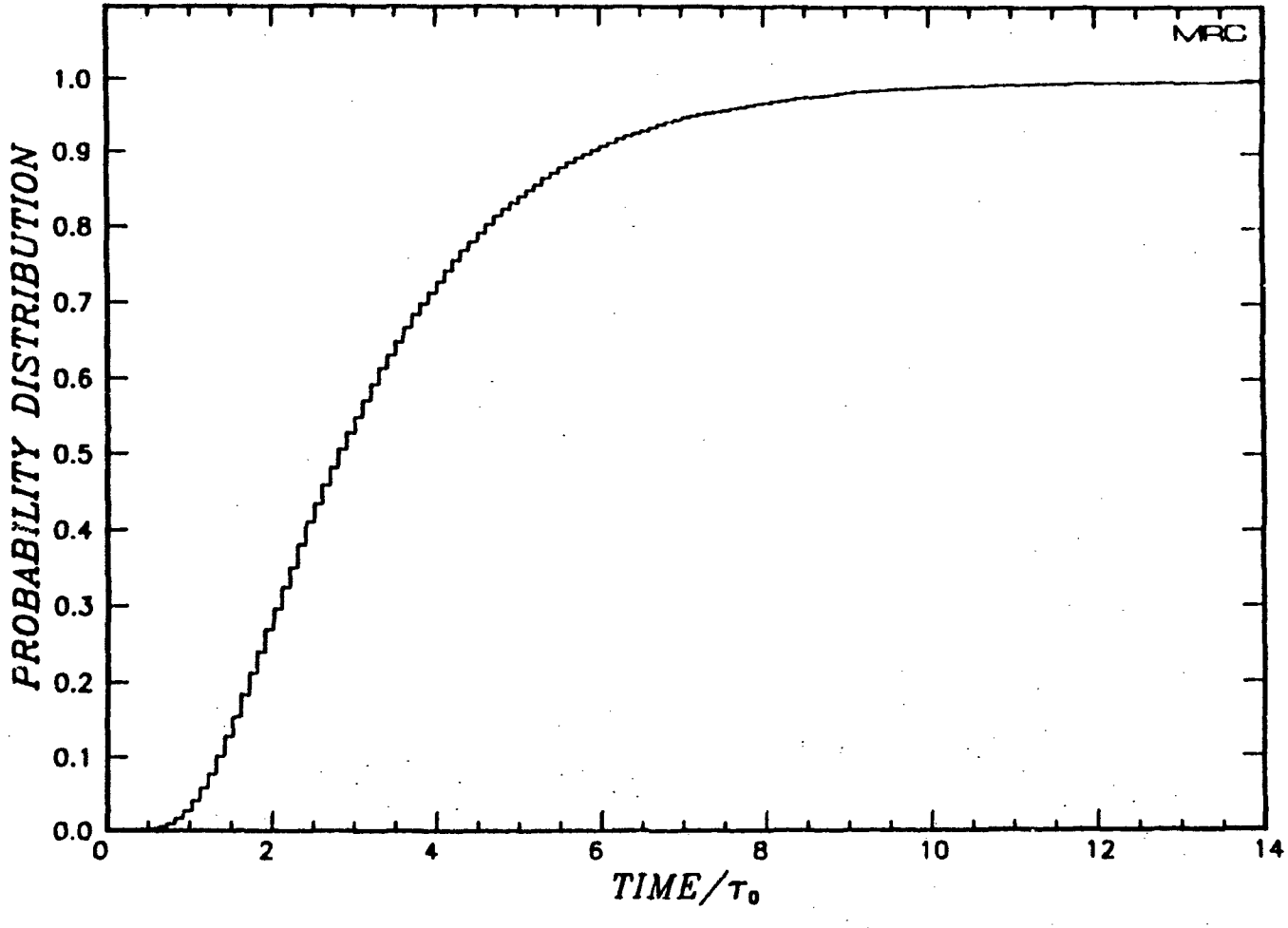

Figure D-24. Cumulative probability distribution of the separation of flares above 0 dB.

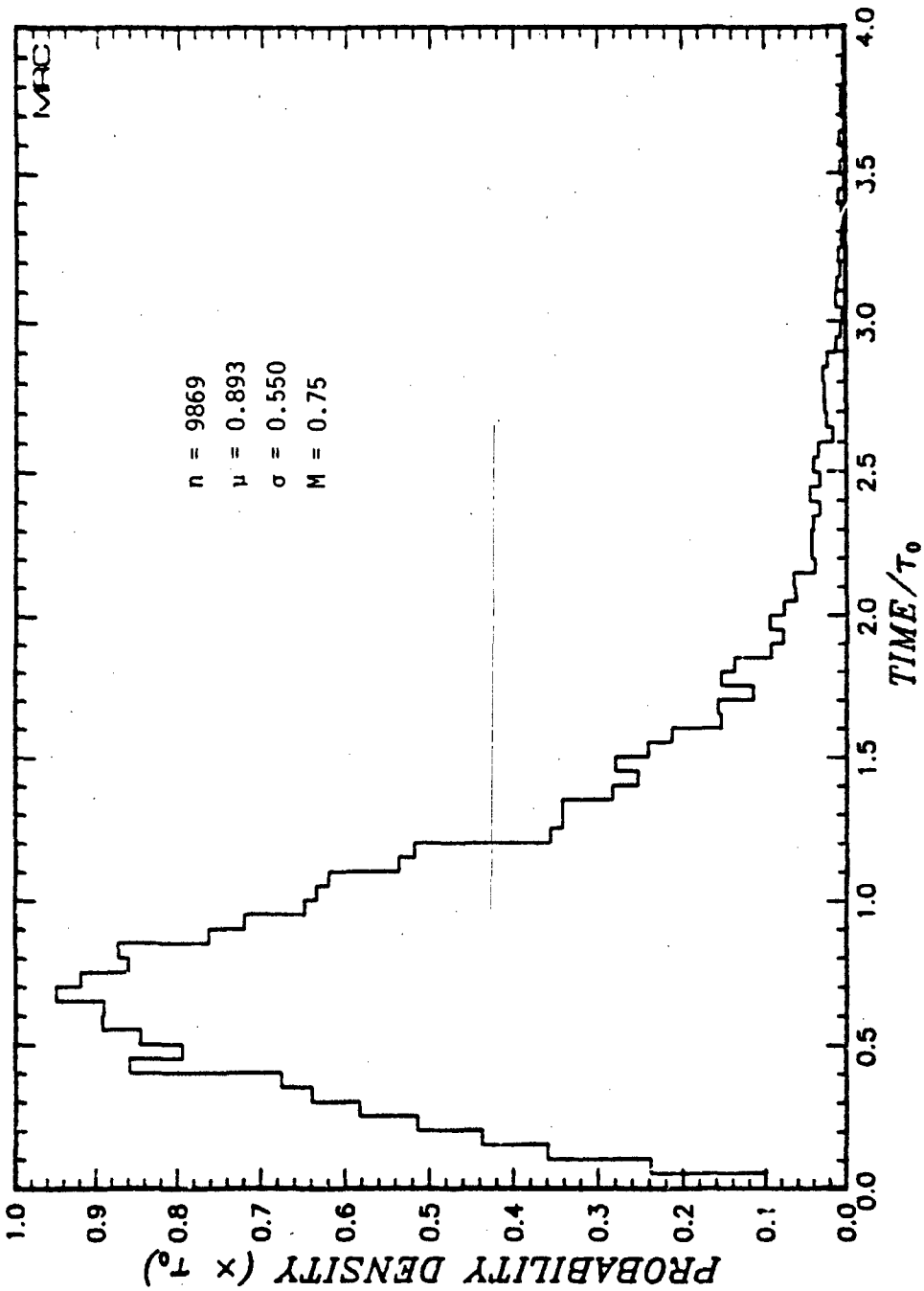

Figure D-25. Probability density function of the duration of flares above 3 dB.

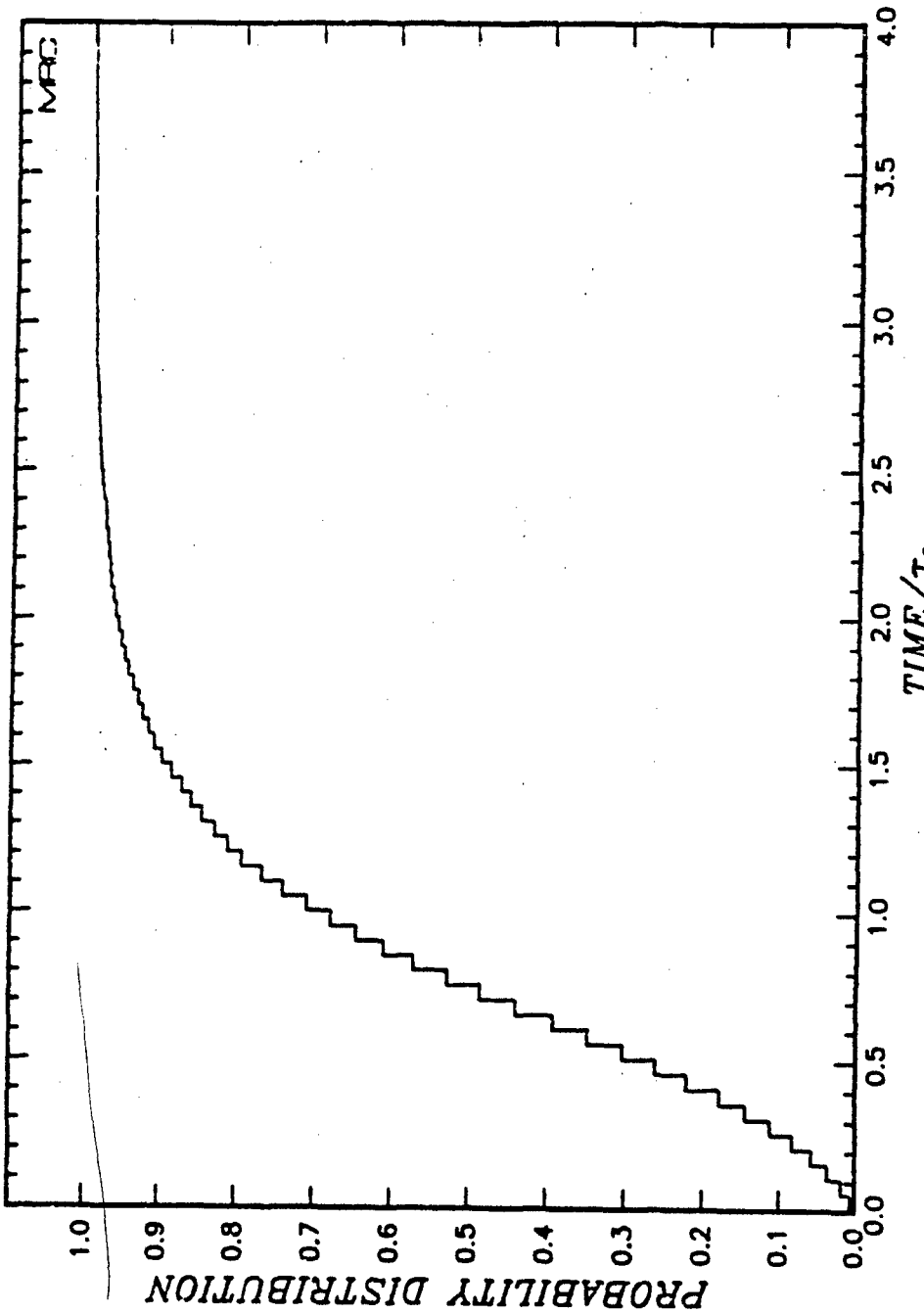

Figure D-26. Cumulative probability distribution of the duration of flares above 3 dB.

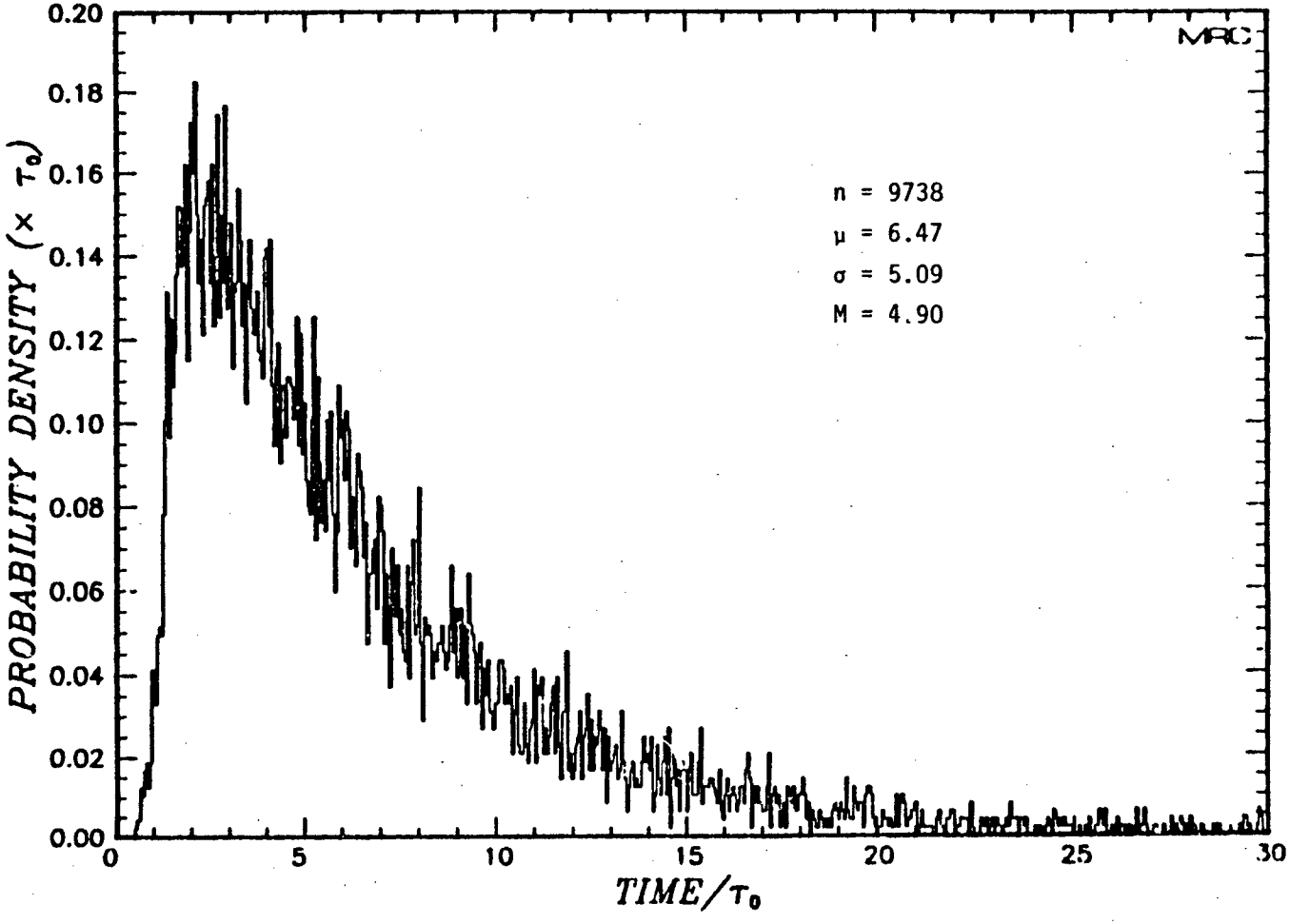

Figure D-27. Probability density function of the separation of flares above 3 dB.

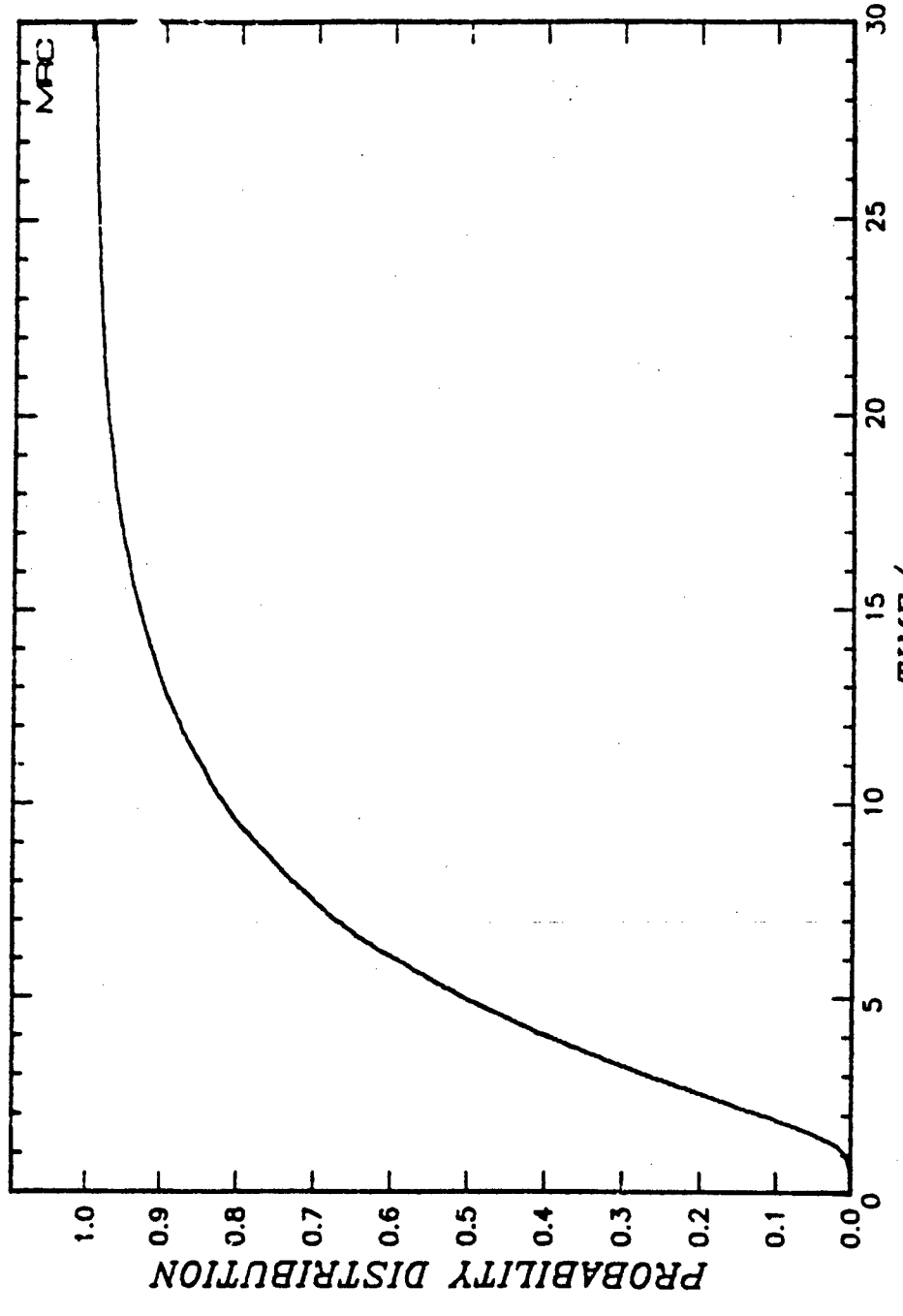

Figure D-28. Cumulative probability distribution of the separation of flares above 3 dB.

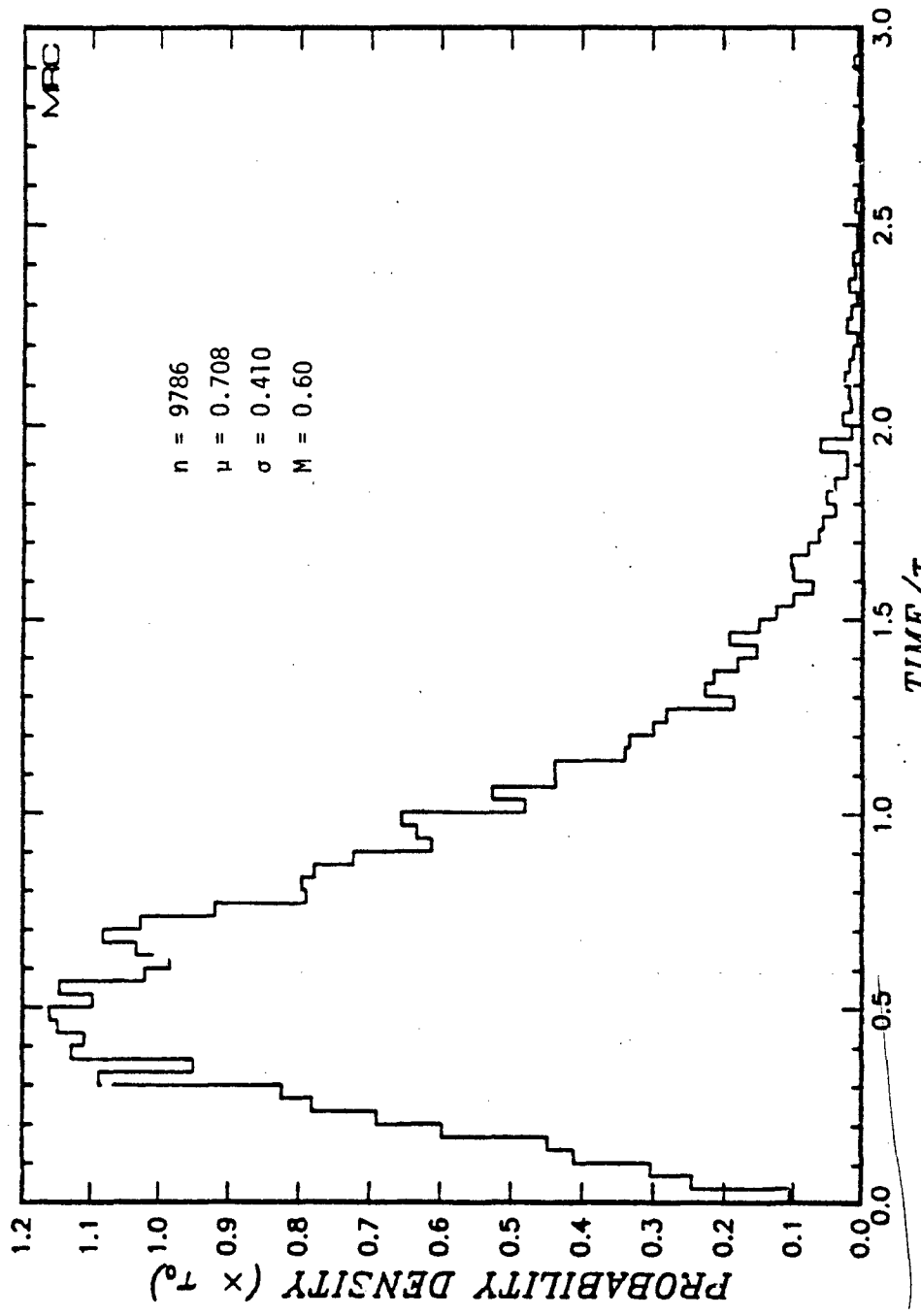

Figure D-29. Probability density function of the duration of flares above 5 dB.

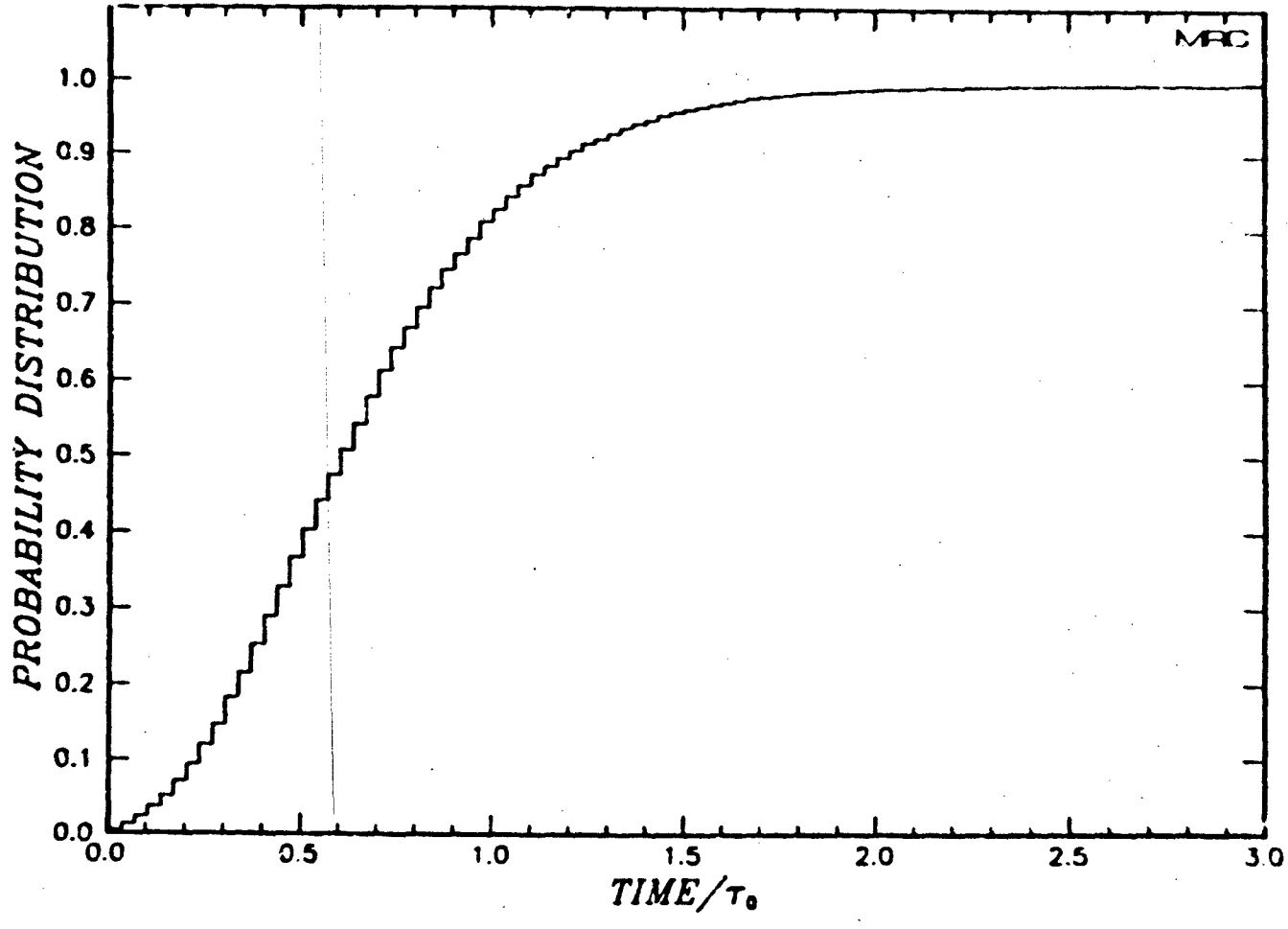

Figure D-30. Cumulative probability distribution of the duration of flares above 5 dB.

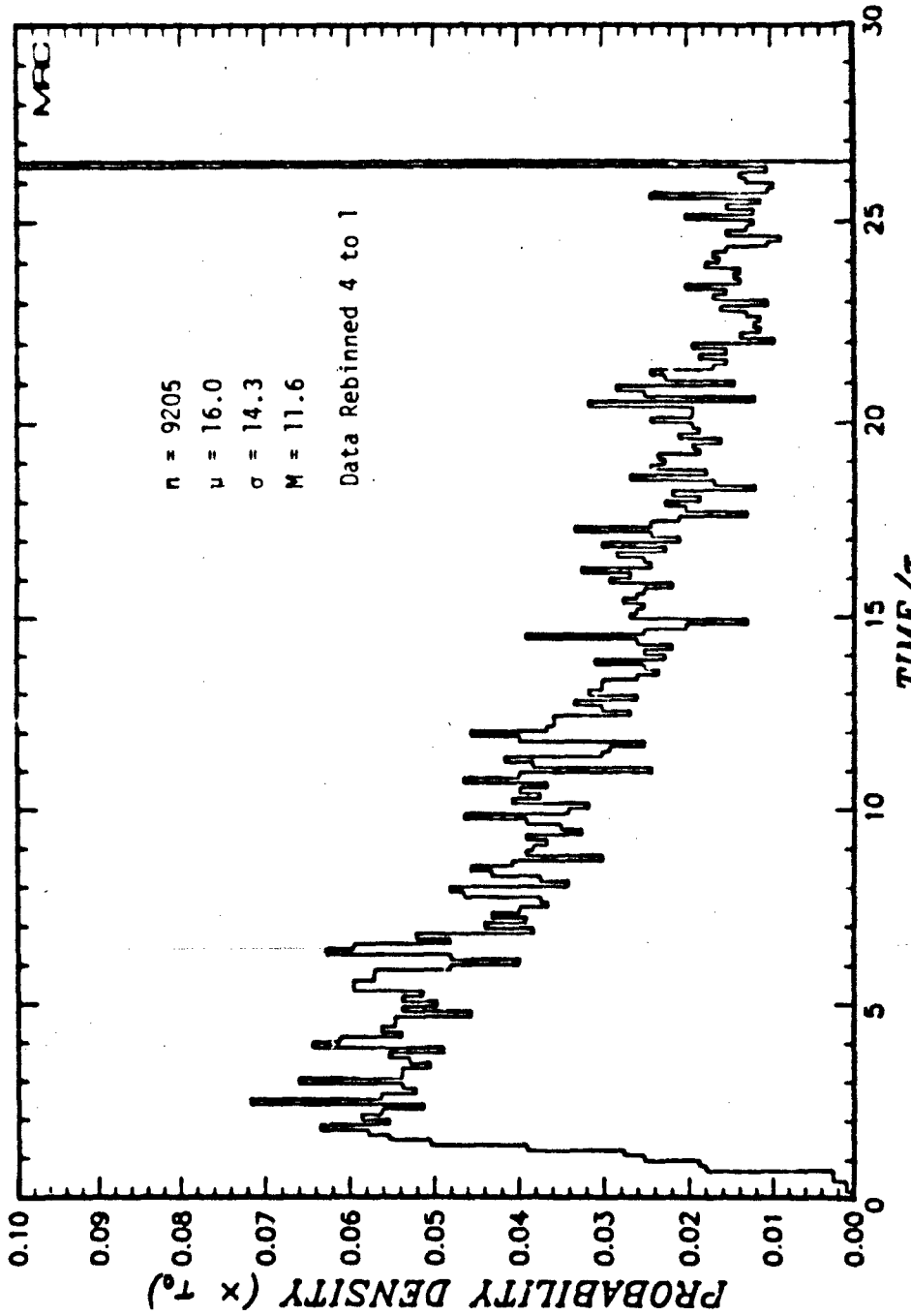

Figure D-31. Probability density function of the separation of flares above 5 dB.

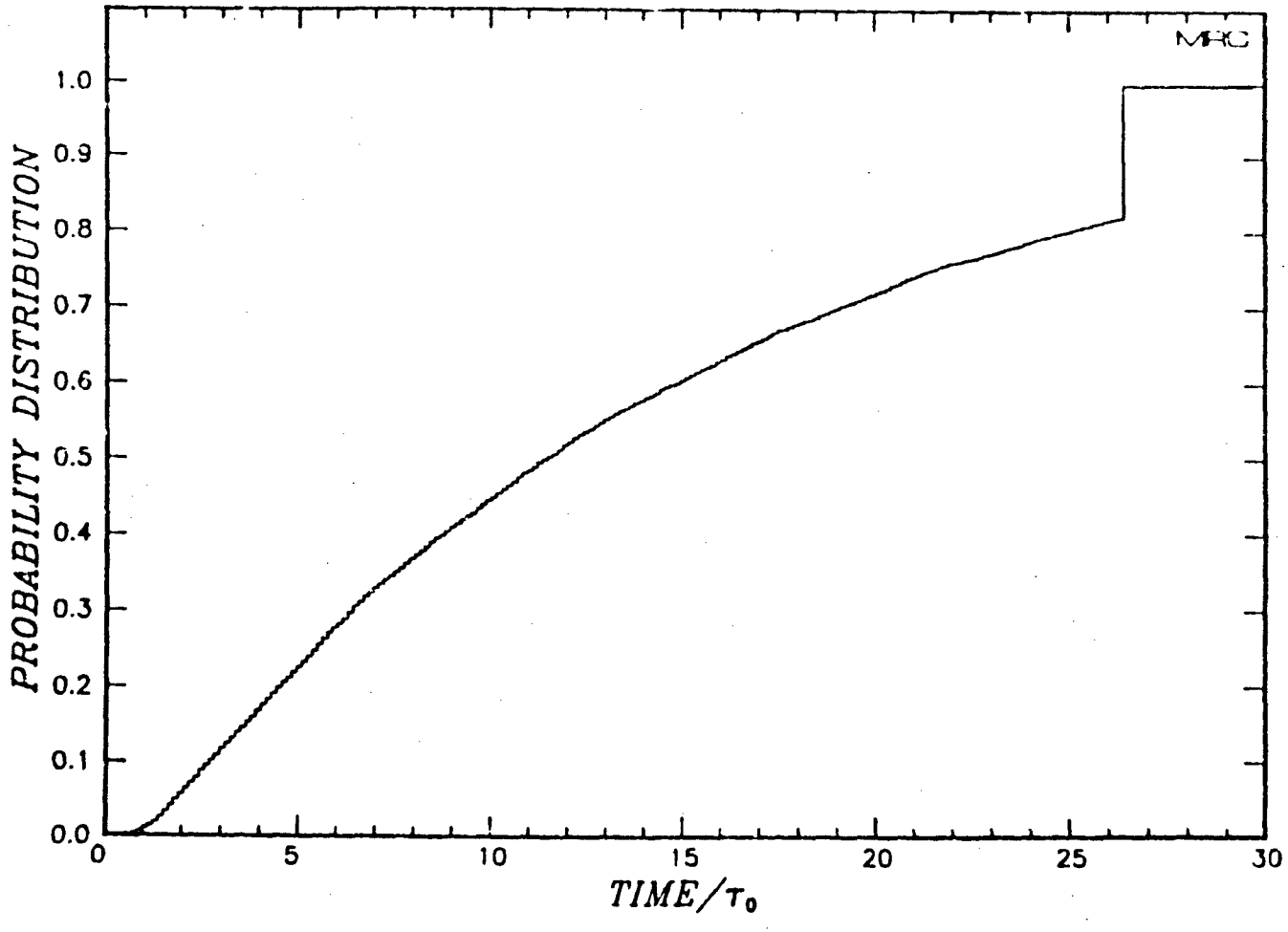

Figure D-32. Cumulative probability distribution of the separation of flares above 5 dB.

DISTRIBUTION LIST

DEPARTMENT OF DEFENSE

Command & Control Tech Ctr
ATTN: C-312, R. Mason
ATTN: C-650, G. Jones
ATTN: C-650
3 cy ATTN: C-650, W. Heidig

Defense Comm Engr Ctr
ATTN: Code R410, N. Jones
ATTN: Code R410
ATTN: Code R410, R. Craighill
ATTN: Code R123

Defense Nuclear Agcy
ATTN: STNA
ATTN: NAFD
ATTN: RAEE
ATTN: NATD
ATTN: RAAE, P. Lunn
3 cy ATTN: RAAE
4 cy ATTN: TITL

Defense Tech Info Ctr
12 cy ATTN: DD

Field Command Defense Nuclear Agcy
Det 1
Lawrence Livermore Lab
ATTN: FC-1

Interservice Nuclear Wpns School
ATTN: TTV

WWMCCS Sys Engrg Org
ATTN: R. Crawford

DEPARTMENT OF THE ARMY

USA Comm Cmd
ATTN: CC-OPS-WR, H. Wilson
ATTN: CC-OPS-W

USA Satellite Comm Agcy
ATTN: Doc Con

DEPARTMENT OF THE NAVY

Naval Electronic Sys Cmd
ATTN: Code 501A
ATTN: PME 117-211, B. Kruger
ATTN: PME 106-4, S. Kearney
ATTN: PME 117-2013, G. Burnhart
ATTN: PME 117-20
ATTN: PME 106-13, T. Griffin
ATTN: Code 3101, T. Hughes

Naval Ocean Sys Ctr
ATTN: Code 532
ATTN: Code 5322, M. Paulson
ATTN: Code 5323, J. Ferguson

Office of Naval Rsch
ATTN: Code 414, G. Joiner
ATTN: Code 412, W. Condell

DEPARTMENT OF THE NAVY (Continued)

Naval Rsch Lab
ATTN: Code 4720, J. Davis
ATTN: Code 7500, B. Wald
ATTN: Code 4780, S. Ossakow
ATTN: Code 4187
ATTN: Code 4700
ATTN: Code 4780
ATTN: Code 6700
ATTN: Code 7950, J. Goodman

DEPARTMENT OF THE AIR FORCE

Air Force Geophysics Lab
ATTN: OPR, H. Gardiner
ATTN: OPR-1
ATTN: LKB, K. Champion
ATTN: CA, A. Stair
ATTN: PHY, J. Buchau
ATTN: R. Babcock
ATTN: R. O'Neil

Air Force Tech Applications Ctr
ATTN: TN

Air Force Wpns Lab
ATTN: SUL
ATTN: NTYC
ATTN: NTN

Air Force Wright Aeronautical Lab
ATTN: W. Hunt
ATTN: A. Johnson

Air University Library
ATTN: AUL-LSE

Foreign Tech Div
ATTN: NIIS Library
ATTN: TQTD, B. Ballard

Rome Air Dev Ctr
ATTN: OCS, V. Coyne
ATTN: TSLD

Space Div
ATTN: YKM, Maj Alexander
ATTN: YKM, Capt Norton

OTHER GOVERNMENT AGENCY

Institute for Telecommunications Sciences
National Telecomm & Info Admin
ATTN: A. Jean
ATTN: L. Berry
ATTN: W. Utlaut

DEPARTMENT OF ENERGY CONTRACTORS

Los Alamos National Lab
ATTN: MS 670, J. Hopkins
ATTN: D. Simons
ATTN: MS 664, J. Zinn
ATTN: T. Kunkle, ESS-5
ATTN: P. Keaton
ATTN: R. Jeffries
ATTN: J. Wolcott

DEPARTMENT OF ENERGY CONTRACTORS (Continued)

Sandia National Lab
ATTN: Tech Lib 3141
ATTN: Space Proj Div
ATTN: D. Dahlgren
ATTN: ORG 4231, T. Wright
ATTN: D. Thornbrough
ATTN: ORG 1250, W. Brown

DEPARTMENT OF DEFENSE CONTRACTORS

Aerospace Corp
ATTN: D. Olsen
ATTN: I. Garfunkel
ATTN: R. Slaughter
ATTN: J. Straus
ATTN: T. Salmi
ATTN: V. Josephson

Analytical Systems Engrg Corp
ATTN: Radio Sciences

Analytical Sys Engrg Corp
ATTN: Security

BDM Corp
ATTN: T. Neighbors
ATTN: L. Jacobs

Berkeley Rsch Assoc, Inc
ATTN: J. Workman
ATTN: S. Brecht
ATTN: C. Prettie

Boeing Aerospace Co
ATTN: MS/87-63, D. Clauson

Boeing Co
ATTN: G. Hall
ATTN: S. Tashird

BR Communications
ATTN: J. McLaughlin

University of California at San Diego
ATTN: H. Booker

Charles Stark Draper Lab, Inc
ATTN: A. Tetewski
ATTN: D. Cox
ATTN: J. Gilmore

COMSAT Labs
ATTN: D. Fang
ATTN: G. Hyde

Cornell University
ATTN: D. Farley, Jr
ATTN: M. Kelly

E-Systems, Inc
ATTN: R. Berezdivin

Electrospace Systems, Inc
ATTN: P. Phillips
ATTN: H. Logston

EOS Technologies, Inc
ATTN: B. Gabbard

DEPARTMENT OF DEFENSE CONTRACTORS (Continued)

General Rsch Corp
ATTN: B. Bennett

Geo-Centers, Inc
ATTN: E. Marram

Harris Corp
ATTN: E. Knick

Honeywell, Inc
ATTN: G. Terry, Avionics Dept
ATTN: G. Collyer, Avionics Dept

HSS, Inc
ATTN: D. Hansen

IBM Corp
ATTN: H. Ulander

Institute for Defense Analyses
ATTN: E. Bauer
ATTN: H. Wolfhard
ATTN: J. Aein
ATTN: H. Gates

International Tel & Tel Corp
ATTN: Tech Library

International Tel & Tel Corp
ATTN: G. Wetmore

JAYCOR
ATTN: J. Sperling

Johns Hopkins University
ATTN: J. Newland
ATTN: T. Evans
ATTN: P. Komiske
ATTN: J. Phillips

Kaman Sciences Corp
ATTN: T. Stephens

Kaman Tempo
ATTN: B. Gambill
ATTN: DASIAC
ATTN: J. Devore
ATTN: W. McNamara
ATTN: W. Knapp
ATTN: K. Schwartz

MIT Lincoln Lab
ATTN: D. Towle

MA/COM Linkabit, Inc
ATTN: H. Van Trees
ATTN: A. Viterbi
ATTN: I. Jacobs

Mitre Corp
ATTN: G. Harding
ATTN: C. Callahan
ATTN: A. Kymmel
ATTN: MS J104, M. Dresp

Pensylvania State University
ATTN: Ionospheric Rsch Lab

DEPARTMENT OF DEFENSE CONTRACTORS (Continued)

Mission Rsch Corp
ATTN: F. Fajen
ATTN: R. Hendrick
ATTN: R. Bogusch
ATTN: R. Bigoni
ATTN: C. Lauer
ATTN: S. Gutsche
ATTN: R. Kilb
ATTN: D. Knepp
ATTN: Tech Library
ATTN: G. McCartor
ATTN: F. Guigliano
4 cy ATTN: R. Dana
5 cy ATTN: Doc Con

Mitre Corp
ATTN: M. Horrocks
ATTN: W. Hall
ATTN: J. Wheeler
ATTN: W. Foster

Pacific-Sierra Rsch Corp
ATTN: E. Field, Jr
ATTN: F. Thomas
ATTN: H. Brode, Chairman SAGE

Physical Dynamics, Inc
ATTN: E. Fremouw

Physical Rsch, Inc
ATTN: R. Deliberis

R&D Assoc
ATTN: R. Lelevier
ATTN: W. Karzas
ATTN: W. Wright
ATTN: R. Turco
ATTN: M. Gantsweg
ATTN: C. Greifinger
ATTN: F. Gilmore
ATTN: H. Ory

R&D Assoc
ATTN: B. Yoon

DEPARTMENT OF DEFENSE CONTRACTORS (Continued)

Rand Corp
ATTN: E. Bedrozian
ATTN: C. Crain

Rockwell International Corp
ATTN: R. Buckner

Science Applications, Inc
ATTN: E. Straker
ATTN: D. Hamlin
ATTN: L. Linson
ATTN: C. Smith

Science Applications, Inc
ATTN: J. Cockayne

SRI International
ATTN: R. Tsunoda
ATTN: J. Vickrey
ATTN: V. Gonzales
ATTN: W. Chesnut
ATTN: R. Livingston
ATTN: D. McDaniels
ATTN: M. Baron
ATTN: R. Leadabrand
ATTN: G. Price
ATTN: D. Neilson
ATTN: A. Burns
ATTN: G. Smith
ATTN: J. Petrickes
ATTN: W. Jaye
ATTN: C. Rino

Sylvania Systems Gp
ATTN: I. Kohlberg
ATTN: J. Concordia

Visidyne, Inc
ATTN: O. Shepard
ATTN: W. Reidy
ATTN: C. Humphrey
ATTN: J. Carpenter